N O T I C E

THIS DOCUMENT HAS BEEN REPRODUCED FROM MICROFICHE. ALTHOUGH IT IS RECOGNIZED THAT CERTAIN PORTIONS ARE ILLEGIBLE, IT IS BEING RELEASED IN THE INTEREST OF MAKING AVAILABLE AS MUCH INFORMATION AS POSSIBLE

CONCEPTS FOR 18/30 GHz
SATELLITE COMMUNICATION SYSTEM STUDY
VOLUME I-A - APPENDIX TO FINAL REPORT

Contract NAS3–21362

Prepared for:
NASA LEWIS RESEARCH CENTER
Cleveland, Ohio

Ford

**Ford Aerospace &
Communications Corporation**
Western Development
Laboratories Division

3939 Fabian Way
Palo Alto, California 94303

CONCEPTS FOR 18/30 GHz

SATELLITE COMMUNICATION SYSTEM STUDY

VOLUME I-A - APPENDIX TO FINAL REPORT

Contract NAS3-21362

Prepared for:

NASA LEWIS RESEARCH CENTER
Cleveland, Ohio

APPENDIX A

PRECIPITATION ATTENUATION FOR 18/30 GHz SYSTEM DESIGN

CONTENTS

CONTENTS (Continued)

SECTION 1

SUMMARY

A summary of this appendix report on 18/30 GHz rain attenuation is fully contained within subsection 2.3 of the main report. All of this work was prepared by Future Systems Incorporated for Ford Aerospace & Communications Corporation under subcontract.

SECTION 2
INTRODUCTION

This study report has been prepared by Future Systems Incorporated (FSI) for Ford Aerospace & Communications (FACC) in accordance with Purchase Order Number SP-605387-AP, Task 1. The Statement of Work for this Task is repeated below.

> Future Systems Incorporated shall perform the following tasks in support of the 18/30 GHz fixed service satellite communications systems study (FACC, Prime Contract NAS 3-21362 to NASA Lewis Research Center, dated 18 May 1978):
>
> FSI Task 1   Propagation Study
>
> Prepare summary of available propagation data collected at 18/30 GHz for use in support of NASA RFP Task 2, Trunking Concepts, and Task 3, Direct User Concepts. Define link margins required for availabilities ranging from 0.99 to 0.9999. The use of spatial diversity shall be evaluated to achieve the higher availabilities. This Study shall apply to the CONUS area only.

NASA Lewis Research Center commissioned FACC to perform an 18/30 GHz fixed service satellite communications systems study. The purpose of this study is to establish probable configurations of millimeter wave satellite systems and the resulting need for technology development. The FACC study includes the design of a system based on a major terminal trunking concept and a system based on direct-to-the-user concepts. For both of these systems it is important to establish the relationships between communications link availability and link power margin for different climatic zones within the contiguous United States (CONUS). In addition, it is necessary to establish the availability versus link margin with space diversity for the major terminal trunking concept. The purpose of the present FSI study is to develop and present this information.

The effect of atmospheric precipitation on propagation attenuation has been studied for years, initially in support of the design of terrestrial microwave radio relay systems and later also in support of satellite communications systems. These studies consisted of theoretical analysis, measurement programs and the comparison of measurements and theory. During recent years the interest in these phenomena has increased due to the expectation that higher frequencies will be employed in future communications satellites where the effects of precipitation are more pronounced. The following major programs have been undertaken, some of which are still in progress:

> ATS-5 Propagation Experiments
> ATS-6 Propagation Experiments
> CTS Propagation Experiments
> COMSTAR Beacon Measurements

In addition there are active programs of propagation attenuation evaluation based on Sirio, the Japanese satellite programs and the European OTS/ECS Program.

In performing the propagation study, the following subjects were considered:

1.   Survey of Existing Information

We collected and reviewed a large number of articles and reports on the subject of propagation attenuation. A bibliography is included as an Annex to this report.

2.   Theoretical Models

Section 3 presents an introduction to the phenomenon under study, namely, precipitation attenuation. The other factors affecting propagation through the earth's atmosphere at frequencies above 10 GHz are also outlined. The significant conclusion is that only attenuation caused by hydrometeors, specifically rain, is of sufficient magnitude to cause link outages at these frequencies.

The various theoretical models for precipitation attenuation were also examined. The most reliable models to date include the following items:

a. Laws and Parsons raindrop size distribution as a function of rainfall rate. This distribution has been tested more completely than others which are available.

b. Spherical raindrop shape. The primary effect of non-spherical shape is the difference in attenuation for vertical and horizontal polarization. The values for spherical raindrops lie between those produced by oblate raindrops.

The relation between rain rate and specific attenuation is given by a semi-empirical formula of the form:

$$A = aR^b$$

Values of the parameters a and b were computed and are given in a recent paper by Olsen et. al. (ref. 4).

3. Climatological Models and Rainfall Rate Measurements

Section 4 examines the current data on climate, specifically rainfall amounts and rates in the U.S. Two important sources of data rare available: the U.S. Weather Bureau and the various experimenters who have taken precipitation measurements as an adjunct to propagation measurements. Weather Bureau data, while much more extensive and covering longer periods of time, is not in the desired form. Some type of transformation is required to obtain the needed cumulative time distributions. Several such transformations are available, and we examined that due to Rice and Holmberg (ref. 12). The resulting distributions match some experimental data within a reasonable degree.

4.   Millimeter Wave Experiments

        In Section 5 we review a number of experiments performed at
millimeter wave frequencies. We have assembled results from several of these in
the following categories:

            Terrestrial links
            Experiments using radiometers
            Experiments using weather radars
            Experiments using satellite-borne beacons or transponders

5.   Comparison of Experiment and Theory

        Section 6 provides a brief examination of the comparison between the
various experiments and the theoretical predictions of attenuation. Some of the
possible reasons for discrepancies are investigated.

6.   A Model for Precipitation Attenuation for CONUS

        Section 7 ties together the results of the previous sections to produce a
model for rain margins in the CONUS area. The climatological model used is that
of Rice and Holmberg. We have used the known geographical distribution of the
parameters for this model to divide CONUS into six zones, based on the expected
rainfall rate distribution with time.

7.   Diversity

        Section 8 describes the improvement in link availability that can be
obtained from the use of space diversity.

        In order to provide the results of the propagation study on a timely basis
as input to FACC's system study, it was necessary to limit consideration to those
data that were available by the beginning of February 1979. It should be
recognized that significant additional information will become available within the
coming year, especially as the result of the COMSTAR beacon experiments. Such
new information may make it desirable to update the attenuation model presented
in this report.

SECTION 3

PROPAGATION PHENOMENA AND ATTENUATION MODELS

3.1 Propagation Phenomena

Fading and distortion of electromagnetic waves as the result of transmission through the atmosphere can be caused by the following phenomena:

a) Atmospheric Absorption

The clear sky atmosphere causes propagation attenuation in excess of free space attenuation. The attenuation depends on the elevation angle, relative humidity and on the transmission frequency. There is a general increase of attenuation with frequency, and in addition there are peaks of attenuation due to molecular resonance at certain frequencies.

b) Rain Attenuation

Atmospheric attenuation increases with the presence of rain, hail, snow, fog and clouds due to absorption and scattering of energy by water particles. This phenomenon is generally called hydrometeor absorption. (The word "meteor" is of Greek origin, meaning "object in the air".) Rain attenuation increases with frequency and is the main subject of this study.

c) Ionospheric Scintillation

Refractive inhomogeneities in the ionosphere cause variations of received signal levels with time. This effect is not significant at frequencies above 10 GHz.

d) Faraday Rotation

The interaction of moving electrons in the ionosphere with the magnetic field of the Earth causes a rotation of the plane of polarization for linearly polarized transmissions. This effect is not significant at frequencies above 10 GHz.

e) Depolarization

Signal scattering due to rain also causes depolarization. This effect increases with frequency and will be a serious limitation in the use of dual polarizations above 10 GHz in areas with heavy rain rates.

f) Other Effects

Other effects in radio propagation include surface propagation, ionospheric reflection and scattering as well as ducting. These effects are present at much lower frequencies and need not be considered at frequencies above 1 GHz.

In summary, the only propagation effects that need to be considered for the 18/30 GHz satellite transmission systems are atmospheric absorption, rain attenuation and depolarization.

3.2 Atmospheric Absorption

Atmospheric absorption has been well described and quantified in CCIR Volume V, Propagation in Non-Ionized Media. An extract of the relevant information is given below.

Figure 3-1 shows the theoretical one-way attenuation for vertical and horizontal transmission through the atmosphere as a function of transmission frequency. The clear sky attenuation at the higher frequencies cannot be neglected, particularly at low elevation angles. Absolute humidity is also a factor that must be considered.

Water vapor absorption has a resonant peak at a frequency of 22.23 GHz, and oxygen absorption has a peak at 60 GHz and another peak at 120 GHz. Atmospheric absorption also causes an increase in systems noise temperature which must be considered at low elevation angles. This is shown in Figure 3-2.

3.3 Attenuation Due to Precipitation

Attenuation due to precipitation arises from the absorption of energy in the water droplets and to a lesser extent from the scattering of energy out of the beam of the antenna. When electromagnetic waves pass through an atmosphere with inhomogeneities such as rain clouds, electric and magnetic dipoles are exited in each particle of the inhomogeneities. Through this process, energy is extracted from incident waves and in part converted into heat and in part scattered through re-radiation. The heat absorption and wave scattering depends on many factors such as:

Figure 3-1
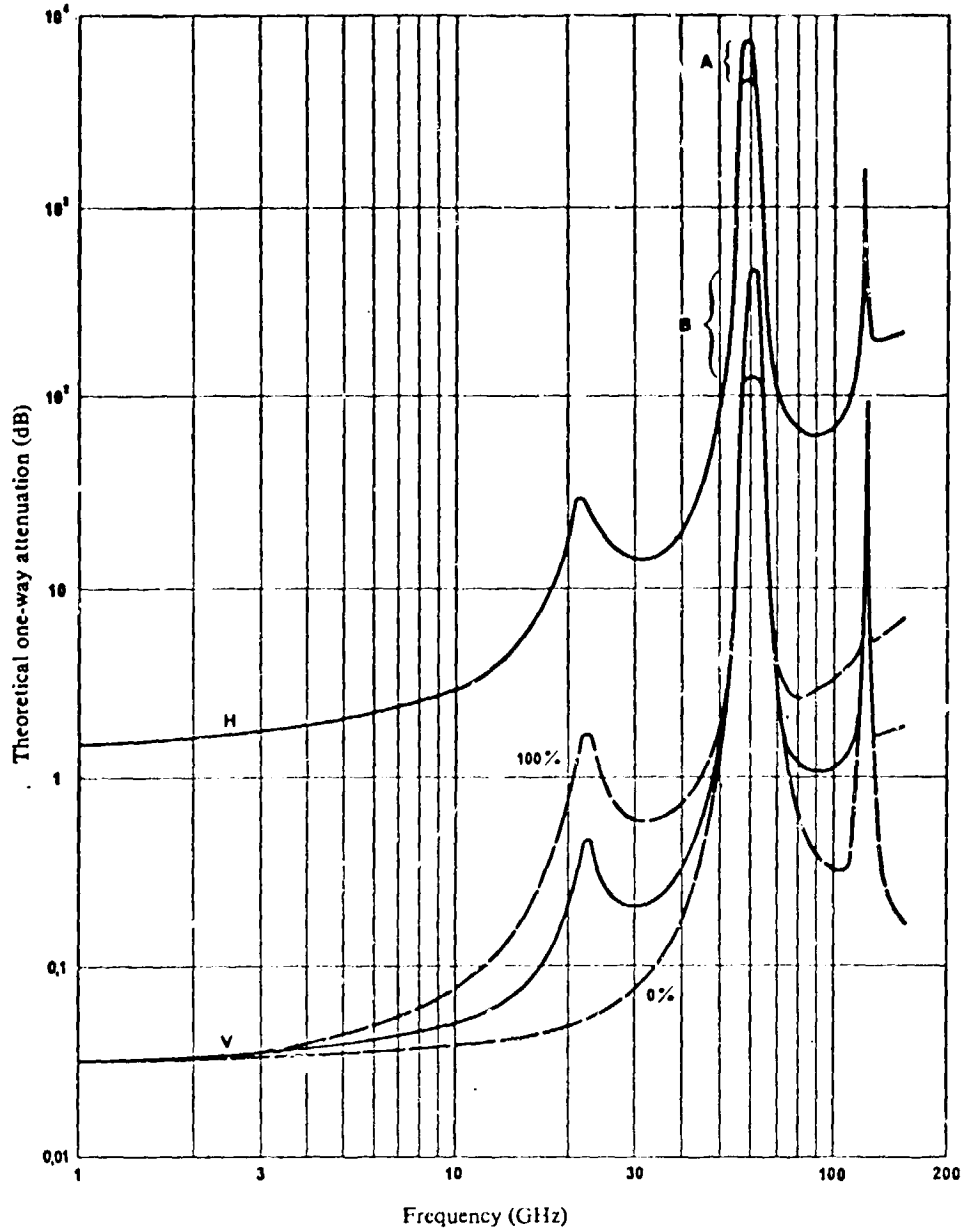
FIGURE 2

*Theoretical one-way attenuation for vertical and horizontal paths through the atmosphere
(calculated using the United States' standard atmosphere for July at 45° N latitude).
Solid curves are for a moderately humid atmosphere (7·5 g/m³ at the surface); dashed curves for
vertical attenuation represent the limits for 0 and 100% relative humidity*

A: Range of values   H: Horizontal

B: Range of values   V: Vertical

Source: CCIR Volume V
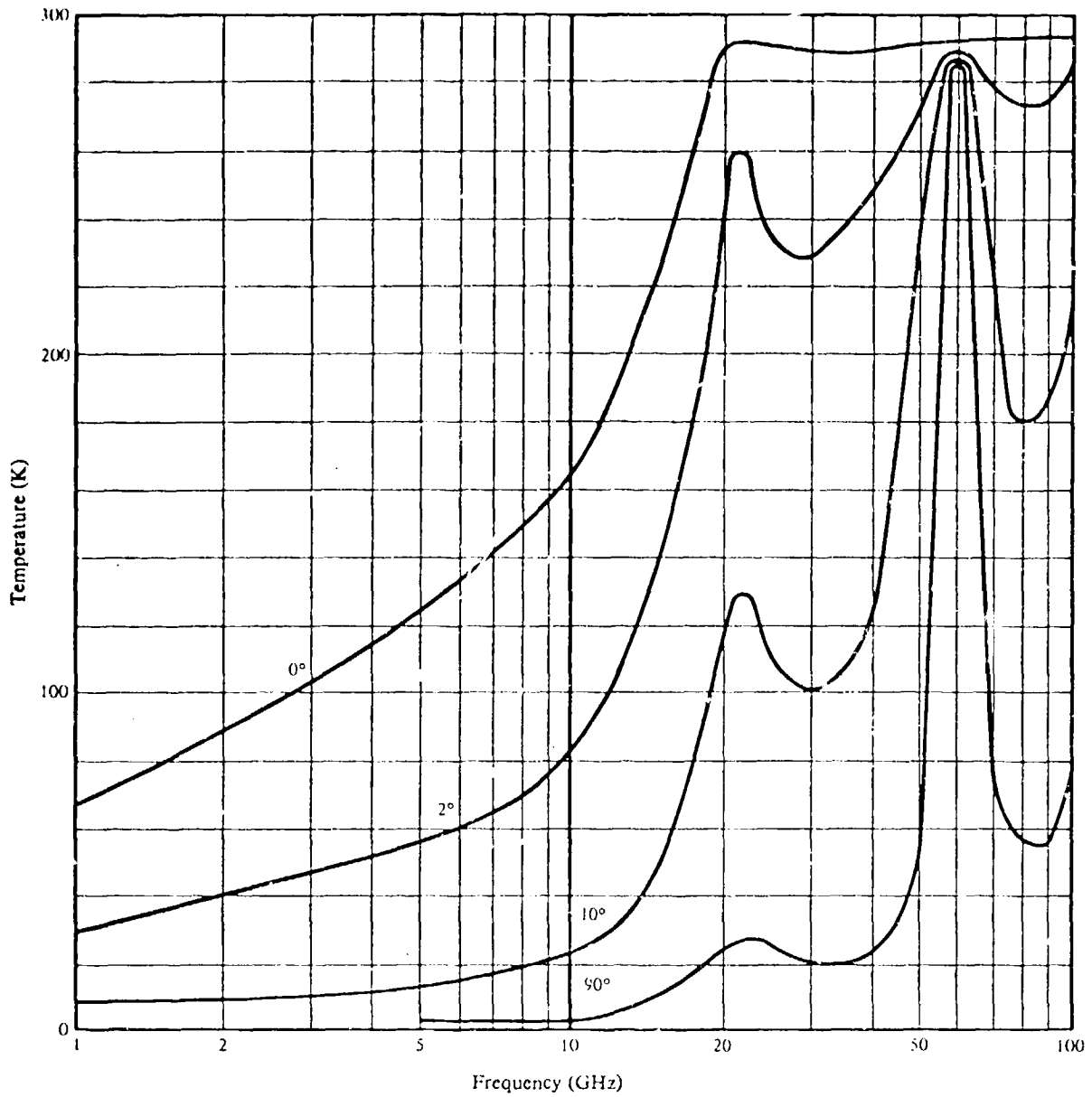
FIGURE 6

Total sky-noise temperature

Surface pressure: 760 mg Hg   Surface temperature: 20°C

Water vapour density: 10 g/m³

Angles of elevation: 0° – 90° as shown

Figure 3-2

Source: CCIR Volume V

a) The chemical processes which produce the particles and determine their electrical properties.

b) The aerodynamic processes which determine the shapes and sizes of the particles.

c) The electromagnetic processes which describe the interaction of waves and particles.

d) The meteorological processes which determine the collective behavior of particles in terms of clouds and precipitation.

However, due to a substantial lack of data concerning the characteristics of precipitation, a complete theoretical treatment of actual precipitation attenuation is not feasible. A practical and commonly used method is to use the theory, modified by some simplifying assumptions to extend the results of propagation experiments to cover a broad geographical and frequency range. Naturally, climatic data is an important component of such a method.

Calculations of attenuation due to rain generally yield results in units of d3/km. Further assumptions, guided by actual propagation experiments where possible, must be made to produce a value for the total excess attenuation in the earth/space path.

3.4   Models of Rain-Induced Attenuation

The primary factor which produces excess attenuation and depolarization phenomena is the presence of rain in the radio path. Several properties of rain are essential to any model of such phenomena, to wit:

Rainfall Rate
Raindrop Size (volume)
Raindrop Shape
Rain Temperature

The first item is significant in that it determines the density with which raindrops are present. The rain rate is usually treated differently for convective rain such as occurs in thundershowers, due to the intense updrafts which can increase the drop density over that expected from the ground level rainfall rate.

The other three items are significant in that they determine the scattering properties of the individual drops. Scattering is an important mechanism which produces attenuation and depolarization effects. The other contributor which is dependent on drop parameters is the absorption, which produces attenuation in a straightforward way.

In a given rainstorm, there will be areas of differing rain rate; likewise, even at a fixed rain rate not all drops will be of the same size. Raindrop shape is generally assumed to be spherical, although several authors have reported calculations based on oblate spheroidal drop shapes.

Given a set of assumptions for drop shape and size distribution, the attenuation at a given rain rate can be calculated. Such a calculation is given by Setzer (ref. 1), based on Mie scattering, and using a drop size distribution due to Laws and Parsons (ref. 2). Spherical raindrops are assumed. Figure 3-3 shows the Laws and Parsons drop size distribution for a 50 mm/hr rain rate. Figure 3-4 shows the attenuation at 18.5 and 30 GHz calculated as a function of rain rate from the data given by Setzer.

Another method, assuming oblate spheroidal raindrops, is due to Oguchi (ref. 3). The attenuation at 19.3 and 34.8 GHz given in this reference is shown in Figure 3-5. The raindrop volume is related to the drop size distribution of Laws and Parsons. This model is a closer approximation to reality, since in fact the drops are distorted by their fall through the air. The primary effect of such distortion is to produce different attenuation for horizontal and vertical polarizations.

A recent paper by Olsen et. al. (ref. 4) presents a thorough analysis using several models of raindrop size distribution. A useful empirical relation is derived of the form:

$$A = aR^b$$

where

A is attenuation in dB/km

R is rain rate

a,b are parameters dependent on frequency and the drop size distribution
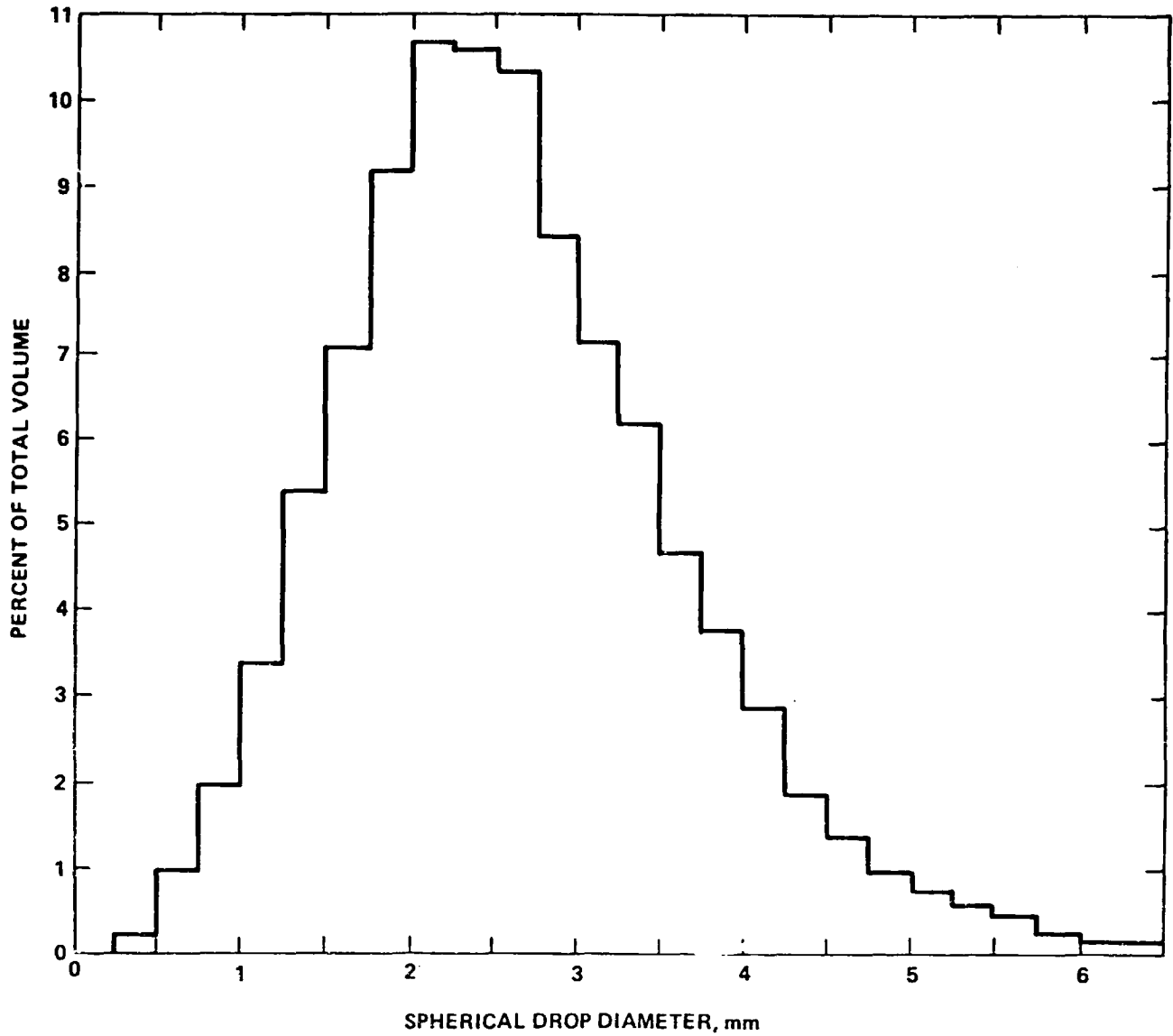
Figure 3-3

LAWS & PARSONS DROPSIZE DISTRIBUTION

RAIN RATE - 50mm/hr.
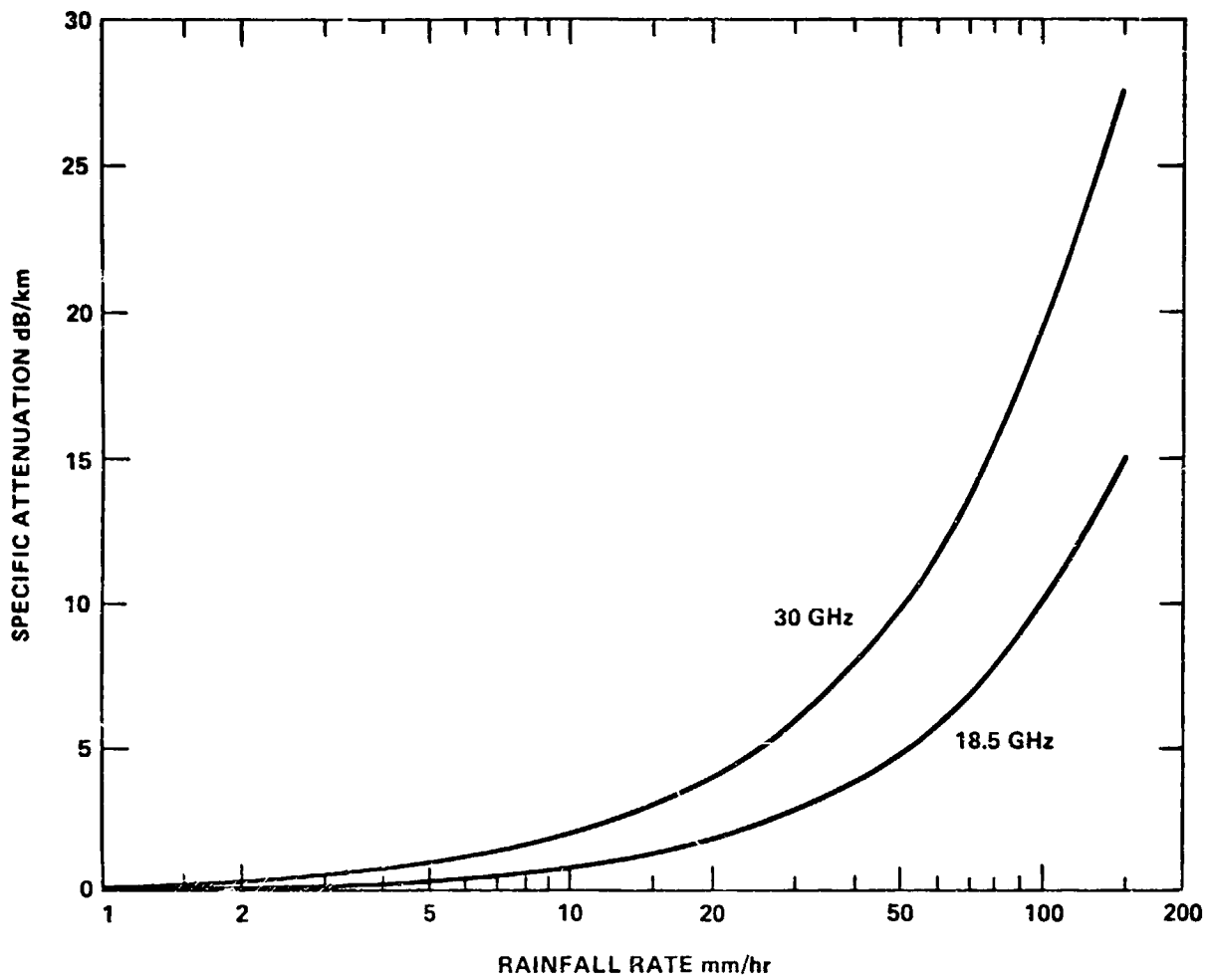
Figure 3-4

SPECIFIC ATTENUATION

ACCORDING TO SETZER (Ref. 2)
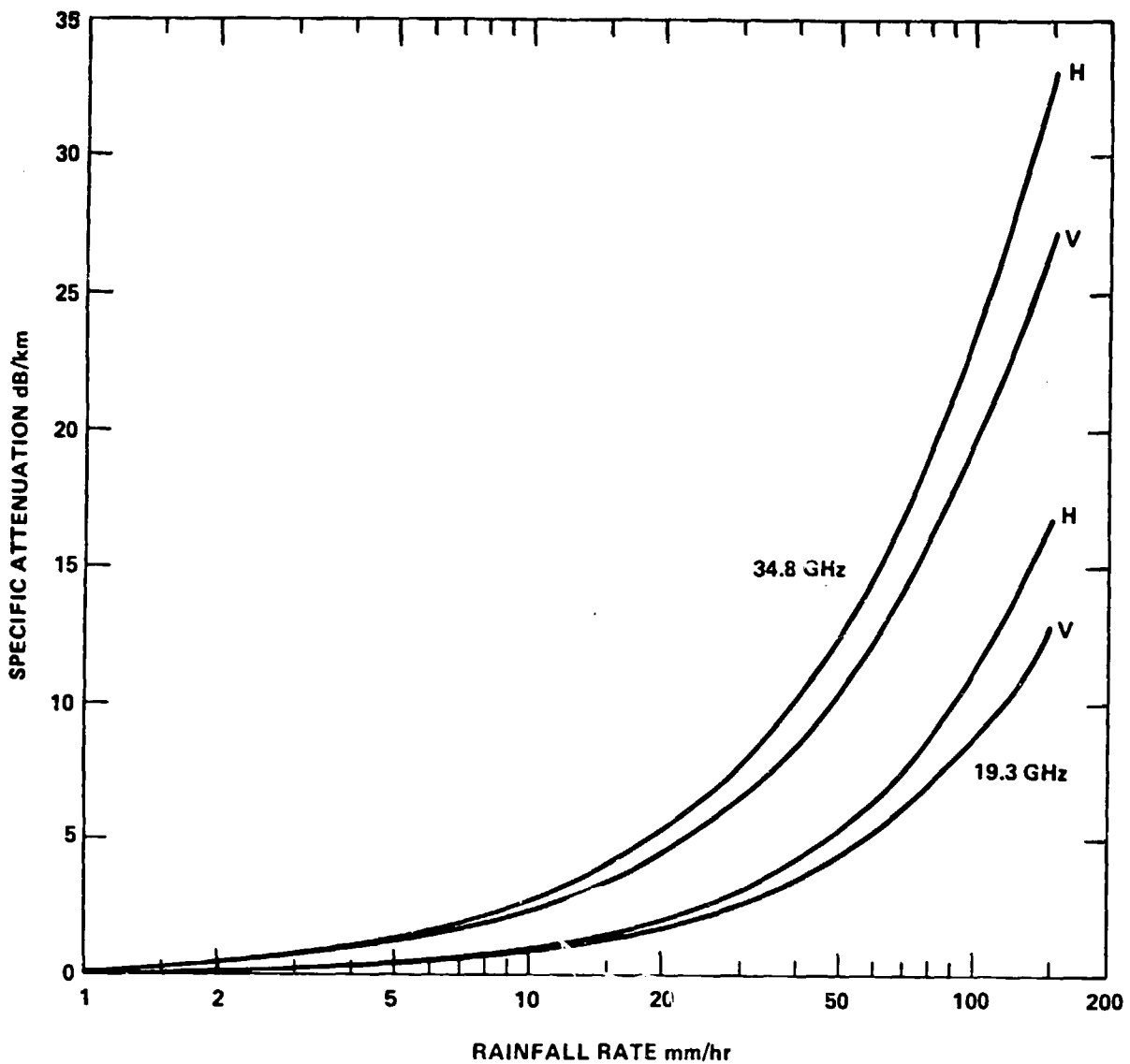
Figure 3-5

ATTENUATION VERSUS RAIN RATE FOR
OBLATE RAINDROPS - OGUCHI (Ref. 3)
V = Vertical polarization
H = Horizontal polarization

The parameters a and b are given for 41 frequencies between 1 and 1000 GHz. Those for 15, 20 and 30 GHz are shown in Table 3-1. The raindrop size distributions are as follows:

1) Laws and Parsons (LP) Distribution (ref. 2)

This tabular distribution has been found to be a reasonable choice for a mean dropsize spectrum in continental temperate rainfall at least at rainrates below about 35 mm/hr. It is probably the most widely tested distribution currently available and has been used for many previous calculations. The LP_1 distribution is for rain rates below 50 mm/hr and the LP_h is for rain rates from 50 mm/hr to 150 mm/hr.

2) Marshall-Palmer (MP) Distribution

This negative exponential distribution is a fairly good fit for the mean dropsize spectra measured by both Marshall and Palmer and Laws and Parsons. It has been found to be most applicable to widespread rain in continental temperate climates, although it has a tendency to overestimate the number of small drops.

3) "Thunderstorm" Distribution (J-T) of Joss et. al.

This negative exponential distribution was fitted by Joss et. al. to the average dropsize spectrum measured in convective rain. It has not yet been widely tested but has been used previously for some specific attenuation calculations.

4) "Drizzle" Distribution (J-D) of Joss et. al.

Again this is a negative exponential distribution obtained by fitting the average dropsize spectrum of very light widespread rain or drizzle composed mostly of small drops. Although the calculations for this distribution are not expected to be used by designers of communications systems, it was included for comparison purposes since even some heavy rains can contain mostly small drops.

Table 3-1
Values of a and b in $A = aR^b$ dB/km

Values of a				
Freq. GHz	LP_1	LP_h	MP	J-T	J-D

Freq. GHz	LP_1	LP_h	MP	J-T	J-D
15	3.21×10^{-2}	3.47×10^{-2}	3.05×10^{-2}	4.37×10^{-2}	3.19×10^{-2}
20	6.26×10^{-2}	7.09×10^{-2}	5.95×10^{-2}	9.22×10^{-2}	6.00×10^{-2}
30	0.162	0.226	0.154	0.257	0.145

Values of b					
15	1.142	1.119	1.139	1.094	0.973
20	1.119	1.083	1.118	1.03	0.99
30	1.061	0.964	1.064	0.907	1.014

It still has to be decided which distribution values are applicable for design purposes. The Laws and Parsons values are generally favored (LP_1 or LP_h, depending on the rain rate). These factors are applicable both for widespread and for convective rain. In addition, the LP distribution has been widely tested and compared against experimental results. Agreement is generally good. In the higher rain rate range which is associated with convective rain and in frequencies above 10 GHz, the LP_h values give higher specific attenuations than the J-T values. In order to perform a worst case design, it is then desirable to use the higher values. In any regions where the J-T distribution is known to apply, it should be used; however, it has not yet been tested for all climatic regions.

Figure 3-6 presents values of attenuation in dB/km given by the aR^b relation for Laws and Parsons rain at 18 and 30 GHz.
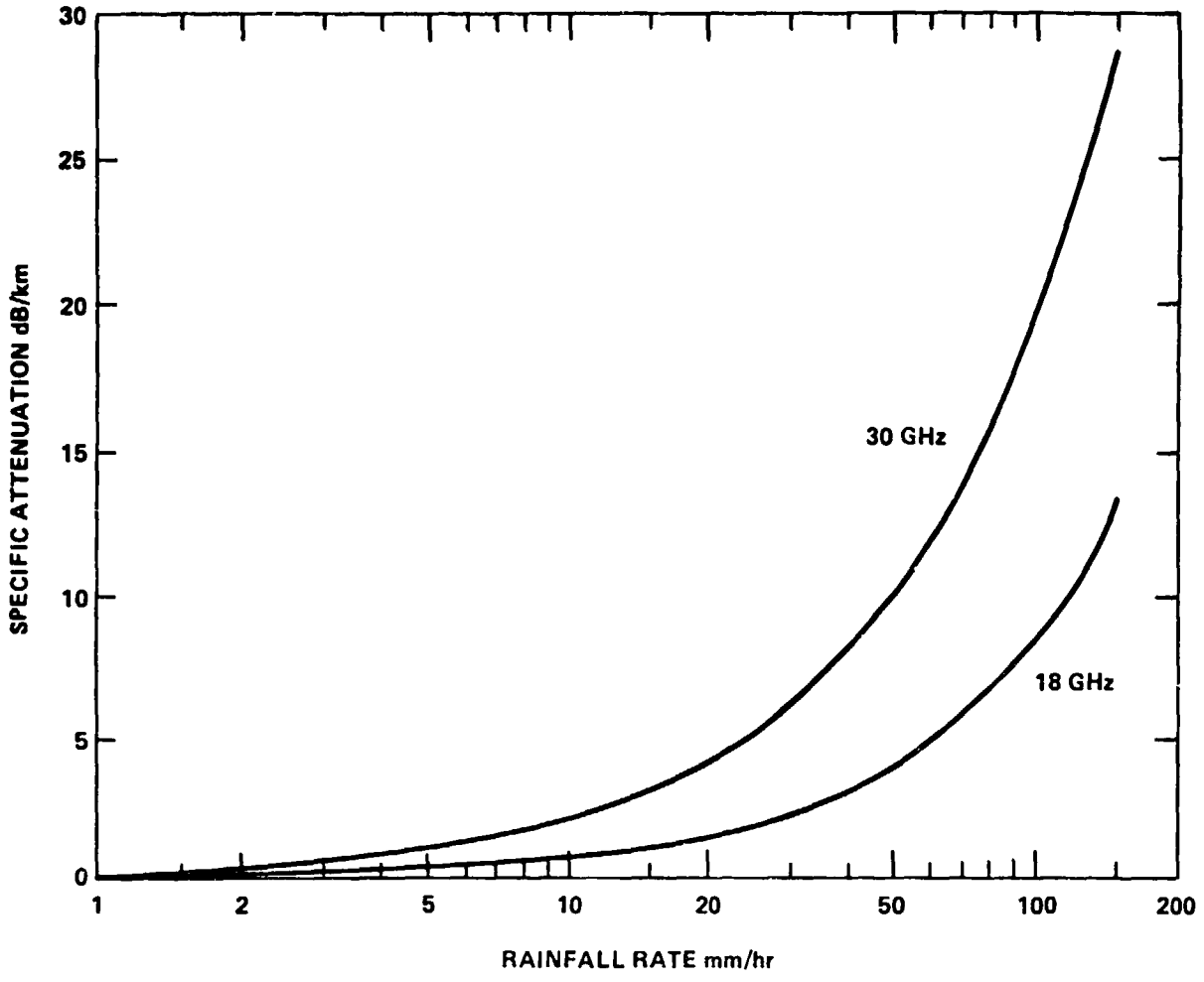
Figure 3-6

SPECIFIC ATTENUATION ACCORDING TO aR^b

LAWS & PARSONS RAIN

3.5 Noise Temperature Increase Due to Rain Attenuation

The satellite receiving antenna always points at the hot earth, representing a mean temperature of about 290 K. Increased path attenuation due to rain attenuation does not cause a significant variation of this temperature. Contrary to this, the earth station antenna normally points at space with a very low temperature, governed primarily by clear sky atmospheric absorption and to a lesser extent by cosmic radiation. (In addition, the effect of the hot earth is introduced through antenna sidelobes.) For a small percentage of the time the noise temperature as seen by the earth station receive antenna is increased greatly as the result of pointing at the sun and by a smaller amount as the result of pointing at the moon. However, during periods of rain the rain attenuation increases the noise temperature of the receive antenna.

This increase has, in fact, been exploited to provide indirect measurements of precipitation attenuation without the use of an orbiting beacon. The relationship between the sky noise and the attenuation is given by the following approximation, valid for antennas with narrow beamwidths:

$$T = \left[1 - 10^{-A/10} \right] T_r$$

where

T_r is the physical temperature of the sky seen by the antenna, generally about 273 K

A   is the attenuation in dB

T   is the apparent temperature increase of the sky, including the effects of precipitation.

This increase in noise temperature must be added to the temperature of the receiving system and the clear-weather sky temperature. This produces a degradation in the receive gain-to-noise temperature ratio or G/T. The decrease is dependent on the initial system G/T. Systems having a low noise antenna and amplifier are affected more than those with a higher receive noise temperature.

SECTION 4
MODELS AND MEASUREMENTS
OF RAINFALL PATTERNS IN THE U.S.

4.1   Introduction

The climatological model for rainfall is the crux of the overall model. No matter how accurate the relation between rain and attenuation, if a reasonable approximation to the rain rate distribution is not used, the predictions given by the model will not be reliable.

There are at least two sources of important climate data for the U.S.: the Weather Bureau and the various experimenters around the country who have taken data. The Weather Bureau has data covering a much longer period of time but it has not had an interest in correlating this data with space-link attenuation. The experimenters, on the other hand, have devoted a great deal of effort to the attempt to relate the observed weather to attenuation (and depolarization) but have data only for relatively short periods of time.

An additional difficulty with the satellite link is that the length of the path that extends through the precipitation is not readily determined. This factor is most important, for the results given by theory and the various models of attenuation are for specific attenuation (i.e., dB per km). Thus the path length (or an "equivalent" path length with constant rain rate) is needed to produce a value for total attenuation. Some assumptions must be made for this in a working model.

4.2   General Considerations

From the standpoint of attempting to describe (in statistical terms) the future precipitation patterns of a particular locale, there is not much latitude. Rain storms vary in their individual characteristics (such as drop shape), and we have seen that these are not very important anyway. We are forced to choose a

distribution of drop sizes (as a function of rain rate) and a shape for our models of the attenuation mechanism. We could not reasonably expect to predict such detail in any case.

We are left then with several parameters to use. The most important of these is the distribution of rain rates that we may expect in the future. If we make the assumption that the local climate is a stationary process (that is, that there are no shifts in climate) over periods of 20 or 30 years, we can use such data as have been collected by the Weather Bureau. These cover relatively long periods of time and have good reliability. The main hazard is the inherent large variability in the weather from year to year. A conservative approach is indicated.

The data provided by experimenters, while much more applicable than that of the Weather Bureau, has the drawback that it covers only short periods of time. The year-to-year variability in the rainfall amounts and rates is such that periods on the order of a year only provide confidence to the level of many hours in a year, rather than the 5-minute to 1-hour level required by systems designers. Furthermore, most of the experiments have been designed to enhance our knowledge of the attenuation process, rather than to characterize a locale for long-term predictions. However, these data are useful in determining the relation of path length to rain rate.

4.3 Available Measurements and Experiments

Typical of the data available from the National Weather Service is the paper entitled "Five-to-60 Minute Precipitation Frequency for the Eastern and Central United States" (ref. 6). This paper presents an analysis of data collected from over 2,000 rain gauges in the United States. Figure 4-1 shows a presentation of the 2-year, 60-minute data. The interpretation of the contours is as follows. The value given for each contour line is the amount of precipitation (liquid water equivalent) that will fall in "t" minutes (60 minutes in the Figure) on the average every N_t years (2 years in the Figure). The rain rate implied is merely 60/t times the precipitation amount. This rate will be equalled or exceeded for "t" consecutive minutes on the average every N_0 years. The 5-minute values are of particular interest since 0.001 percent of a year is about 5.3 minutes.
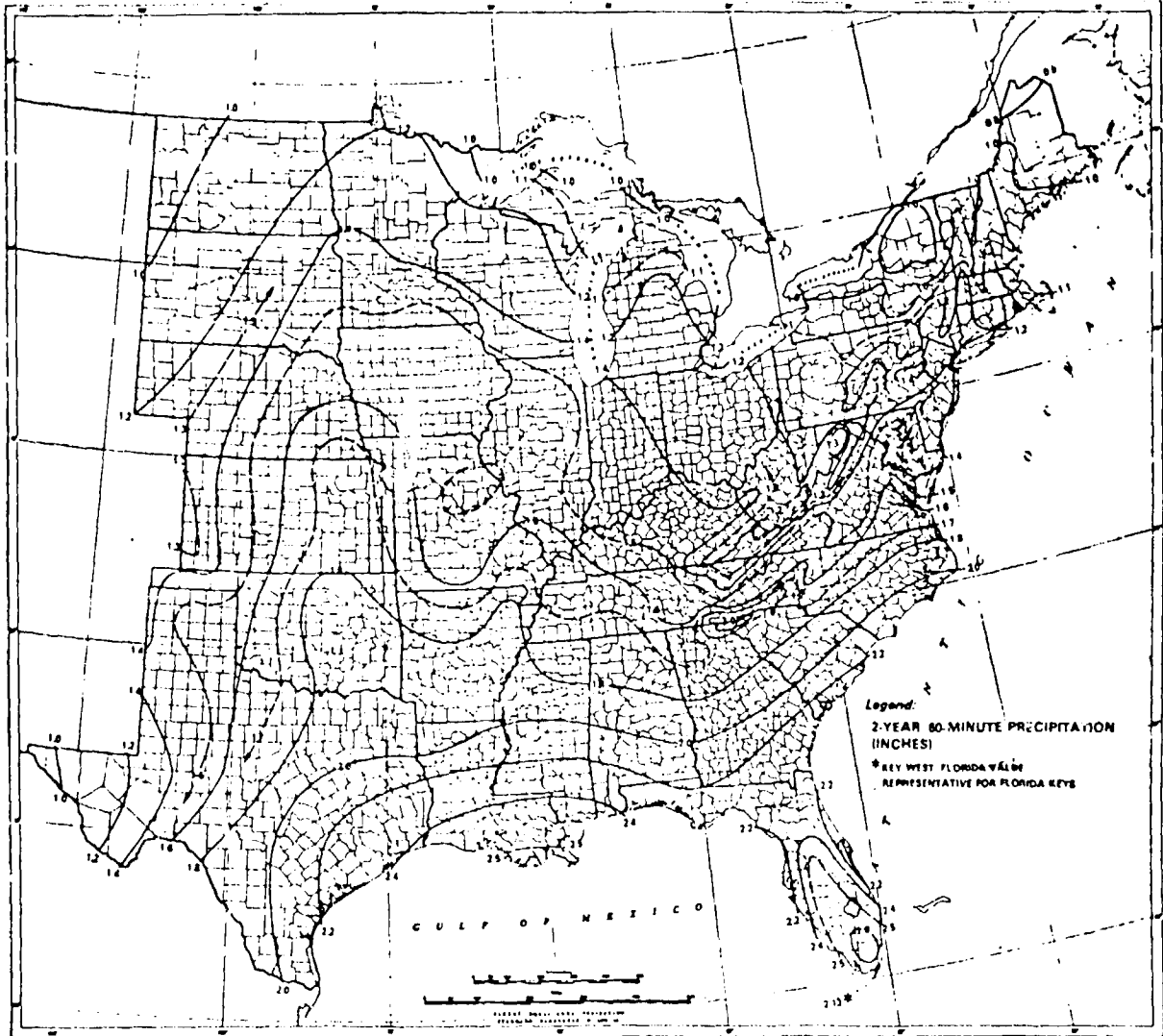
Figure 4.--2-year 60-min precipitation (inches)--adjusted to partial duration series.

Figure 4-1

Source: NOAA/National Weather Service (ref. 6)

A study by the FAA entitled "Rain Attenuation Study for 15 GHz Relay Design" (ref. 7) is also of interest. The authors of this report have expended substantial effort on the analysis of storm patterns in the United States. A number of charts and tables of data that are relevant to more elaborate models are also represented in the study report. An interesting example is presented in Figures 4-2 and 4-3. The map shows the 5-minute rainfall rate to be expected, on the average, once in 2 years, or about 2.5 minutes a year. Figure 4-3 then presents approximate curves to be used with the map giving the precipitation distributions as a function of rain rate. The proper curve from the family is selected by the 5-minute, 2-year rainfall rate, as read from the map.

Bell Telephone Laboratories has made provisions for detailed measurements of rainfall within a limited area. In Holmdel, New Jersey, Bell Labs has erected a rain gauge field consisting of nearly 100 gauges covering an area of about 130 square kilometers. This is described in Reference 8. Freeny and Gabbe (ref. 9) present an analysis of data taken from this rain gauge network during storms. Due to the detail with which the rain storms could be observed, this data is quite useful for examining the possibility of diversity operations. The spatial extent and movement of storms were also examined in some detail. The rainstorm data were non-stationary, and no attempts to fit a known distribution to the data were successful.

The data reports for the ATS-6 Millimeter Wave Experiment (ref. 10) contain some climate data. The report from the University of Texas, particularly, has some interesting examinations of thunderstorm data for Central Texas. Table 4-1 shows thunderstorm statistics for Central Texas as presented in the report. A fairly good correlation between the attenuation and the height of the cloud tops (as indicated by radar) was also found. This is shown in Figure 4-4.
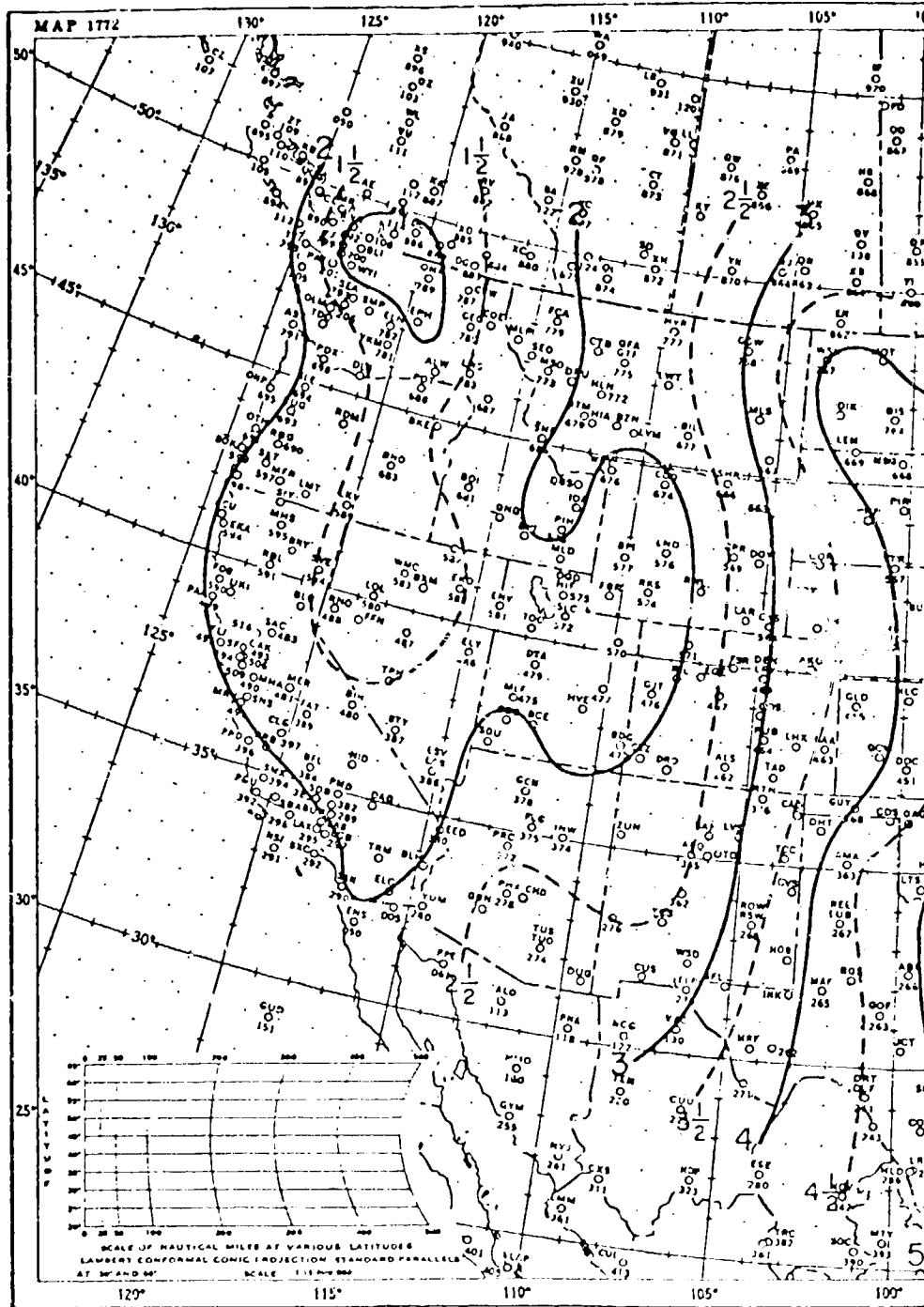
Figure 4-2a

CONTOURS OF 5-MINUTE RAIN RATES WITH
A TWO YEAR RETURN PERIOD

Source: Rain Attenuation Study for
15 GHz Relay Design (ref. 7)

A-23
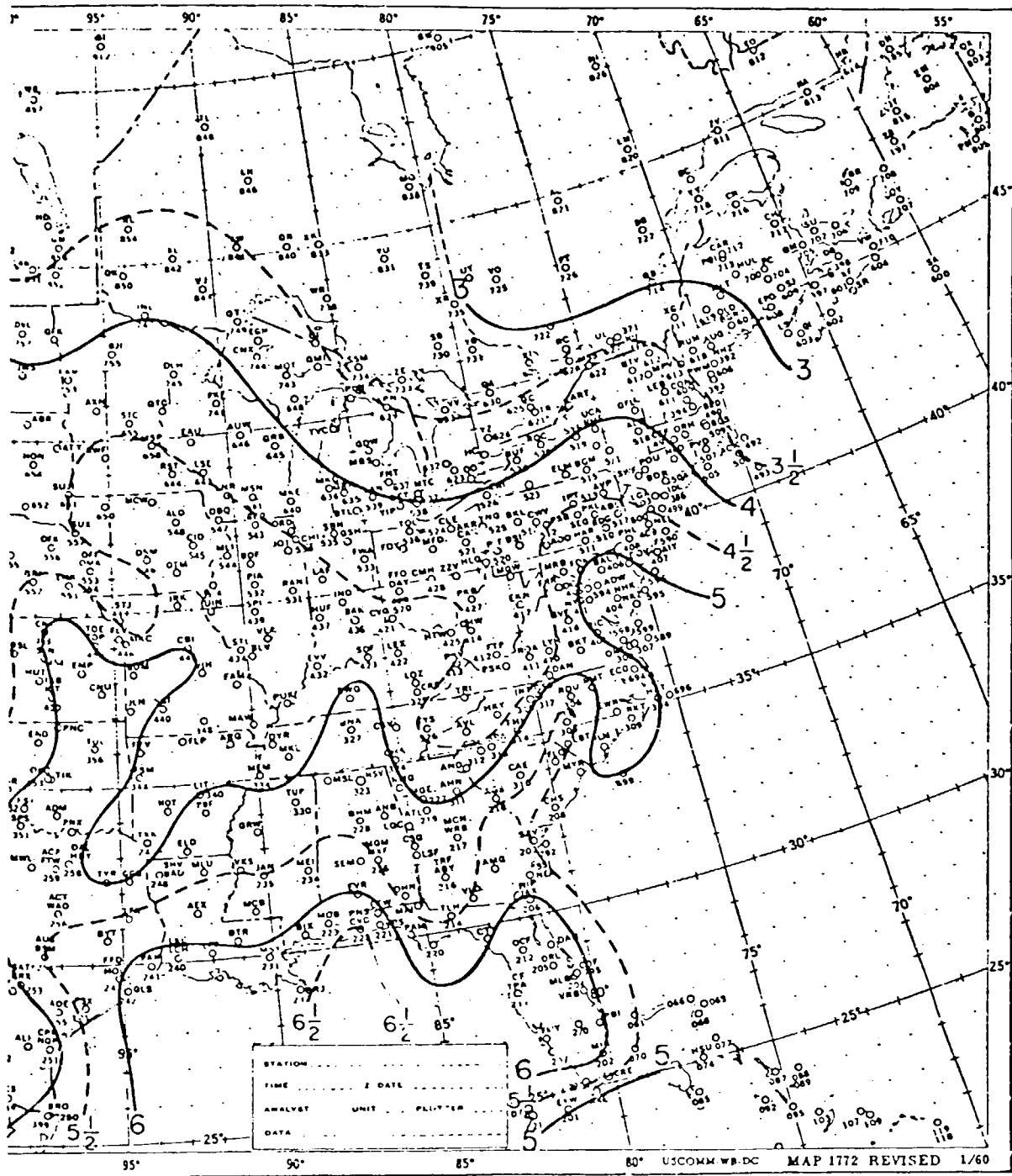
Figure 4-2b

Figure 4-3

CUMULATIVE DISTRIBUTIONS OF PRECIPITATION RATES – AFTER BUSSEY
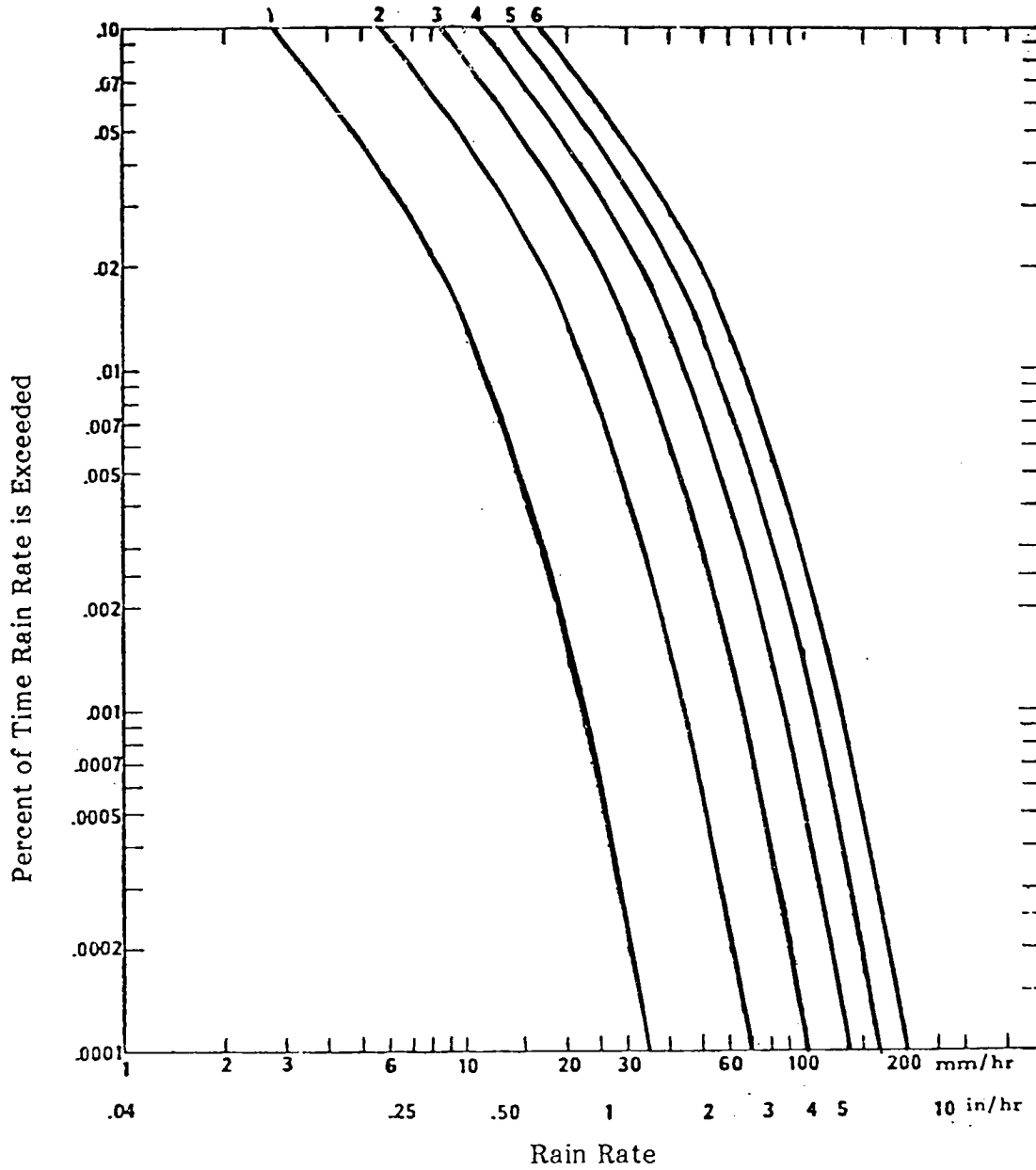
Source: Rain Attenuation Study for
15 GHz Relay Design (ref. 7)
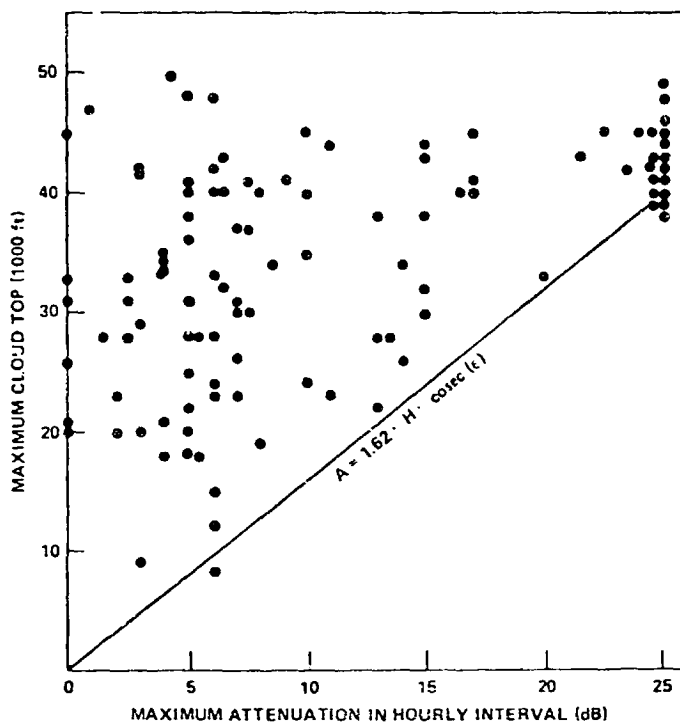
Figure 13. Cloud top height versus attenuation at 30 GHz (1 ft = 0.304 m).

Figure 4-4

Source: 20 & 30 GHz Millimeter Wave Experiments
with the ATS-6 Satellite (ref. 10)

Table 4-1

Thunderstorm Statistics for Central Texas

Month	Frequency of Occurrence	Height of Cloud Tops meters (ft)	Cell Speed m/s (knots)	Direction of Movement degrees
January	1	8.51 (28)	12.8 (25)	240
February	2	9.12 (30)	15.4 (30)	250
March	3	11.55 (38)	17.9 (35)	270
April	5	12.16 (40)	15.4 (30)	250
May	7	12.76 (42)	12.8 (25)	240
June	4	10.64 (35)	10.3 (20)	180
July	4	9.72 (32)	7.7 (15)	170
August	5	9.72 (32)	7.7 (15)	150
September	4	12.16 (40)	12.8 (25)	230
October	3	11.55 (38)	12.8 (25)	230
November	2	9.12 (30)	12.8 (25)	240
December	1	8.51 (28)	12.8 (25)	240

The COMSAT Propagation Experiment using ATS-6 (ref. 11) also produced a considerable amount of rain rate data. The rain gauges used were of the tipping-bucket type and recorded each 0.01 inch of rain. A single point gauge was installed at each site in the experiment, as follows:

Location	Location
Andover, ME COMSAT Earth Station	Boston, MA Waltham
Detroit, MI Selfridge Air Force Base	Boston, MA Sudbury
Philadelphia, PA McGuire Air Force Base	Boston, MA Cambridge
Washington, D.C. Clarksburg, MD	Boston, MA Marlboro
Wallops Island, VA Burton's Cave	Columbus, OH Mechanicsburg
Nashville, TN Fort Campbell	Columbus, OH London
Asheville, NC Fort Bragg	Columbus, OH Scientific Advances, Inc.
Fayetteville, NC Rosmann NASA Station	Columbus, OH Ohio State University
Atlanta, GA Georgia Tech	Starkville, MS Mathiston
New Orleans, LA NASA Michoud Missile Test Facility	Starkville, MS Adaton
Tampa, FL MacDill Air Force Base	Starkville, MS Mississippi State University
Miami, FL Homestead Air Force Base	Starkville, MS Sessums

Table 4-2 shows a comparison of the total rain amounts collected by the COMSAT experiment with the average expected amounts taken from Weather Service data. As a first approximation, the Weather Service amounts were scaled by the fraction of the full year that the COMSAT experiment took data for each location. A further refinement is possible since the COMSAT data are available on a seasonal basis, as are the Weather Service data.

From the Table one can see that several of the sites were in marked disagreement with the average data. There are several possible sources for the discrepancy:

1) Errors in the rain gauges or the data reduction process

2) Errors in the average rainfall values due to the low density of rain gauges operated by the Weather Service in a particular locale. It has been observed that the heavy rains responsible for much of the rainfall in thunderstorms are highly localized.

3) Errors due to the high variability of the local climate itself from year to year

The data reduction was done manually, and with such a large quantity of data the possible errors are many. However, the other reasons noted above are far from insignificant. In addition, the cumulative distribution curves of some sites with large total errors look quite reasonable, which would likely not be so had some large bias been inserted during processing. Figures 4-5 and 4-6 show this quite well for the Tampa and Boston #2 sites, while in Figure 4-7, the data for the Detroit location which has a smaller error in total rainfall, clearly has some sort of problem at the high rain rates.

Table 4-2

ATSF Propagation Experiment

Total Rainfall From May 19, 1974 to May 31, 1975

Site	Rain (mm)[1]	Total Data (Hours)[2]	Percent of Year Data Collected	Average Expected Rainfall (mm)[3]	Percent Differences Between Data and Expected Rainfall
Boston #2	508.1	7115.0	81	875	-42
Columbus #3	651.8	7999.0	91	855	-24
Starkville #4	843.2	6366.2	73	912	-8
Miami #5	63.0	4413.5	50	759	-92
Ithaca #6	98.5	1943.5	22	186	-47
Detroit #7	117.1	1948.2	22	173	-32
Andover #8	0.0	0.0	0	0	0
Philadelphia #9	12.4	453.7	5	51	-76
Washington #10	391.8	3651.7	42	415	-6
Nashville #11	619.0	4562.9	52	608	+2
Asheville #12	0.0	48.0	0	0	0
Fayettesville #13	761.0	5354.1	61	658	+16
New Orleans #14	813.3	6026.7	69	995	-18
Atlanta #15	289.7	641.5	7	86	+236
Tampa #16	352.4	6058.0	69	1030	-66
Boston #17	0.0	0.0	0	0	0
Boston #18	750.3	7835.7	89	961	-22
Boston #19	405.0	6219.5	71	767	-47
Wallops Island #20	326.8	5145.9	59	670	-51
Columbus #21	594.9	6667.3	76	714	-17
Columbus #22	508.8	7199.6	82	771	-34
Columbus #23	88.4	4289.5	49	460	-81
Starkville #24	423.3	2048.6	23	287	+47
Starkville #25	482.2	3270.0	37	462	+4
Starkville #26	636.3	3988.5	46	575	+11

Notes:

1) Total rainfall indicated by the gauge at each site

2) Number of hours data were taken at each site

3) Average Weather Service figures for annual rainfall scaled to the fraction of 1 year for which data were taken

Figure 4-5
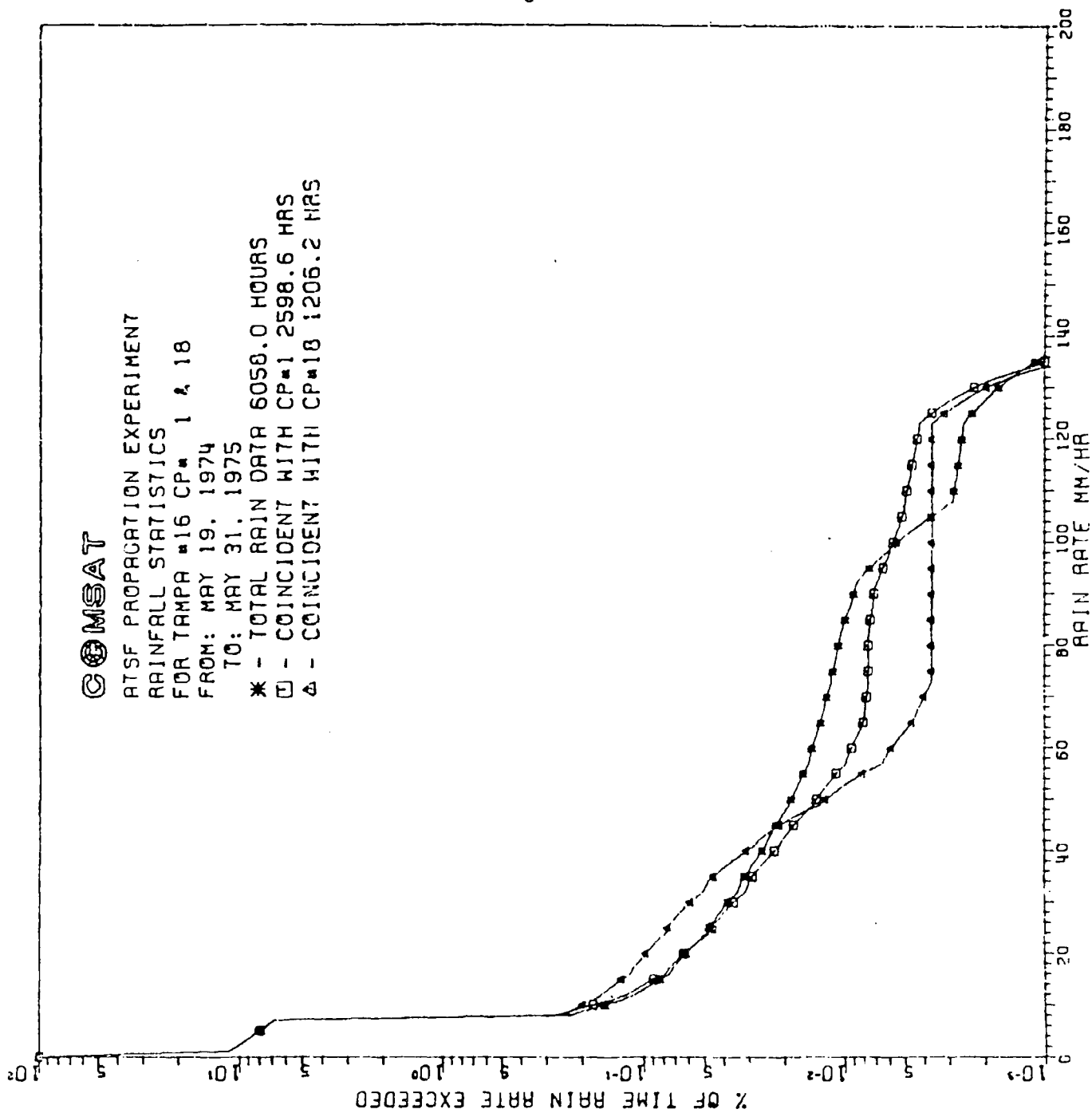
Source: Data Analysis Report on COMSAT ATS-F
Propagation Experiment (ref. 11)

Figure 4-6
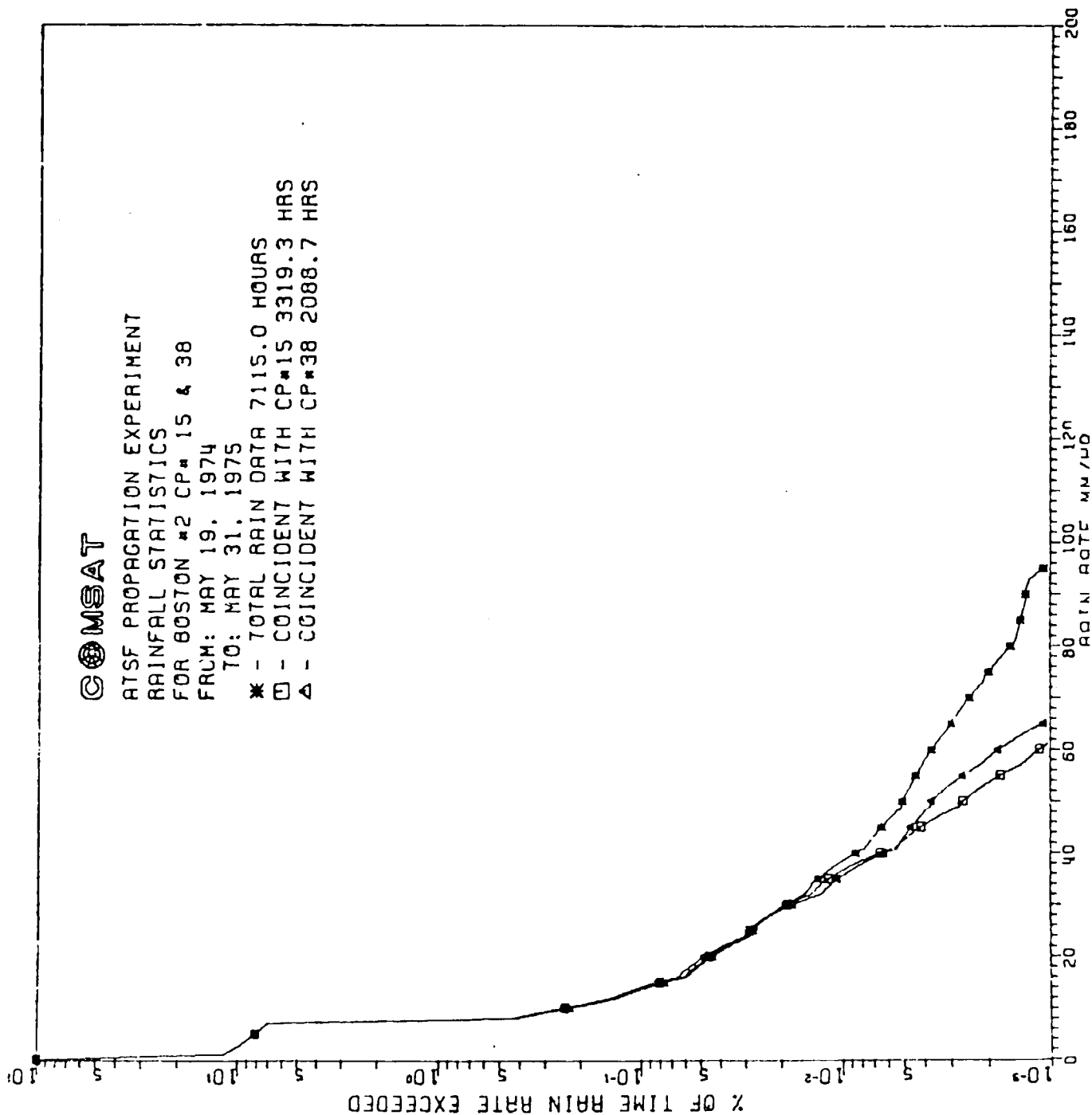
Source: Data Analysis Report on COMSAT ATS-F
Propagation Experiment (ref. 11)

Figure 4-7
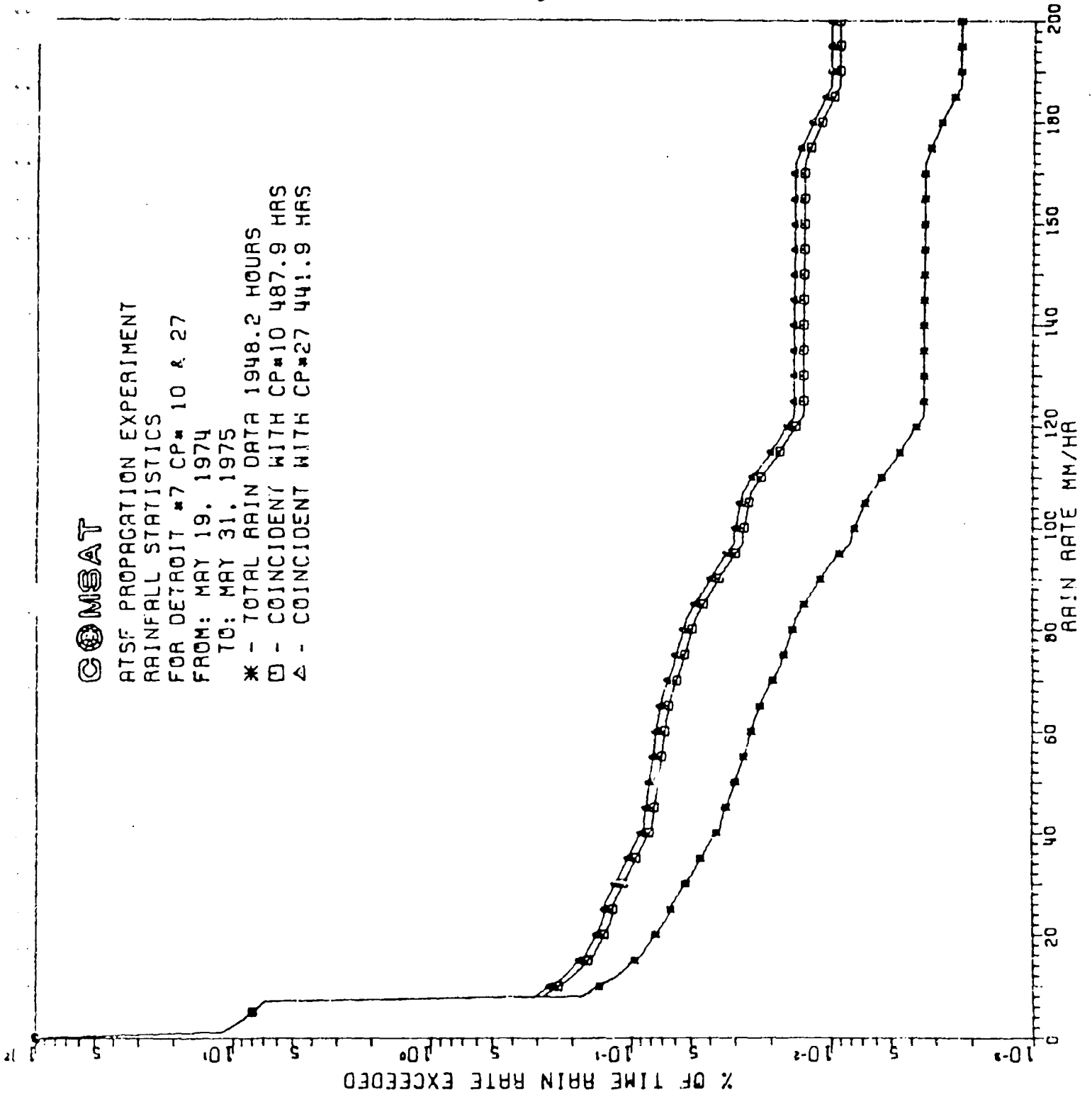
Source: Data Analysis Report on COMSAT ATS-F
Propagation Experiment (ref. 11)

On balance, the best approach is to use the Weather Service data as the primary basis for modeling the frequency of precipitation and its rate. The data from the various experiments is a useful adjunct and can best be used to enhance the model of storm cells and path lengths through rainstorms. It should be borne in mind, however, that even the Weather Service data, which covers about 25 years, is not proof against the variability of the local climate. The systems designer should choose conservative margins whenever possible to guard against this and against the inaccuracies inherent in the modeling process.

4.4   Climatological Models for CONUS

Several models have been formulated to approximate the climate in the contiguous U.S. These are also applicable to other regions due to their general nature. It is our judgement that the model due to Rice and Holmberg (ref. 12) is the most accurate one currently available. It has the advantage of modeling well the mixture of rain types found in the U.S. It is also reasonably accurate at the low percentages of time that are of interest to satellite systems designers. A detailed examination of this model will be instructive.

The statistical model by Rice and Holmberg is the sum of two individual exponential modes of rainfall rates, each having a characteristic average rate rainfall thus described by:

Rainfall = Mode 1 Rain + Mode 2 Rain

The exponential distribution that was chosen to describe mode 1 rain is based on an analysis of thunderstorms. Mode 2 rain is all other rain. In temperate climates only convective storms associated with strong updrafts and thunder can produce the high rainfall rates identified by mode 1. The average annual rainfall depth M is the sum of the contributions from the two modes:

$$M = M_1 + M_2$$

The ratio of thunderstorm rain to total rain is defined as:

$$\beta = M_1/M_2$$

The number of hours of rainy periods for which the surface point rainfall rate R is exceeded is the sum of contributions from the two modes. These relationships are shown in Figure 4-8.
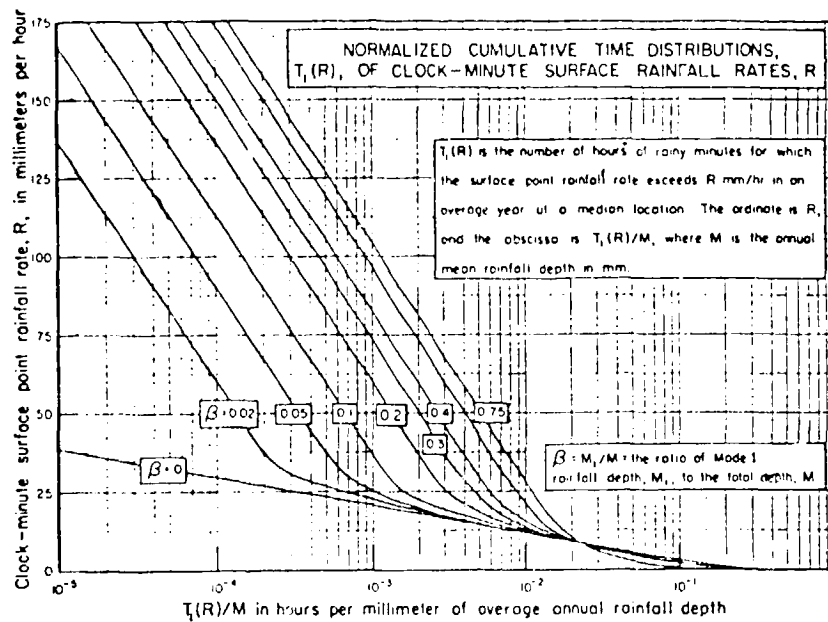
Fig. 1. Normalized cumulative time distributions.

Figure 4-8

Source: Rice and Holmberg: Statistics of
Rainfall Rates (ref. 12)

Figures 4-9 and 4-10 are maps of M and β .

A-35

Figure 4-9

Inches → mm	
0	0
10	250
20	500
40	1000
80	2000
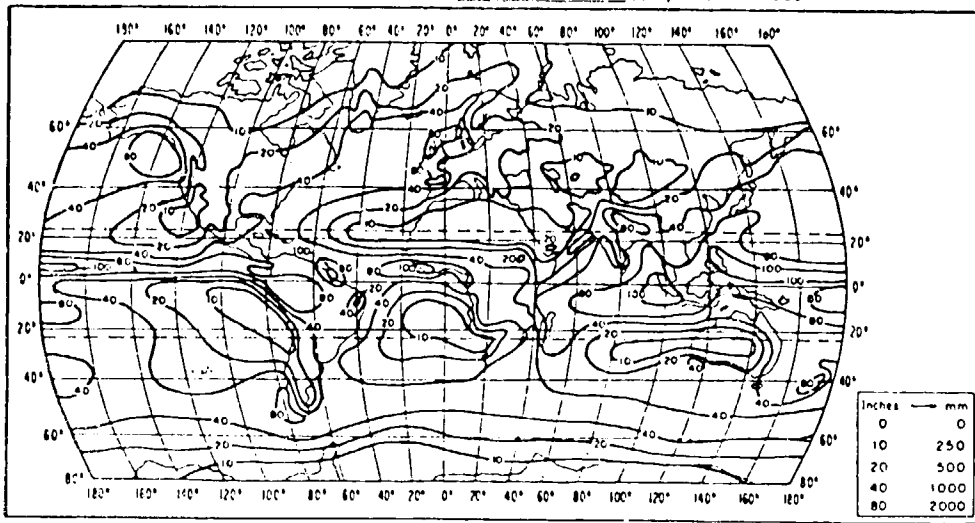
Fig. 2. Mean annual precipitation in inches (equal to $M/25.4$).

Source: Rice and Holmberg: Statistics of
Rainfall Rates (ref. 12)

Figure 4-10
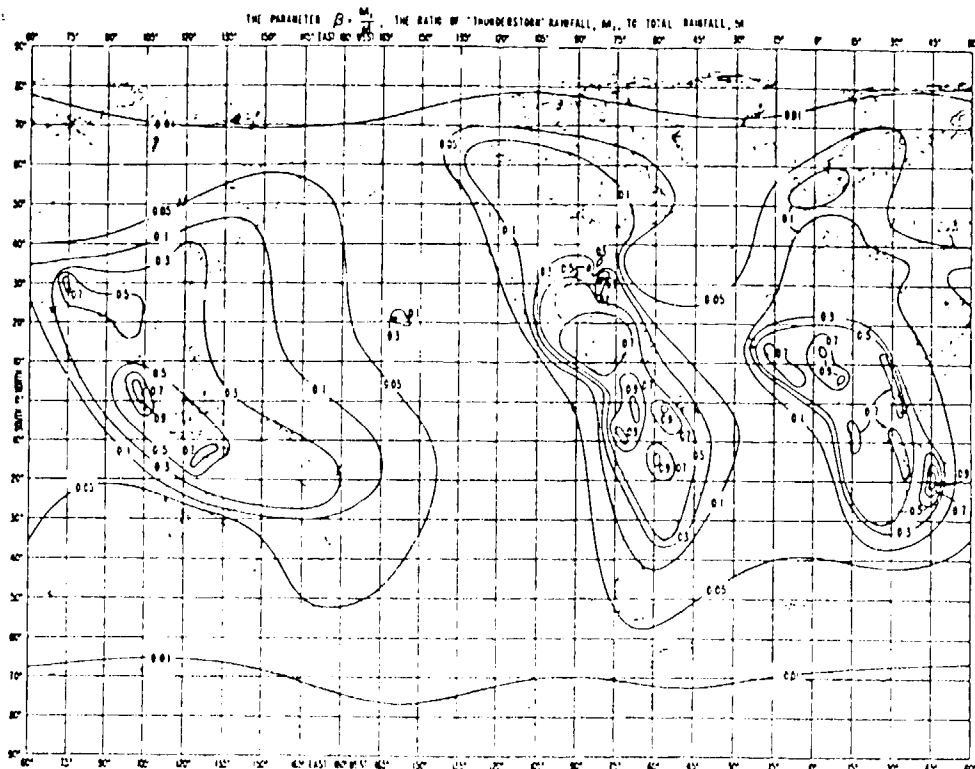
Fig. 3. The parameter β.

Source: Rice and Holmberg: Statistics of
Rainfall Rates (ref. 12)

Figure 4-11 shows the average year cumulative distributions for the annual rainfall rate of 40 inches and thunderstorm rain representing 12.5 percent of the total rain.
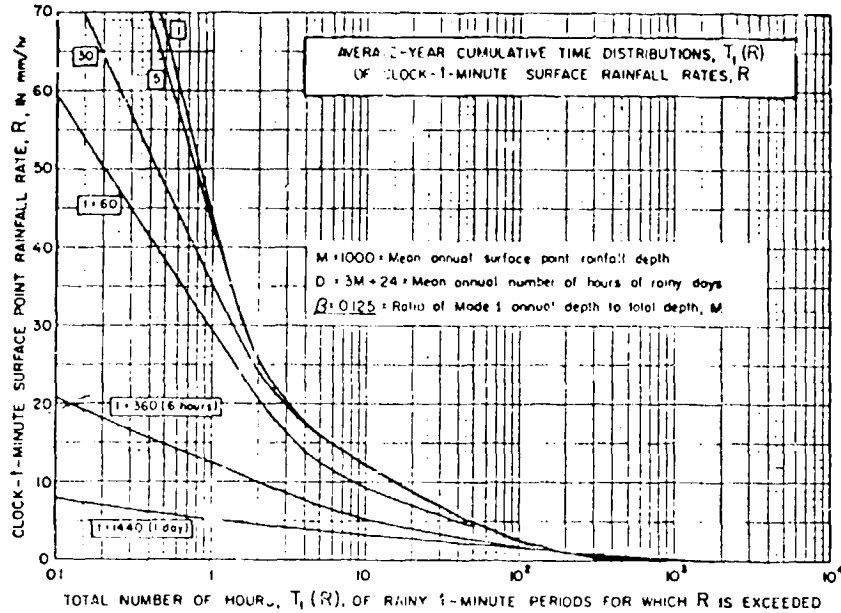
Fig. 4 Average year cumulative time distributions $T_t(R)$.

Figure 4-11

Source: Rice and Holmberg: Statistics of
Rainfall Rates (ref. 12)

Table 4-3 shows a comparison of the Rice and Holmberg prediction for Starkville, Mississippi with the COMSAT ATS-6 rain rate data for the four sites at Starkville. The parameters used in the R-H model were M = 1250 mm/year and beta = 0.4. The agreement is rather good, save for the site #24 which also has the fewest total hours of data and the largest error in cumulative rainfall for the experiment.

Table 4-3
Comparison of Rice and Holmberg Model With
COMSAT Data for Starkville, Mississippi

R mm/hr.	R-H Percent of Time	Site #4	Site #24	Site #25	Site #26
10	0.26	0.34	0.52	0.37	0.48
20	0.10	0.15	0.20	0.10	0.17
50	0.04	0.05	0.06	0.038	0.04
100	0.035	0.009	0.013	0.007	0.003
150	0.002	0.001	0.001	0.0004	0

Tables 4-4 through 4-8 present similar results for the five other sites in the COMSAT experiment which had an error in the total rainfall of less than 20 percent. In several of the cases the agreement with the Rice and Holmberg model is good.

Table 4-4
Cumulative Time Distributions of Rainfall Rates
For Washington

Rainfall Rate (mm/hr.)	Rice-Holmberg Model (Percent of Time)	ATS-6 COMSAT Data (Percent of Time)
10	0.18	0.29
20	0.039	0.088
50	0.011	0.025
100	0.0025	0.005
150	0.0006	0.001

Table 4-5
Cumulative Time Distributions of Rainfall Rates
for Nashville

Rainfall Rate (mm/hr.)	Rice-Holmberg Model (Percent of Time)	ATS-6 COMSAT Data (Percent of Time)
10	0.23	0.41
20	0.077	0.12
50	0.027	0.039
100	0.006	0.004
150	0.0013	0.0008

Table 4-6
Cumulative Time Distributions of Rainfall Rates
for Fayetteville

Rainfall Rate (mm/hr.)	Rice-Holmberg Model (Percent of Time)	ATS-6 COMSAT Data (Percent of Time)
10	0.21	0.37
20	0.061	0.14
50	0.021	0.037
100	0.005	0.007
150	0.001	0.002

Table 4-7

Cumulative Time Distributions of Rainfall Rates
for New Orleans

Rainfall (mm/hr.)	Rice-Holmberg Model (Percent of Time)	ATS-6 COMSAT Data (Percent of Time)
10	0.31	0.37
20	0.14	0.15
50	0.055	0.05
100	0.012	0.009
150	0.0027	0.003

Table 4-8

Cumulative Time Distributions of Rainfall Rates
for Columbus #21

Rainfall (mm/hr.)	Rice-Holmberg Model (Percent of Time)	ATS-6 COMSAT Data (Percent of Time)
10	0.18	0.25
20	0.045	0.055
50	0.014	0.011
100	0.003	0.0015
150	0.0007	0.0003

4.5   Modeling the Effective Path Length

As noted previously, the models for precipitation and attenuation given so far yield a value for specific attenuation only. In order to find the total attenuation produced by a given rain rate, it is necessary to have a model for the length of the path through the precipitation. This is generally held to be a function of rain rate itself and of the elevation angle to the satellite. The logic of this is as follows. The dependence on rain rate stems from the fact that the low rain rates are the product of a storm system that is large in physical extent. The low rain rates are to be found throughout the storm system. Thus the path will traverse the area of precipitation through much of its length near the earth. The high rain rates are the products of much smaller storm cells which have height comparable to their horizontal extent. The section of the path that lies within the area of precipitation will thus be shorter.

The dependence on the elevation angle is quite natural. In general, because of the relative dimensions of low and high rain rate storm cells, the dependence on elevation angle will decrease as the rain rate increases.

The effective path length can be modeled based on the results of experiment. Several such models are available in the literature. Two general procedures are used for such models. In one, the statistical distributions of attenuation as measured at the site and the statistical distributions of rainfall rate as measured at the same location are assumed to be equivalent. In other words, a rainfall rate that occurs "p" percent of the time is assumed to cause the attenuation that also occurs "p" percent of the time. From this equivalence and the theoretical formula for the specific attenuation, the effective path length as a function of rain rate can be derived. The main drawbacks of this method are: 1) the resulting expression for path length generally displays a strong dependence on frequency, and this is not realistic, and 2) the statistics must be collected over a substantial period of time (on the order of a year or more) before the distributions can be considered to be representative. The latter is due to the poor correlation between point rain gauge data and attenuation at the same location.

The second method, which displays a substantial degree of frequency independence, requires simultaneous measurements at two or more frequencies. The ratio of attenuation at two frequencies is determined for each instant, and the composite ratio function is determined statistically in the form:

$$A_{F1} = xA_{F2}{}^y$$

Since this is the same form that the relationship for specific attenuation takes, the two can be combined to yield an expression for the effective path length that depends only on the rain rate. This procedure is explained in detail in Reference 13.

Of course refinements can be added to either model, such as a dependence on the earth station elevation angle or the height of the melting layer, below which the precipitation is in liquid form, this producing the bulk of the attenuation.

Several experimenters have determined such functions for the effective path length. This has been done for ATS-5 data by Ippolito and for COMSAT data from the Comstar beacon by Harris and Hyde (ref. 13). The curve from Ippolito is shown in Figure 4-12 and that of Harris and Hyde in Figure 4-13. Elevation angles are about 47 degrees for the ATS-5 data and 20 degrees for the Comstar beacon data. Effective path lengths for thunderstorm type rain (rain rate about 40 mm/hr. or higher) range from 5 to less than 2 km. The empirical formulae for these curves are:

$$L = 67.6 \ R^{-0.7887} \qquad \text{for the ATS-5 data}$$
$$L = 2.6 \ R^{-0.1} \qquad \text{for the Comstar data}$$

The curve marked "A" in Figure 4-12 is computed from data given in Figure 8 of Reference 33. As can be seen from the Figure, it lies quite close to the ATS-5 data.
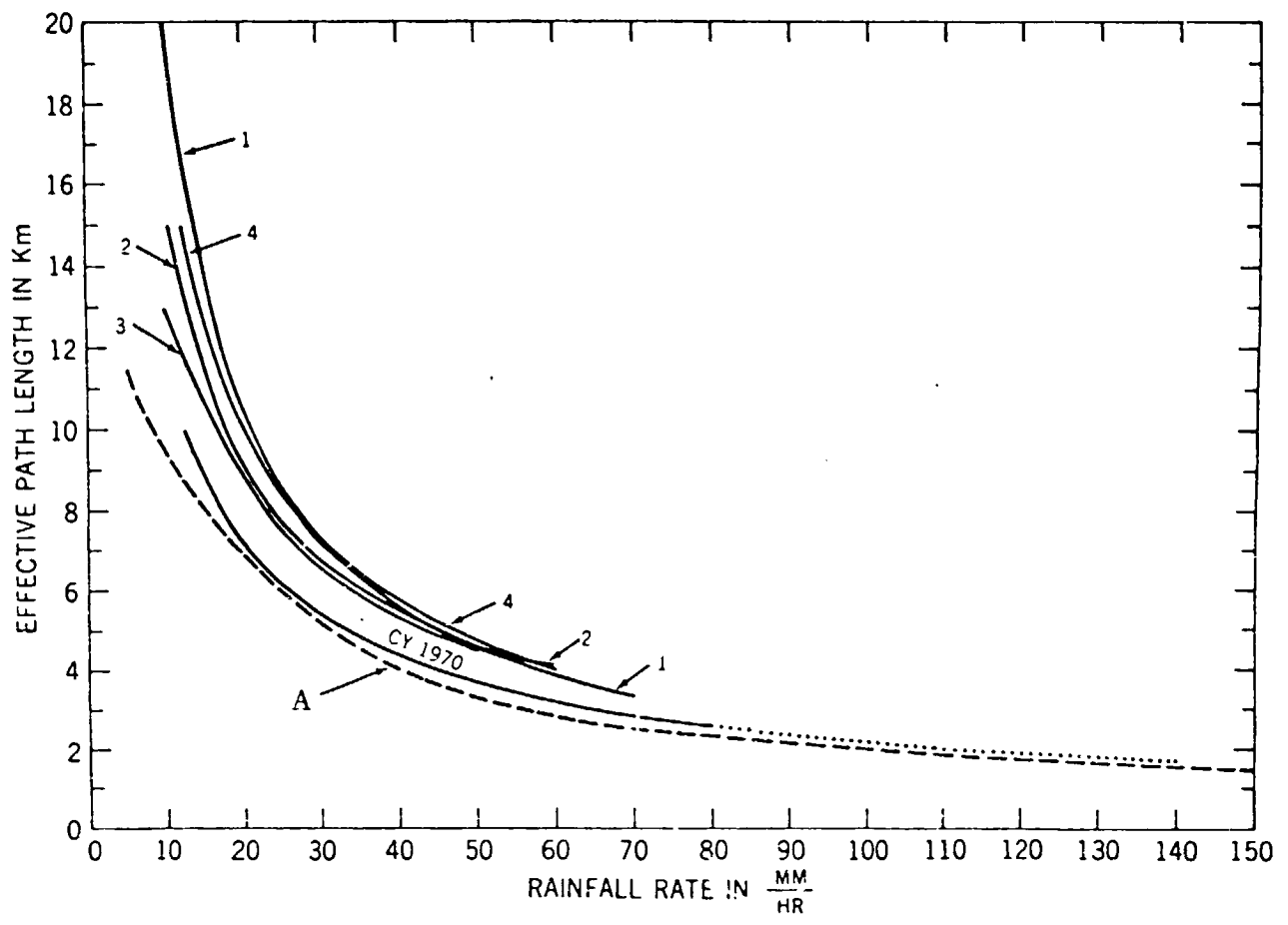
Figure 4-12

EFFECTIVE PATH LENGTH VERSUS RAIN RATE

Figure 4-13
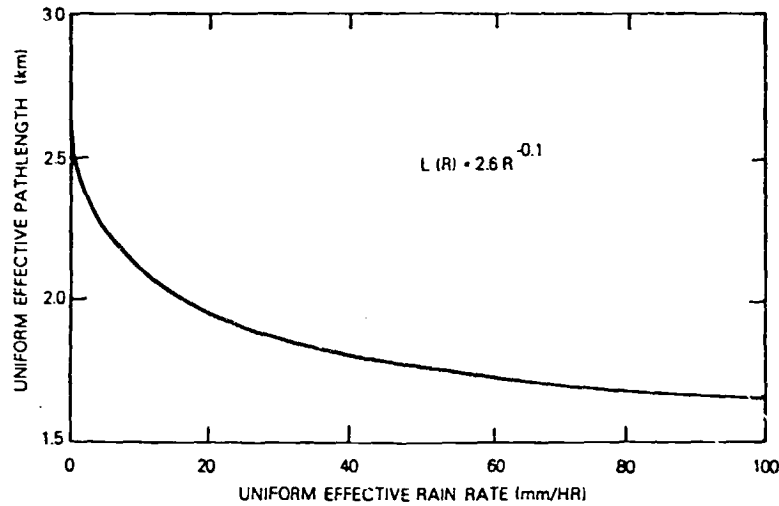
Figure 10. *Variation of Uniform Effective Path Length with Uniform Effective Rain Rate*

Source: (ref. 13)

Table 4-9 shows the composite correlation of 13 and 18 GHz fading for seven of the ATS-6 transmitting sites in the COMSAT Propagation Experiment. The relation between 13 GHz fading and 18 GHz fading from these data (best fit) is:

$$A_{18} = 1.889 \ A_{13}^{0.934}$$

Using the theoretical values from Olsen, et. al. (ref. 4), we derive the following expression for the path length as a function of rain rate:

$$L(R) = 2.74 \ R^{-0.487}$$

Table 4-9

Composite Correlation of 13 & 18 GHz Attenuation
(Attenuation in dB)

13 GHz Attenuation	Mean of 18 GHz Attenuation	Standard Deviation of 18 GHz Attenuation
1	2.350	1.757
2	3.336	1.497
3	4.562	1.819
4	6.189	2.109
5	7.713	2.439
6	9.721	2.481
7	12.300	3.200
8	13.709	2.654
9	15.086	2.905
10	16.217	2.602
11	17.082	2.654
12	19.304	3.413
13	20.477	2.935
14	22.209	3.708
15	28.125	1.166
16	26.226	3.118
17	29.667	0.472
18	24.143	0.833

Sites not considered are 5, 7, 8, 9 and 12.

Source: Data Analysis Report on COMSAT ATS-F Propagation Experiment

CCIR Document F5/003 presents a method for calculating attenuation distributions which incorporates most of the possible features described above. An explicit expression for the path average rain rate as a function of the point rain rate is also included. The expression for the attenuation is as follows:

$$A = \frac{H}{\sin\theta} \; a(f) \, \gamma(D) \; R_p^{\left[b(f) - \delta(D)\right]}$$

where

A	=	Attenuation in dB
H	=	Height of the 0°C isotherm (Figure 4-14)
θ	=	Earth station elevation angle
D	=	$\dfrac{H}{\tan\theta}$

a(f) b(f)	Factors in the aR^b function for specific attenuation (ref. 14)
$\gamma(D)$ =	Obtained from Figure 4-15
$\delta(D)$ =	Obtained from Figure 4-16

One of the significant points about the CCIR model, aside from its completeness, is that it yields generally larger values for the effective path length than the formulas shown previously. It is apparent that, whatever their other features or merits, the aforementioned formulas are lacking in some respect.
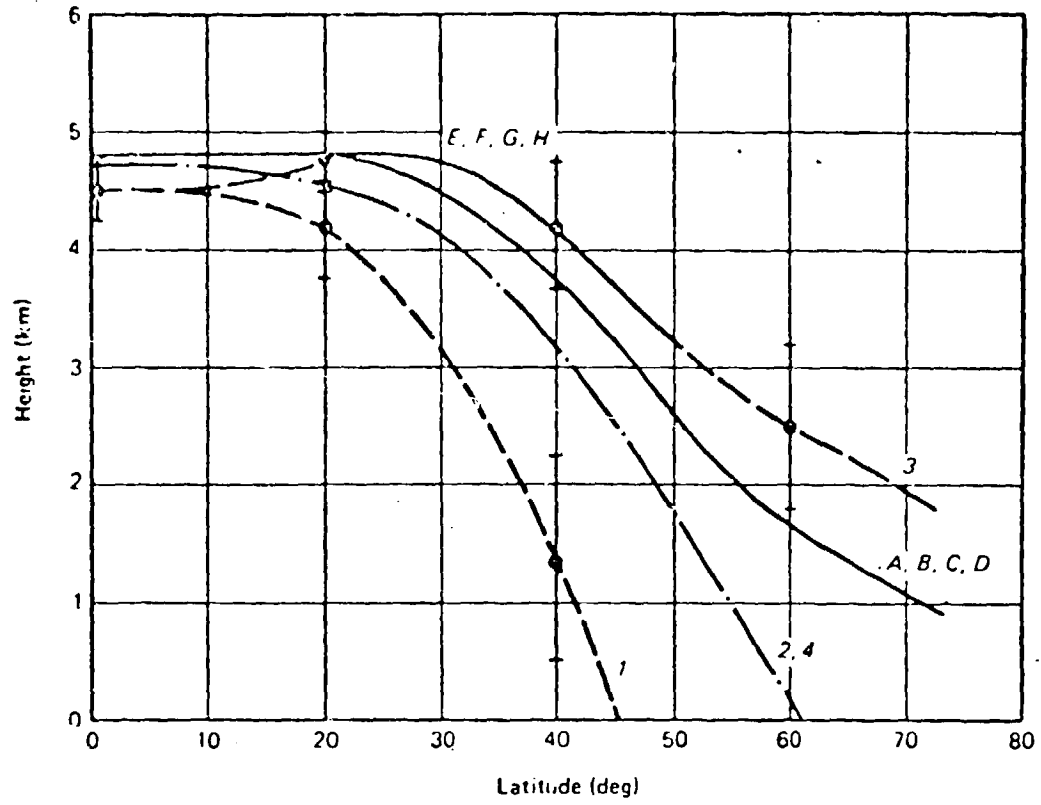
Figure 4-14 | Latitude Dependence of Zonally Averaged 0°C Isotherm Height
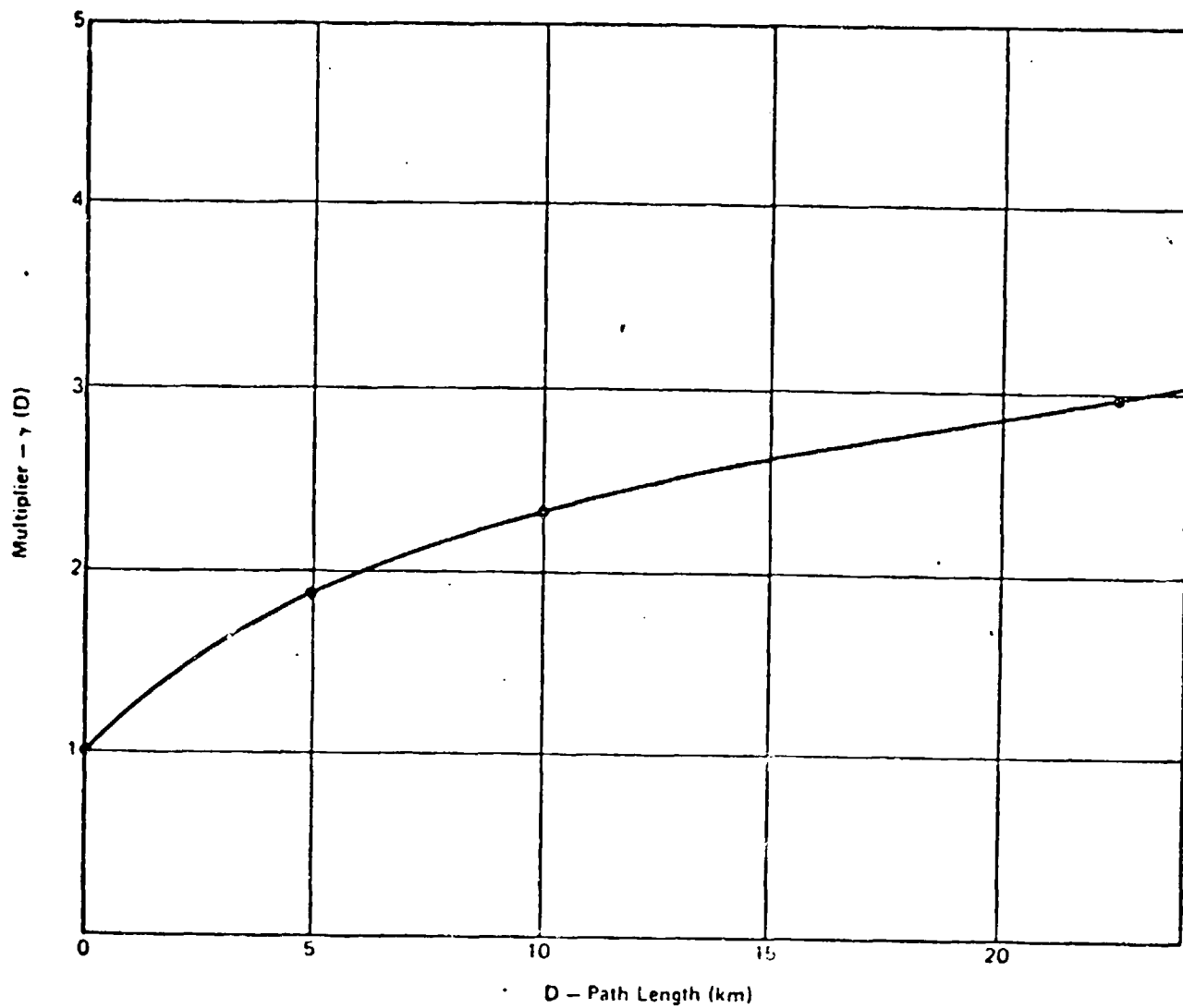
Figure 4-15 | Multiplier in Path Average Model
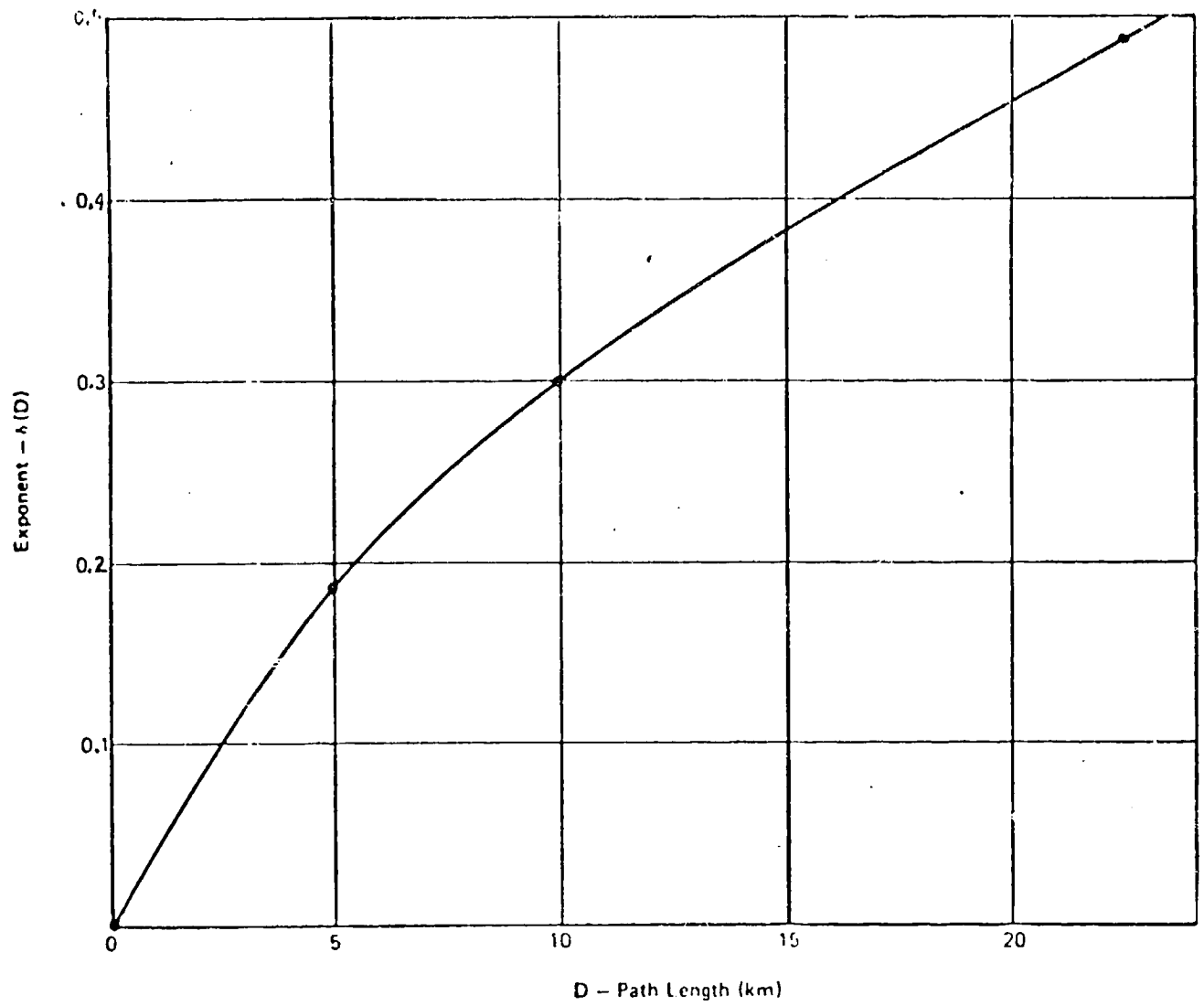
Figure 4-16   Exponent in Path Average Model

SECTION 5
MILLIMETER WAVE PROPAGATION EXPERIMENTS

5.1   Introduction

In spite of the fact that there exists a firm theoretical base for calculations of propagation effects due to hydrometeors, experiments have consistanily played a significant role. There are at least two good reasons for this: first, the well-founded scientific procedure by which theory is tested by experiment, and secondly, the fact that so many assumptions concerning the properties of rainfall must be made. The validity of such assumptions must be tested against reality.

The history of propagation experiments dates from the 1940's. Naturally, much of the effort has been devoted to the study of propagation along terrestrial microwave paths, at least until recently, Bell Laboratories and the U.S. Bureau of Standards have been significant contributors, with NASA having done a great deal of work since about 1963.

Propagation experiments can be grouped into four categories as follows:

1) Experiments using an actual point-to-point terrestrial link. Bell Labs has collected a great deal of data from such facilities.

2) Experiments using radiometers, either with fixed pointing or sun tracking. While these have been primarily intended to measure attenuation along an earth-to-satellite path, the low-angle measurements could also apply to terrestrial links.

3) Experiments using millimeter wave radars. These have had two directions generally: direct measurement of attenuation and determination of rain storm and rain cell characteristics.

WDL-TR8457

4) Experiments using satellite-borne beacons or transponders. These, of course, are the most useful since the results apply directly to the problem considered in this report.

All of the above categories include, in most cases, some form of rain measurement in addition to the attenuation measurements. Some, such as radars, are primarily aimed at an accurate determination of the characteristics of rainstorms.

It will be useful to examine the structure and results of some of the more important experiments. We have limited our interest to those specifically dealing with millimeter wave propagation.

5.2 Experiments Using Terrestrial Links

The most significant of these have been performed using the rain gauge field at Bell Laboratories in Holmdel, New Jersey. The set-up of this field was described in Section 4.

In 1967, Semplak and Turrin (ref. 14) took 18.5 GHz attenuation measurements on a 6.4 km path within the Holmdel rain gauge network. The period of measurement included the Summer of 1967 during which many very heavy showers occurred. Data were examined separately for individual storms. The composite results showed that the attenuation per unit length can be calculated as:

$$A = 0.041 \sum_i d_i R_i^{1.04}$$

In this equation R_i is the rainfall rate in millimeters per hour, and d_i is the distance in kilometers over which the rain rate R_i applies. Percent of time distributions are given for the attenuation and the duration of attenuation. It was found that the path attenuation exceeds 30 dB for 0.043 percent of the time.

Figures 5-1 and 5-2 show distributions of attenuation and rain rate resulting from this experiment.
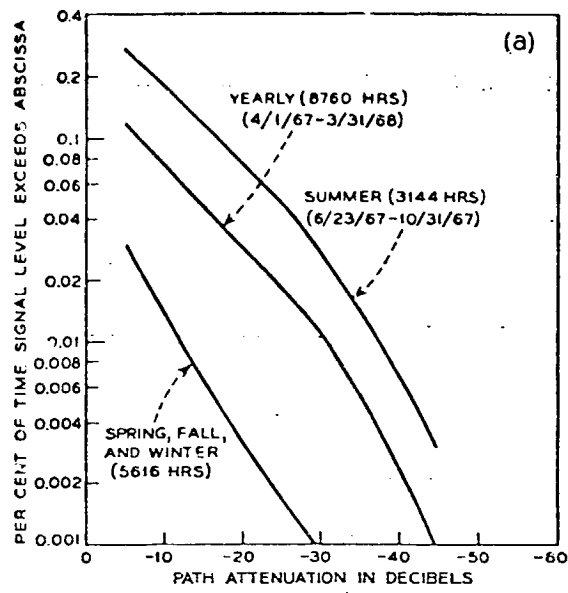
Figure 5-1
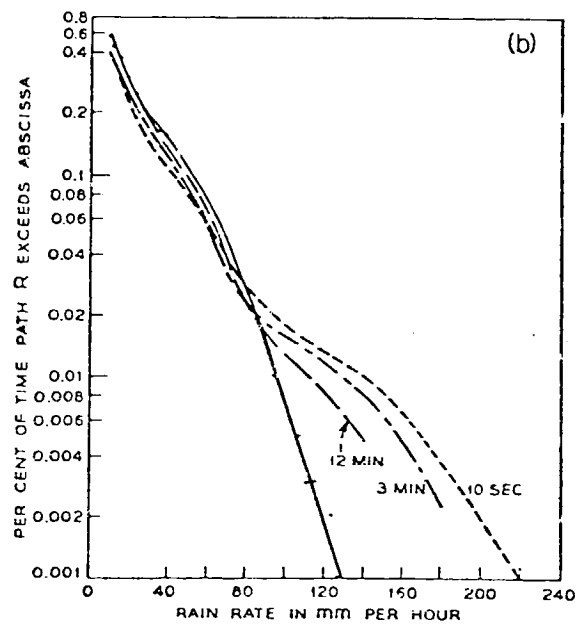
Figure 5-2

Source: (ref. 14)

5.3 Experiments Using Radiometers

Wilson (ref. 15) of Bell Labs published in 1969 the results of measurements using a sun-tracking radiometer to determine attenuation at 16 and 30 GHz. A dynamic range of about 30 dB was available. The sky temperature was used at night with a dynamic range of 10-12 dB. Figures 5-3 and 5-4 show the distribution of attenuation for 16 GHz and 30 GHz, respectively. The measurements were taken at Holmdel, New Jersey.

In 1971-1972, COMSAT Labs (ref. 16) performed propagation attenuation measurements at Utibe, Panama over a period of approximately 1 year using a 15.3 GHz transportable earth station. Attenuation data were determined with the radiometer method where the output was proportional to the sky noise temperature. The tropical site Utibe was selected because good rain statistics were available for it. The antenna was pointed at an elevation angle of 55 degrees, which corresponds with typical synchronous arc use for this location. Attenuation versus percent time was recorded, and distribution functions were plotted. It was found that 4 dB attenuation was exceeded 0.4 percent of the time and 10 dB attenuation was exceeded during 0.1 percent of the time. In addition, rain rate distribution was plotted from rainfall data obtained on an hourly basis from a nearby location. Curve fittings procedures were used to determine plots of instantaneous rain rate versus attenuation at 15.3 GHz. Good correlation was obtained between hourly rainfall and fade durations.

5.4 Experiments Using Radars

Direct observation of the specific variations in rain intensity (and hence attenuation) along a path can only be made by radar. These can also be used to study the size and behavior of intense rain cells of the sort that cause high attenuation. Such measurements have been taken by several investigators, including Crane (ref. 17), Drufuca (ref. 18) and Goldhirsh (ref. 19).
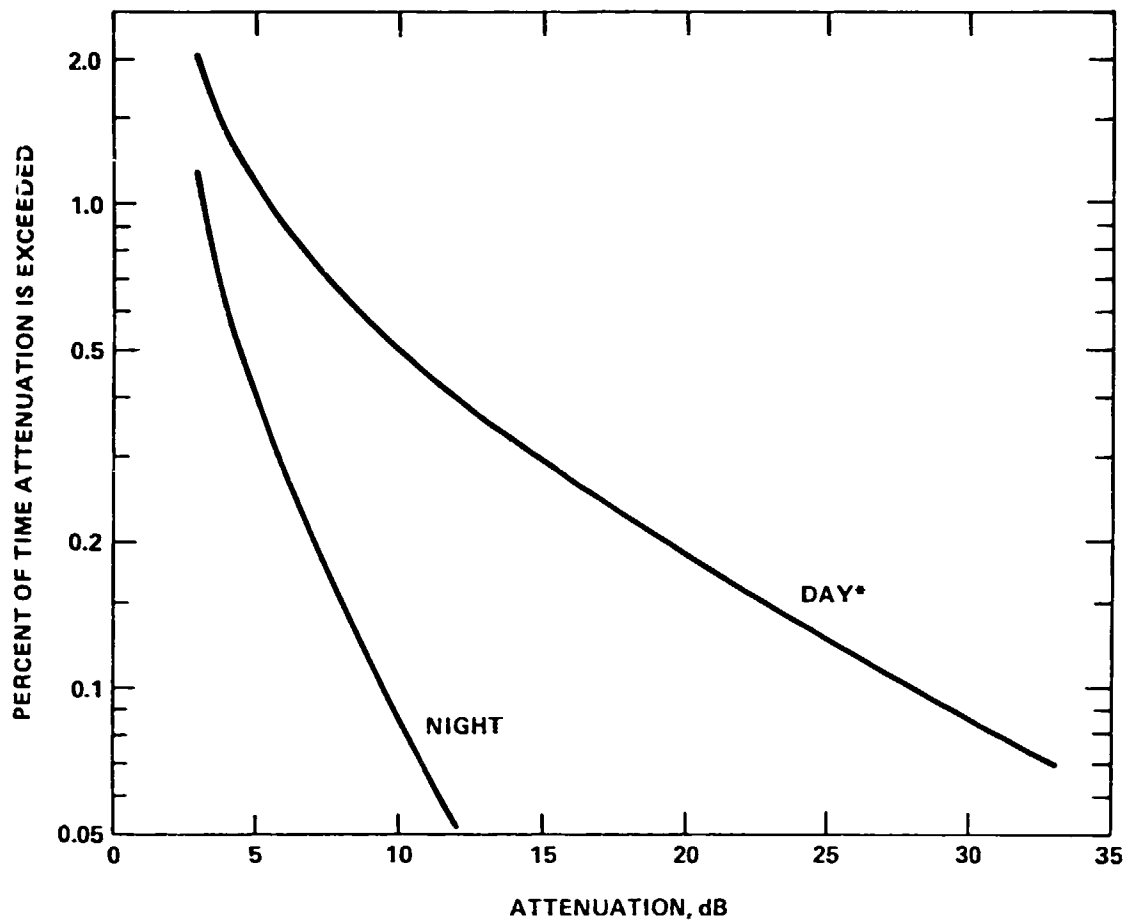
Figure 5-3

CUMULATIVE DISTRIBUTION OF ATTENUATION AT 30 GHz

(Measurements of Wilson)
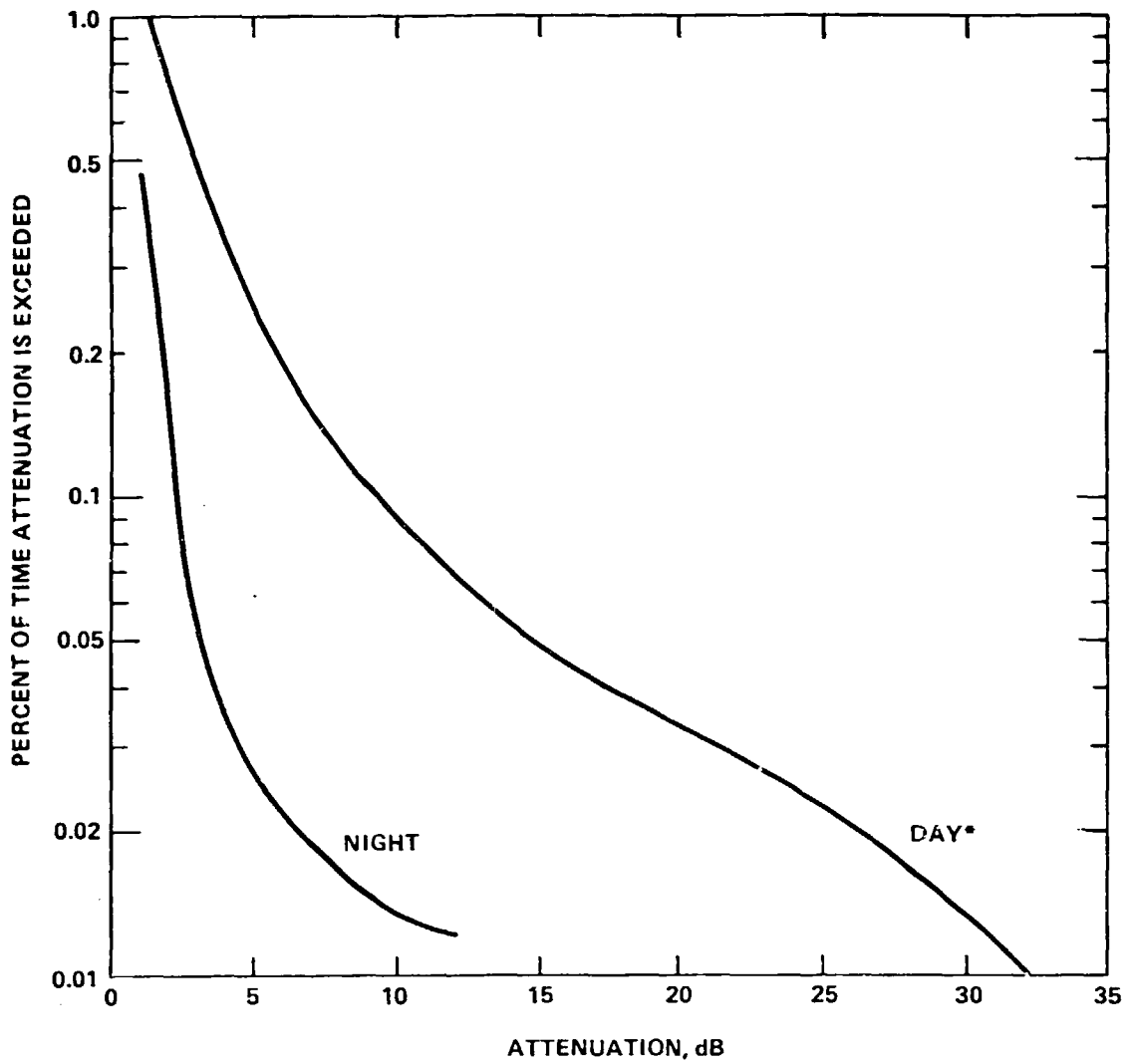
Holmdel, N. J. 12/67 to 12/68

Figure 5-4

CUMULATIVE DISTRIBUTION OF ATTENUATION AT 16 GHz

(Measurements of Wilson)

Holmdel, N. J. 12/67 to 12/68

During the ATS-6 Millimeter Wave Experiment (ref. 10), direct attenuation measurements were taken in addition to correlation measurements using rain gauges. Meteorological radars were used at Rosman, North Carolina to validate attenuation techniques. A dual frequency radar co-located with the Rosman receiver was directed towards the ATS-6 satellite. A set of ten rain gauges was employed along the earth station satellite paths out to a distance of 2.5 kilometers. The frequencies of the radar system were 8.75 GHz and 3 GHz. Their range was 25 kilometers and the range-gated resolution was 100 meters. The attenuation measured with the radar system was then related to the 20 and 30 GHz attenuation through an assumed drop size distribution. Utilizing the following empirical relationship for continuous rain between rainfall rate and reflectivity factor Z,

$$Z = 200 \, R^{1.6}$$
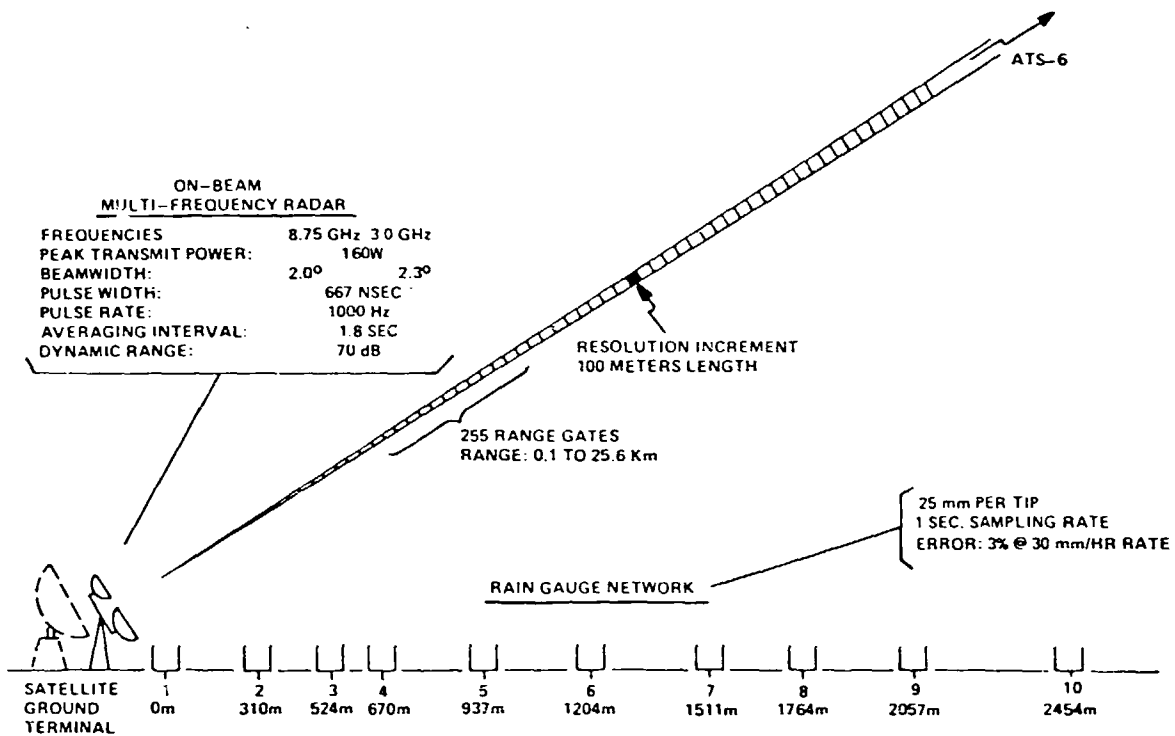
Radar and rain gauge measurements at Rosman, North Carolina.

Source: 20 and 30 GHz Millimeter Wave Experiments
          With the ATS-6 Satellite (ref. 10)

and the attenuation relationship for 20 and 30 GHz, the attenuation at 20 and 30 GHz can be developed. The resulting expressions for the 20 and 30 GHz attenuation are:

$$A_{20}(dB) = \sum_{i=2}^{256} 0.1799 \times 10^{-3} \, Z_i^{0.6875}$$

$$A_{30}(dB) = \sum_{i=2}^{256} 0.5355 \times 10^{-3} \, Z_i^{0.6469}$$

where Z_i is the measured reflectivity factor of the ith range increment in mm^6/m^3. Figures 5-5 and 5-6 are examples of results of direct attenuation measurements compared with predictions from the 8.75 and 3 GHz radars.

Figure 5-5
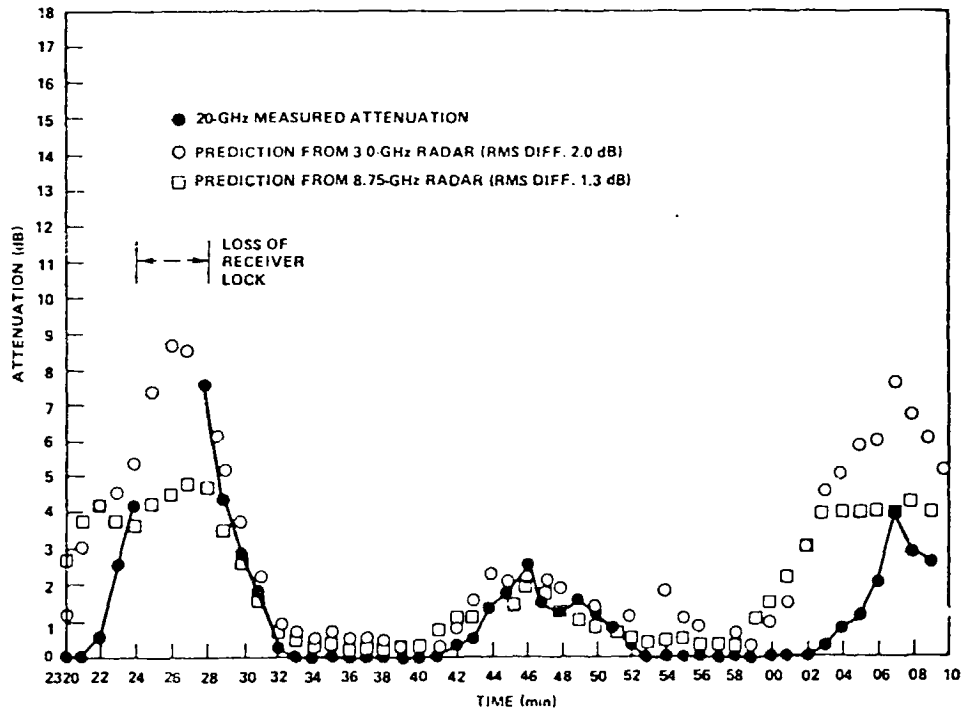
Figure 30. Prediction of 20-GHz attenuation from on-beam radar measurements for September 27, 1974.

Source: 2C and 30 GHz Millimeter Wave Experiments
With the ATS-6 Satellite (ref. 10)

Figure 5-6
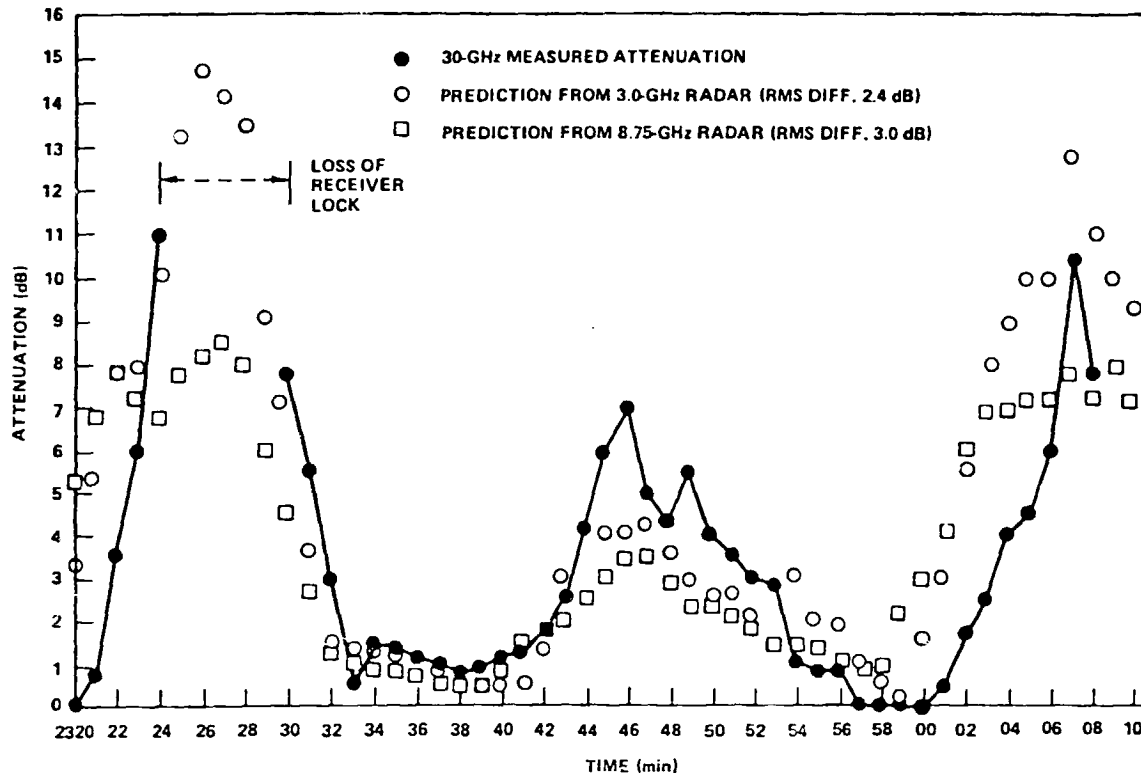
Figure 31. Prediction of 30-GHz attenuation from on-beam radar measurements for September 27, 1974.

Source: 20 and 30 GHz Millimeter Wave Experiments With the ATS-6 Satellite (ref. 10)

Since the reflectivity factor Z is empirically related to the rainrate R, it is possible to also use the radar to predict the rainfall rate along the path directly. This computed value can then be compared to the rainfall rate measured by the rain gauge directly under that point in the path. As expected, the results show that the correlation for the nearer rain gauge is good but degrades as the distance along the path increases.

5.5   Experiments Using Satellites

ATS-V

As reported by Ippolito (ref. 19), a millimeter wave propagation experiment was included on ATS-V. It was the first experiment for the earth-satellite link at 15.3 and 31.65 GHz. Seven stations participated in these experiments in 1969 providing amplitude and phase measurements on the two independent test links during defined weather conditions. The satellite did not achieve proper three-axis stabilization and remained in a spinning condition in geosynchronous orbit. For this reason the data analysis program was modified so as to permit meaningful propagation measurements even though the received data was spin modulated.

The propagation characteristics were determined from analysis of signals transmitted through the satellite at both frequency bands. The 15.3 GHz link consisted of a transmitter in the spacecraft and corresponding receivers at several ground stations. The 31.65 GHz link consisted of ground transmitters at two locations and a receiver on the spacecraft.

In addition to five NASA-funded sites operating with ATS-V, COMSAT Labs, Bell Labs, the Communications Research Center of Ottawa and several other entities used the 15.36 GHz down-link for measurements.

The experimental arrangements at the NASA site at Rosman, North Carolina were most ambitious. The measurement system included the following:

> 15.3 GHz down-link measurement
> 31.65 GHz up-link measurement
> Weather radar
> 10 rain gauges along the short path
> 16 and 35 GHz radiometers

Despite the problems caused by the undesired satellite spin, useful data were collected.

ATS-6

Of particular interest to this report are the COMSAT propagation experiments at 13 and 18 GHz and the millimeter wave experiment at 20 and 30 GHz.

COMSAT Propagation Experiment (CPE) (ref. 11)

The CPE was designed to sample the effects of climate on earth-satellite links (13 and 18 GHz) at 15 widespread locations throughout the Eastern U.S. with minimum spacing of at least 160 km. These locations were near Miami, FL., Atlanta, GA., Starkville, MS., New Orleans, LA., Nashville, TN., Asheville, NC., Fayetteville, NC., Wallops Island, VA., Clarksburg, MD., Philadelphia, PA., Columbus, OH., Detroit, MI., Boston, MA. and Andover, ME. Three of these locales, Starkville, Columbus and Boston, were also equipped with appropriately spaced 18 GHz space diversity terminals, thus providing the CPE with the capability of measuring the effectiveness of diversity as a function of spacing. About 50,000 hours of processed 13 GHz transmit path data and about 51,000 hours of processed 18 GHz transmit path data were collected in the 10 months of the experiment. Additionally, about 113,000 hours of processed point rain data at these sites were collected.

Two of the authors of the present report were heavily involved in the set-up of and data processing for this experiment. We have the following judgements about the results:

1) The results are best for the moderate levels of fading, from about 1.5 dB to 12-15 dB.

2) The rain data are useful and compare favorably with the long-term statistics for the areas covered. This is reassuring because several previous investigators have commented on the rather wide year-to-year variability in the rainfall rates and distributions.

Figures 5-7 through 5-10 show some of the cumulative distributions of attenuation and rainfall rate produced from the COMSAT experiment.

Figure 5-7
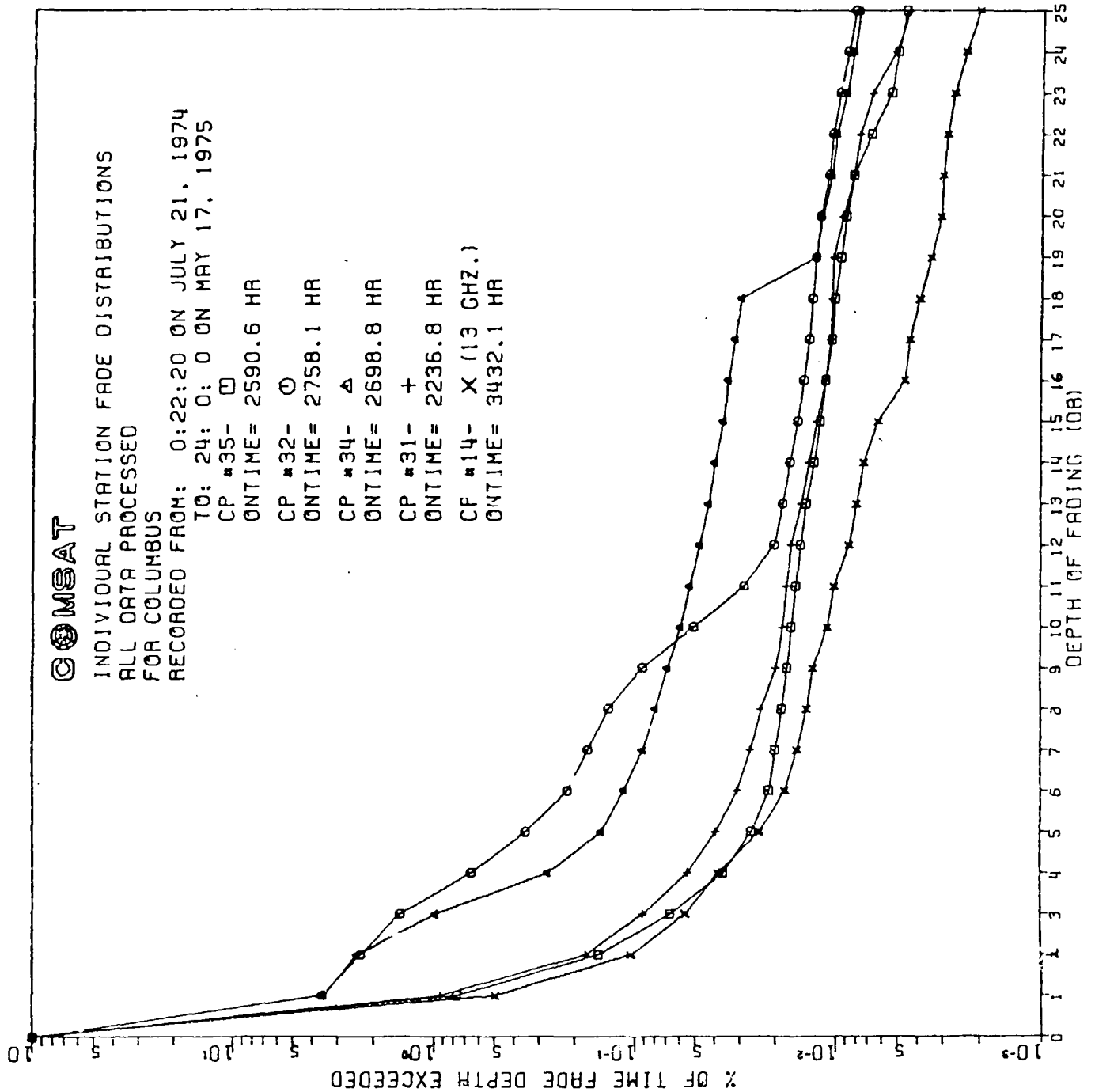
SAMPLE OF ATS-6 DATA

Source: Data Analysis Report on ATS-F
COMSAT Propagation Experiment (ref. 11)

Figure 5-8
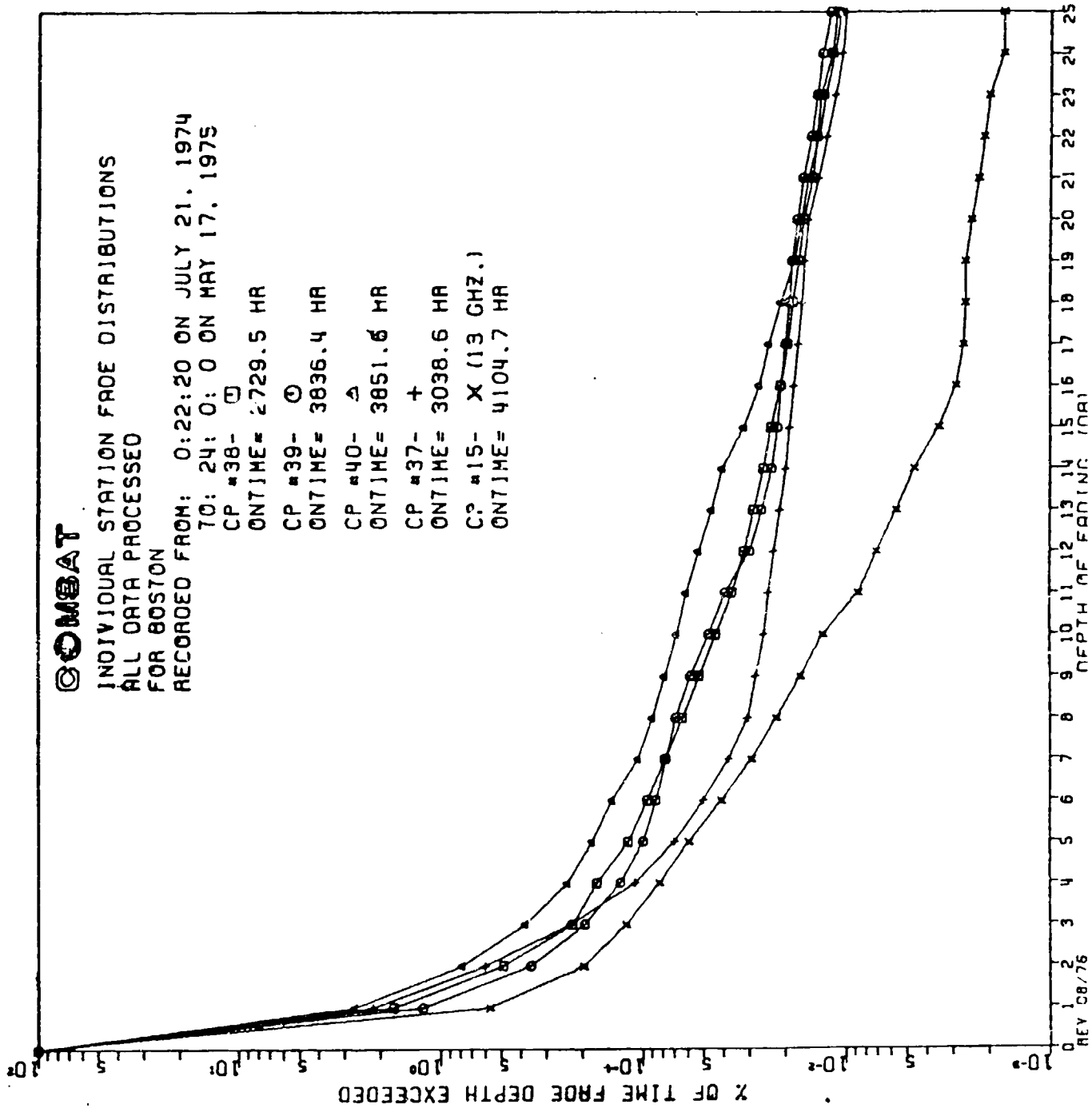
SAMPLE OF ATS-6 DATA
Source: Data Analysis Report on ATS-F
COMSAT Propagation Experiment (ref. 11)

Figure 5-9
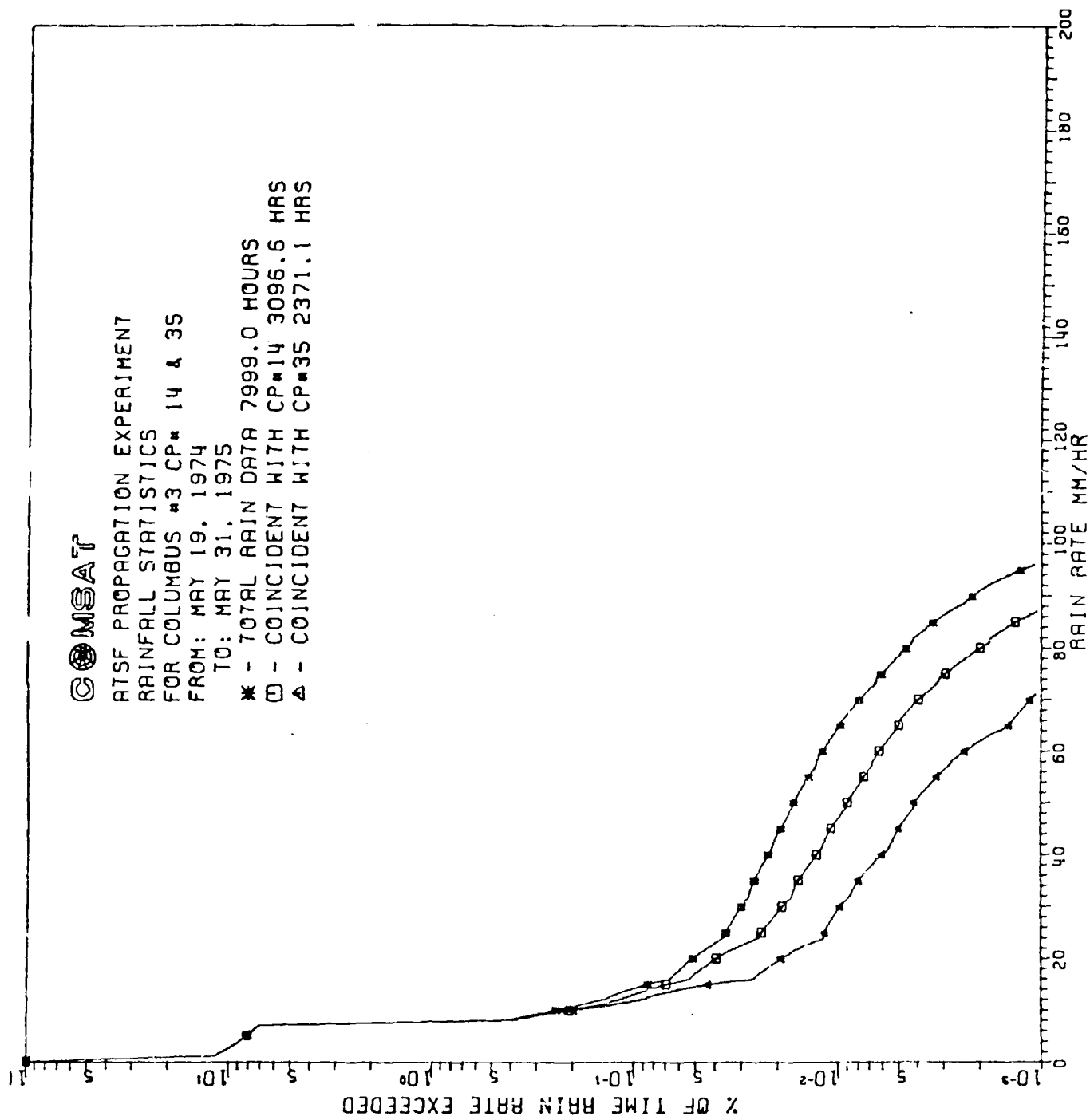
COMSAT

ATSF PROPAGATION EXPERIMENT
RAINFALL STATISTICS
FOR COLUMBUS #3 CP= 14 & 35
FROM: MAY 19, 1974
TO: MAY 31, 1975
※ - TOTAL RAIN DATA 7999.0 HOURS
▣ - COINCIDENT WITH CP=14 3096.6 HRS
△ - COINCIDENT WITH CP=35 2371.1 HRS

RAIN RATE MM/HR

% OF TIME RAIN RATE EXCEEDED

SAMPLE OF ATS-6 DATA
Source: Data Analysis Report on ATS-F
COMSAT Propagation Experiment (ref. 11)

Figure 5-10

COMSAT

ATSF PROPAGATION EXPERIMENT
RAINFALL STATISTICS
FOR BOSTON #2 CP=15 & 38
FROM: MAY 19, 1974
    TO: MAY 31, 1975
  ✳ - TOTAL RAIN DATA 7115.0 HOURS
  ⊟ - COINCIDENT WITH CP=15 3319.3 HRS
  △ - COINCIDENT WITH CP=38 2068.7 HRS

RAIN RATE MM/HR

% OF TIME RAIN RATE EXCEEDED
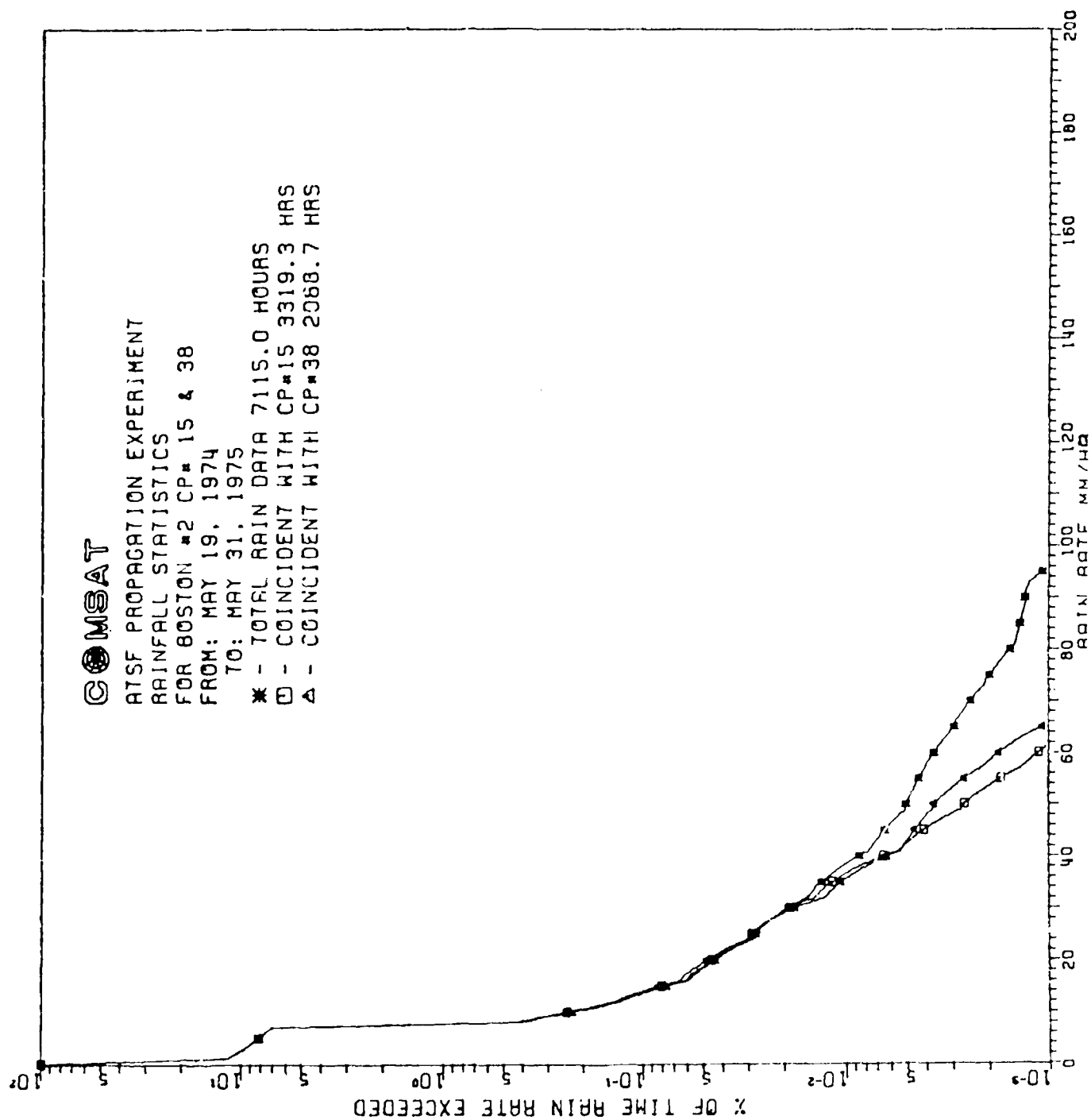
SAMPLE OF ATS-6 DATA
Source: Data Analysis Report on ATS-F
COMSAT Propagation Experiment (ref. 11)

ATS-6 Millimeter Wave Experiment (MWE)

The ATS-6 millimeter wave propagation experiment provided the first direct attenuation measurements at 20 and 30 GHz from an orbiting satellite. Studies were performed at eleven locations within CONUS to determine rain attenuation effects, scintillations, depolarization, site diversity, coherent bandwidth and transmission techniques. In addition, indirect methods of attenuation prediction were used using radars, rain gauges and radiometers for comparison with directly measured attenuation. The locations of the ATS-6 ground terminals are shown below.

ATS-6 MWE Participating Terminals

Location Organization	Major Areas of Investigation
Rosman, NC NASA GSFC	Prime facility 20 and 30 GHz – Attenuation, coherence bandwidth, differential phase effects, scintillation, communications links, radars, radiometers, rain gauge network
Greenbelt, MD NASA GSFC	20 and 30 GHz - Attenuation, site diversity, radiometers
Austin, TX Univ. of Texas (2)	30 GHz – Attenuation, 2-terminal site diversity, radiometer
Blacksburg, VA VPI & SU	20 GHz – Attenuation, depolarization
Clarksburg, MD COMSAT (2)	20 and 30 GHz – Attenuation, site diversity, radiometers
Columbus, OH Ohio State Univ. (3)	20 and 30 GHz – Attenuation, 3-terminal site diversity, scintillation, radars, radiometers

Location Organization	Major Areas of Investigation
Holmdel, NJ Bell Laboratories	20 GHz – Depolarization
Baltimore, MD Westinghouse	20 GHz – Attenuation, site diversity
Waldorf, MD NRL	20 and 30 G... – Attenuation, site diversity, radiometers
Richland, WA Battelle Northwest Laboratories	20 GHz – Attenuation, radiometer
Ft. Monmouth, NJ USASCA	30 GHz – Attenuation

All terminals measured rain attenuation at 20 or 30 GHz or at both frequencies, and most had rain gauge measurements as well. The Washington area diversity experiments used four terminals which jointly observed 20 GHz attenuation events from which it was possible to develop site diversity statistics.

COMSTAR

The COMSTAR satellites owned by COMSAT General and leased to AT&T carry transmit beacons at 19 and 28.5 GHz. These are currently being used for attenuation measurements by Bell Labs and COMSAT Labs, among others.

The Bell Labs experiments are set-up to measure a number of signal parameters, including the following:

1) Co-polarized vertical signal amplitude (TVRV)

2) Cross-polarized signal amplitude coupled from vertical to horizontal (TVRH)

3) Co-polarized horizontal signal amplitude (THRH)

4) Cross-polarized signal amplitude coupled from horizontal to vertical (THRV)

5) Phase difference between vertical and horizontal signals (TVRV and THRH)

6) Phase difference between vertical signal (TVRV) and its cross-polarized component (TVRH)

7) Phase difference between horizontal signal (THRH) and its cross-polarized component (THRV)

There are also two sites devoted to a space diversity experiment. One site is near Atlanta, Georgia and the other near Chicago, Illinois. Preliminary results from this segment of the project have been published. Figures 5-11 and 5-12 show some of these data (ref. 20 and 21).
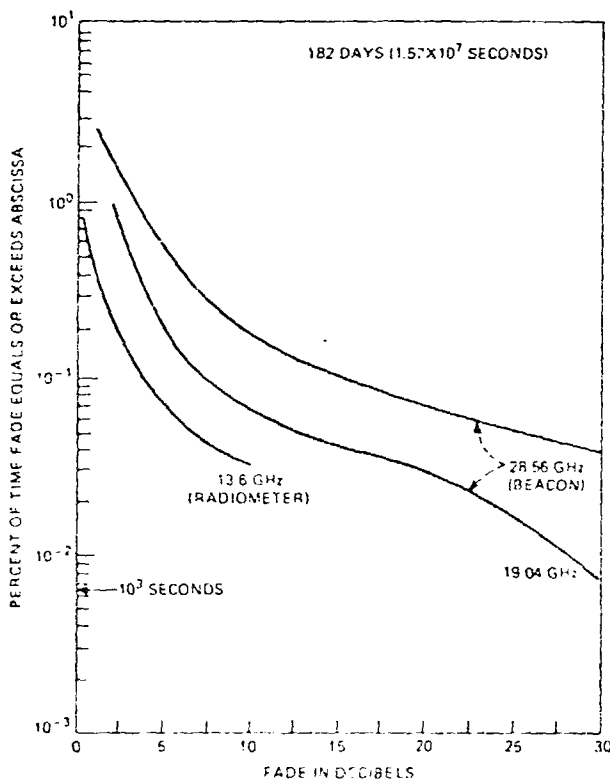
Fig. 12—Grant Park fading.

Figure 5-11

Source: The Bell System
Technical Journal (ref. 20)

Figure 5-12
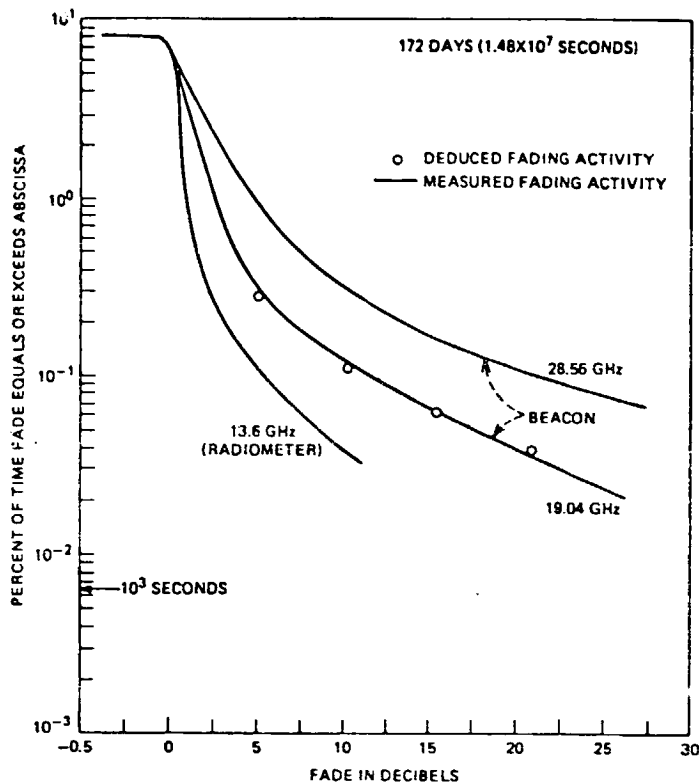
Fig. 13—Fade distribution in Palmetto, Georgia.

Source: The Bell System Technical Journal (ref. 20)

Preliminary results from the COMSAT Labs experiment using COMSTAR have also been published (ref. 13). This was a single-site experiment at Clarksburg, Maryland. Rain gauge data were also collected here. Figures 5-13 and 5-14 show some of the preliminary results from these observations.

A total of 4,200 hours of data were collected out of which the dynamic attenuation range of 30 dB was exceeded for about 100 minutes or 0.04 percent of the time at 19 GHz. At 28.56 GHz, the same range was exceeded twice as long; that is, for 0.08 percent of the time. The fade level was referenced to a nominal clear sky condition.
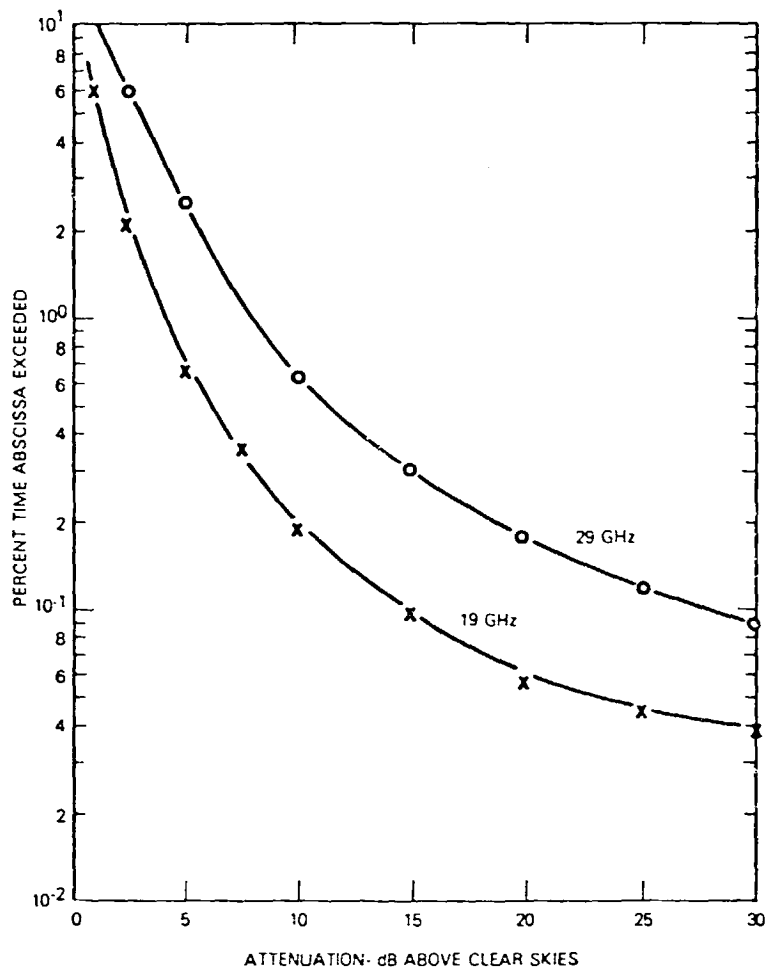
Figure 3. *Cumulative Fading Statistics of 19.04- and 28.56-GHz Vertically Polarized Beacons from Mid-July 1976 to Mid-January 1977*

Figure 5-13

Source: COMSAT Technical Review
Volume 7, No. 2
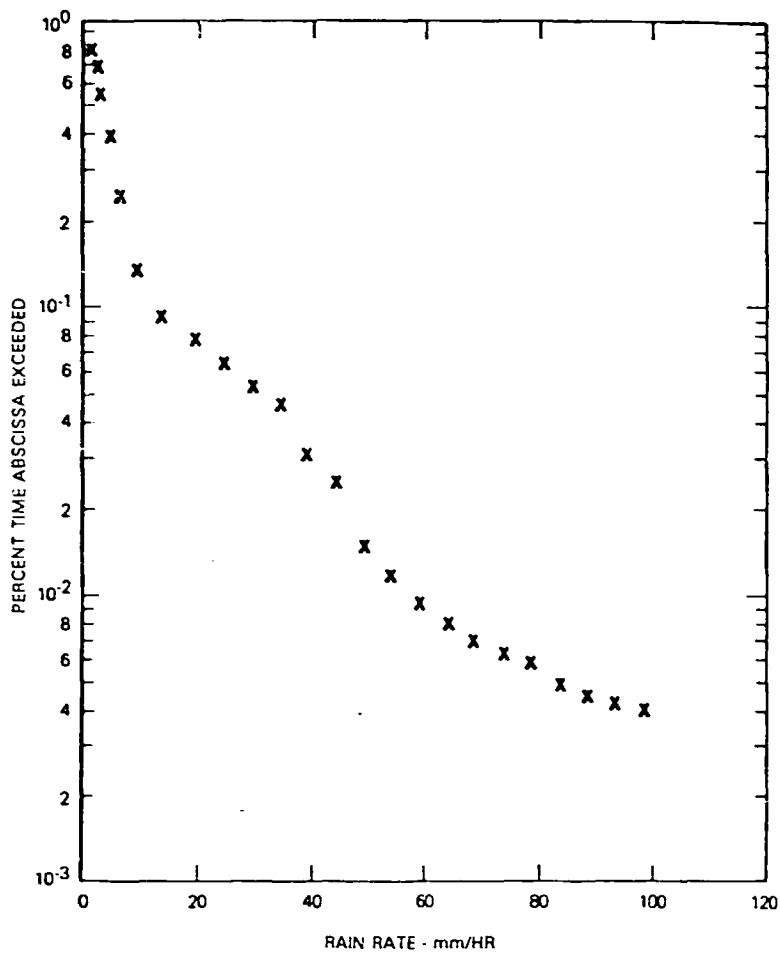
Figure 4. *Cumulative On-Site Rain Rate Statistics from Mid-July 1976 to Mid-January 1977*

Figure 5-14

Source: COMSAT Technical Review
Volume 7, No. 2

The cumulative rain rate statistics for the same site and periods of time are given in Figure 5-14. Measurable rain occurred for about 1.5 percent of the time, but measurable attenuation occurred for more than 10 percent of the time. This higher percentage of the time was explained through the presence of clouds and fog.

Most of the deep fades with attenuations of 15 dB or more at 19 GHz occurred during the late summer months. Lesser fades, however, were more evenly distributed throughout the period of measurements.

SECTION 6
COMPARISON OF THEORY AND EXPERIMENT

6.1   Introduction

An important indication that a theory includes all significant contributors to a phenomenon is the verification of the theory by experiment. In the area of precipitation attenuation, most of the theories proposed before the advent of the digital computer contained some substantial shortcomings due to the approximations needed. Often the values of constants given were in error. Medhurst (ref. 27) published in 1965 a survey comparison of the current theory and the experiments performed to date. These were all concerned with terrestrial links. The general agreement between theory and measurement was not particularly good. The experiments tended to produce a substantial number of attenuation values in excess of the maximum attenuation predicted by theory. This tendency was not satisfactorily explainable.

More recent experiments have shown a somewhat improved correspondence with the predictions of theory. In part this is due to a better understanding of the behavior of rainstorms. However, a fairly elaborate field of rain gauges with fast response time and good data analysis techniques is needed to assure good agreement between theory and measurement. Single point rain gauges generally give rather poor correlation between the rain rate and the attenuation, even on a statistical basis. As the period of measurement increases, the point rain gauge statistics will show more agreement with the attenuation statistics. This is due to the fact that in the absence of any strong influences due to local geography, the rain from a large number of storms will be sampled more or less at random by the point rain gauge. The distribution of rainfall rates sampled will then approach the actual distribution over a long period of time. A similar experience will hold for the attenuation statistics. However, in general the path of the antenna beam and the point rain gauge will sample at different points in space, and thus a long measurement period will be needed before the measurement statistics will converge.

6.2   Specific Experiments

Of the specific experiments we have considered in this paper, the agreement of measurement with theory has been a function of the elaborateness of the experimental set-up and the completeness of the data taken.

Terrestrial Link

The experiment described in Reference 14 involved a 6.4 km link within the Bell Labs rain gauge field at Holmdel, New Jersey. The results show a large degree of scatter when plotted against the path average rain rate, as shown in Figure 6-1. The cumulative time distributions, shown previously in Section 5, can be used to derive an effective path length of about 3 to 4 km, depending on the rain rate. The values are quite consistent for rain rates above about 90 mm/hr. This seems to indicate that the average rainfall values produced by the rain gauge field are conservative.

ATS-6

The experimental set-up at Rosman, North Carolina using the ATS-6 satellite (ref. 10) showed good agreement between the attenuation calculated from weather radar measurements and measured space-link attenuation. The weather radar was also reasonably good at detecting the rain rate along the path as measured by rain gauges.

In the data analysis from the COMSAT propagation experiment using ATS-6, the rain gauge data were used to extrapolate the attenuation data to cover periods of time when the millimeter wave link was not collecting data. The resulting distributions do not show radical differences from the original data taken. This seems to indicate that the weather conditions and the attenuation were both sampled for a long enough period that the statistics began to converge. Analysis of the statistical distributions for several sites produced values of mean effective path length ranging from 1.5 to 3.8 km at 50 mm/hr. However, the behavior of the effective path length was not consistent from site to site as shown in Table 6-1.

Figure 6-1
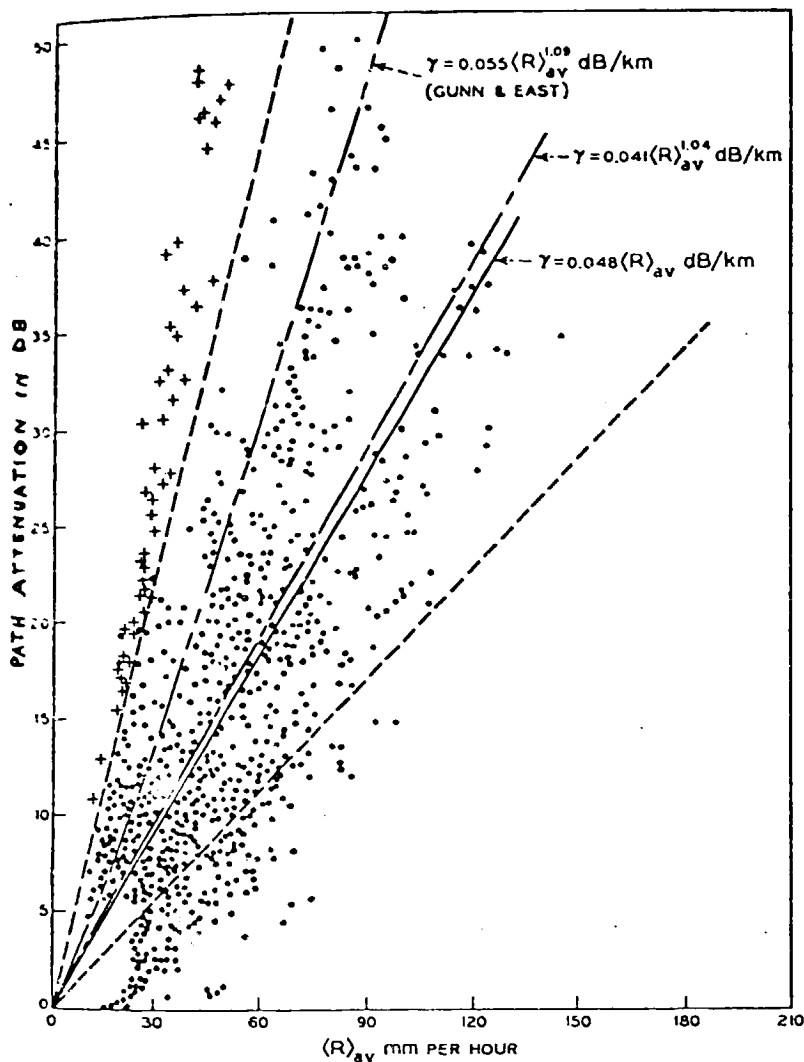
Fig. 7—Plot of observed attenuation versus average path rain rate, $\langle R \rangle_{av}$, as measured by four gauges with an intergauge spacing of 1.6 km, for all storms during the period June 23 through October 31, 1967. The dashed lines are theoretical maxima and minima. The solid line is a least squares regression. The data points represented by crosses pertain to October 25, 1967.

Source: Ref. 14

Table 6-1
Mean Effective Path Length
Computed From COMSAT ATS-6 Data
(L in km)

R	Starkville		Washington	Columbus		Boston	
mm/hr	L_{13}	L_{18}	L_{13}	L_{13}	L_{18}	L_{13}	L_{18}
10	6.8	3.5	4.9	3.6	1.5	4.4	2.4
20	5.0	3.6	2.9	3.4	2.6	4.9	3.0
40	3.8	2.6	1.6	2.4	2.9	4.3	4.0
50	3.8	2.5	1.5	2.5	2.8	4.2	3.6
70	4.2	2.1	1.4	3.1	--	5.6	2.9
100	4.2	1.7	1.9	--	--	4.6	--
120	3.8	1.5	2.0	--	--	--	--
150	--	1.3	1.8	--	--	--	--

SECTION 7

A PRACTICAL RAIN ATTENUATION MODEL FOR CONUS

The specific elements that make up the model for CONUS presented in this report have all been discussed previously; it remains but to explicitly draw them together and explain the relationships involved.

7.1   U. S. Climatological Data

A large amount of rain data is available for the United States, primarily from the U.S. Department of Commerce, Environmental Science Services Administration, National Climatic Center, Asheville, North Carolina. Of particular interest are the Climatic Atlas of the United States and Selected Climatic Maps of the United States.

For the design of the actual system, it will be desirable to use detailed data for individual earth station locations, which are also available from the National Climatic Center. Shown in Tables 7-1 and 7-2, as an example, are extracts of precipitation information for Orlando, Florida which are available on a monthly and on an annual basis. Also available are mean annual number of days with thunderstorms as shown in Figure 7-1, normal annual total precipitation as shown in Figure 7-2 and total monthly precipitation as shown in Figures 7-3 and 7-4. From this and similar information it is possible to develop attenuation versus time statistics for each specific site.

The importance of considering precipitation data for each specific earth station site separately is illustrated in Figures 7-5 and 7-6, which show that significant variations in annual rainfai rates occur for locations which are in close proximity to each other. This is especially true for mountainous areas and for coastal zones. For example, Seattle has about 40 inches of rain annually, but locations 50 miles to the west of Seattle have 150 inches per year; locations 50 miles to the east have 112 inches per year, but locations only 100 miles Southeast of Seattle have only 8 inches of rain per year.

Table 7-1

Rain Data for Orlando

Month of July

C   OCCURRENCES OF PRECIPITATION AMOUNTS:

INTENSITIES	FREQUENCY OF OCCURRENCE FOR EACH HOUR OF THE DAY																									NO DAYS WITH
	AM HOUR ENDING AT											NOON	PM HOUR ENDING AT											MID	
	1	2	3	4	5	6	7	8	9	10	11		1	2	3	4	5	6	7	8	9	10	11		
TRACE	3	1	2	3	2	2		1	1	3	8	8	13	22	23	25	28	22	30	15	9	9	9	6	31
0 in			1	1		1		1	1			4	5	4	4	2	4	4	4		3	3	1	2	7
.02 to .08 in	1	1								1	1	2		11	11	11	13	13	10	10		4	3		17
.10 to .24 in	1		2	1								5	7	3	6	5	4	4	1				1	19
.25 to .49 in	1			1	1	1		1					1		3	3		1	3					14
.50 to .99 in								1			1				1	1		3	5	3				17
1.00 to 1.99 in																2		1						7
2.00 in and over														1		1	1	1	1					5
TOTAL	5	2	3	5	4	3	2	2	2	5	13	21	26	41	48	50	55	51	52	31	21	18	12	92	17

Table 7-2

Rain Data for Orlando

Annual Information

C   OCCURRENCES OF PRECIPITATION AMOUNTS:

#	INTENSITIES	FREQUENCY OF OCCURRENCE FOR EACH HOUR OF THE DAY																									NO DAYS WITH
		AM HOUR ENDING AT											NOON	PM HOUR ENDING AT											MID	
		1	2	3	4	5	6	7	8	9	10	11		1	2	3	4	5	6	7	8	9	10	11		
1	TRACE	13	10	10	9	10	8	10	11	8	12	18	18	25	29	35	36	35	26	29	25	20	16	17	13	52
2	0 in	3	3	3	3	1	1	3	2	3	2	3		4	4	5	6	5	7	5	6	6	4	6	3	9
3	.02 to .08 in	6	5	4	4	6	6	6	6	6	6	7	9	10	13	12	17	14	14	11	12	8	9	7	7	31
4	.10 to .24 in	3	2	2	2	1	2	1	1	1	2	3	5	6	5	5	7	7	6	5	5	5	3	2	2	26
5	.25 to .49 in	1	1	+	+	1	1	+	+	1	1	1	2	2	2	6	3	3	4	2	1	1	+	1	2	20
6	.50 to .99 in	+		1	1	+		+	+	+		1	+	2	1	2	2	2	2	1	1		+	+	+	20
7	1.00 to 1.99 in		+	+						+				+	+	1	1	1	1							12
8	2.00 in and over														+	+	+	+								4
	TOTAL	26	21	20	19	20	19	19	21	20	23	32	39	47	56	63	71	69	58	57	50	39	37	31	26	74
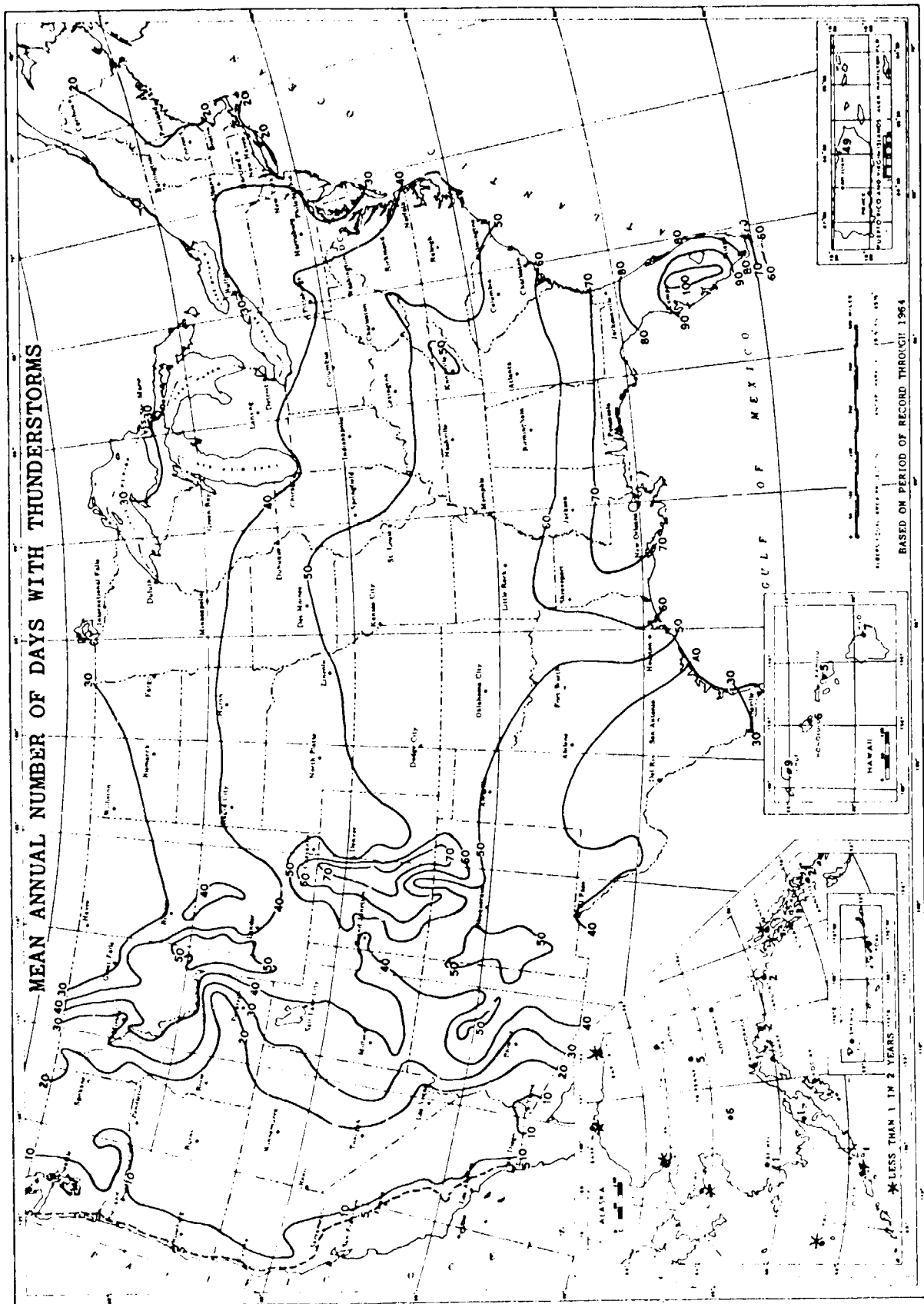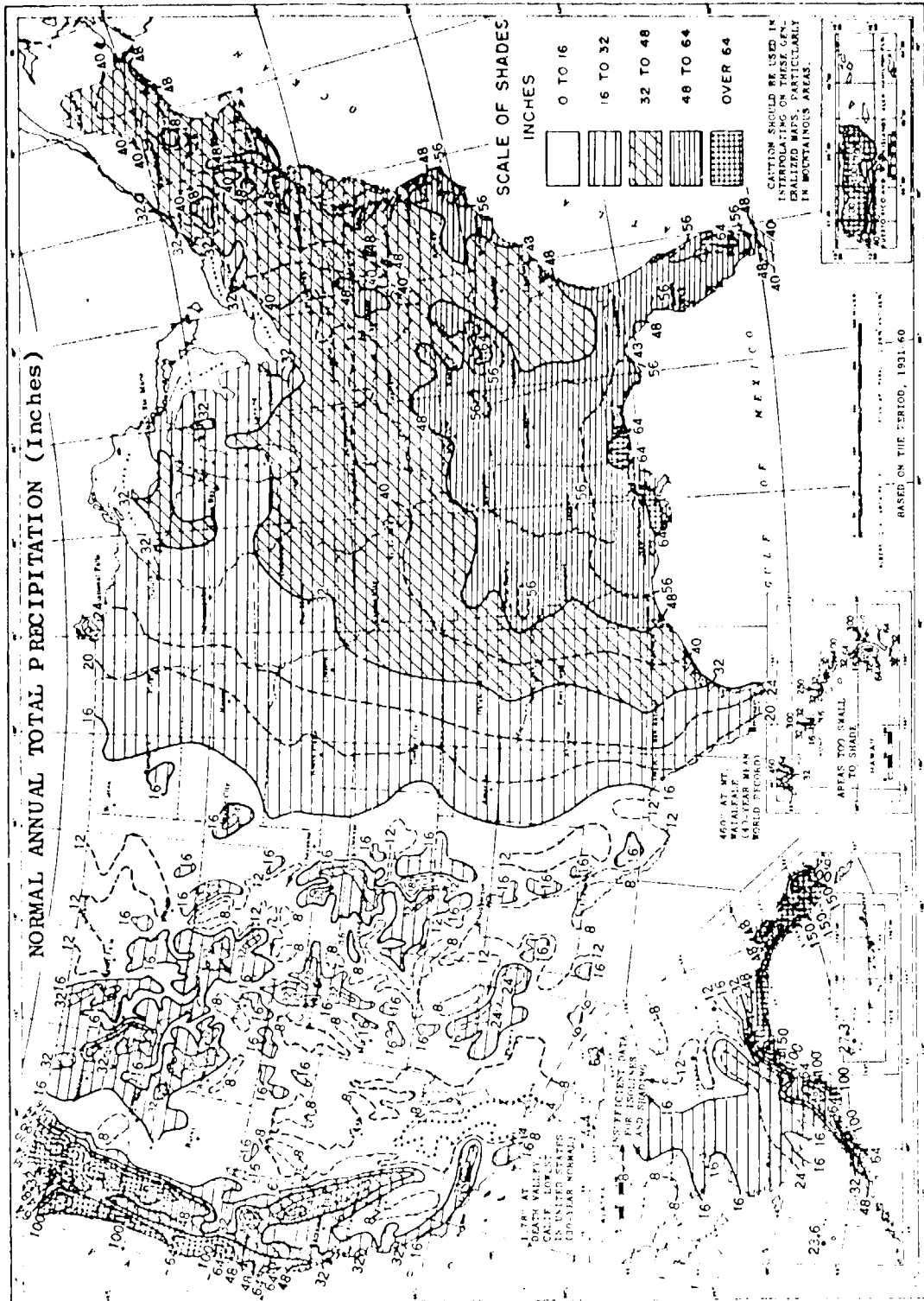
WDL-TR8457

MEAN ANNUAL NUMBER OF DAYS WITH THUNDERSTORMS

Figure 7-1

NORMAL ANNUAL TOTAL PRECIPITATION (Inches)

Figure 7-2

NORMAL MONTHLY TOTAL PRECIPITATION (Inches) EASTERN UNITED STATES
For Selected Stations
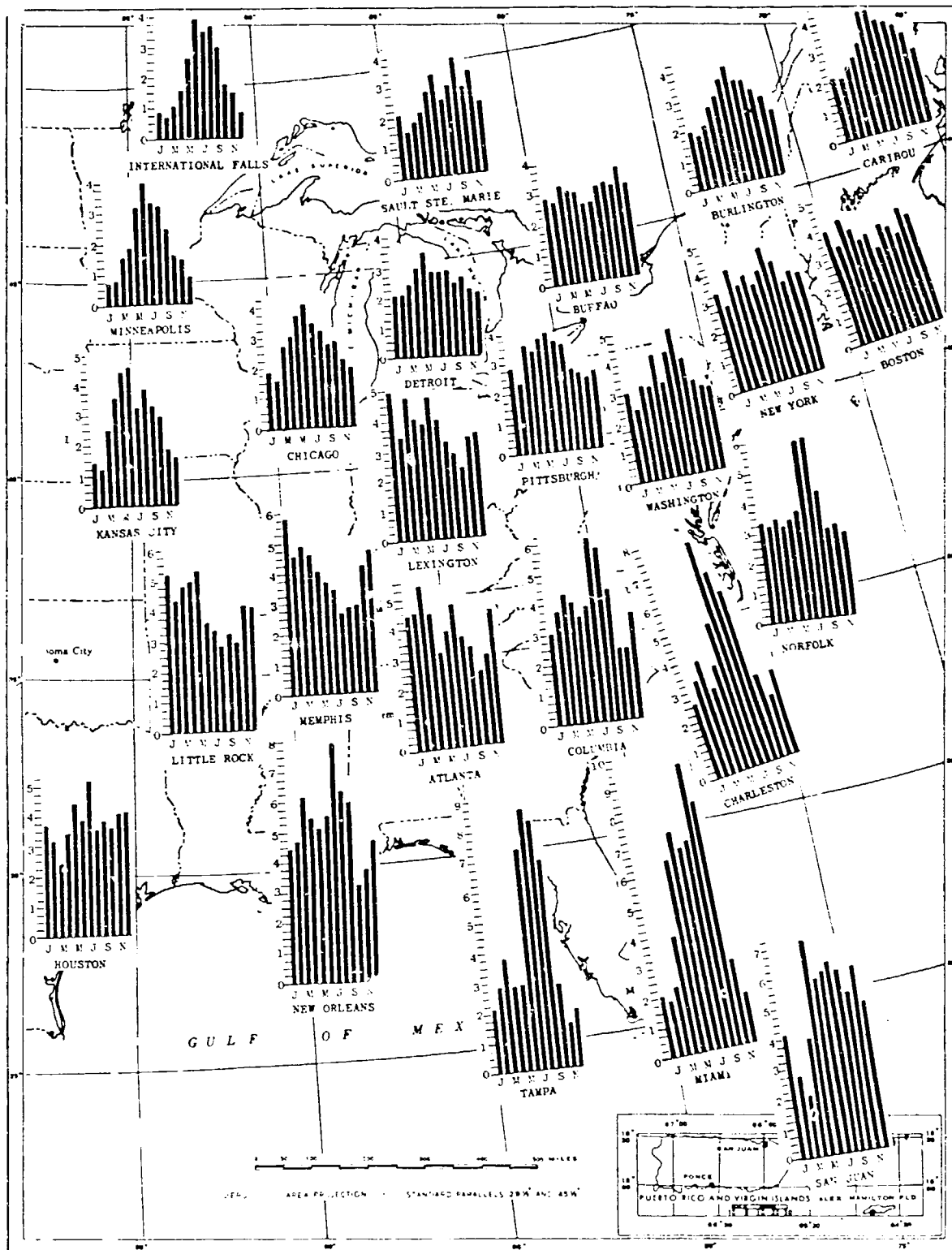
Based on 30-year Period, 1931-60

Figure 7-3

NORMAL MONTHLY TOTAL PRECIPITATION (Inches) WESTERN UNITED STATES
For Selected Stations
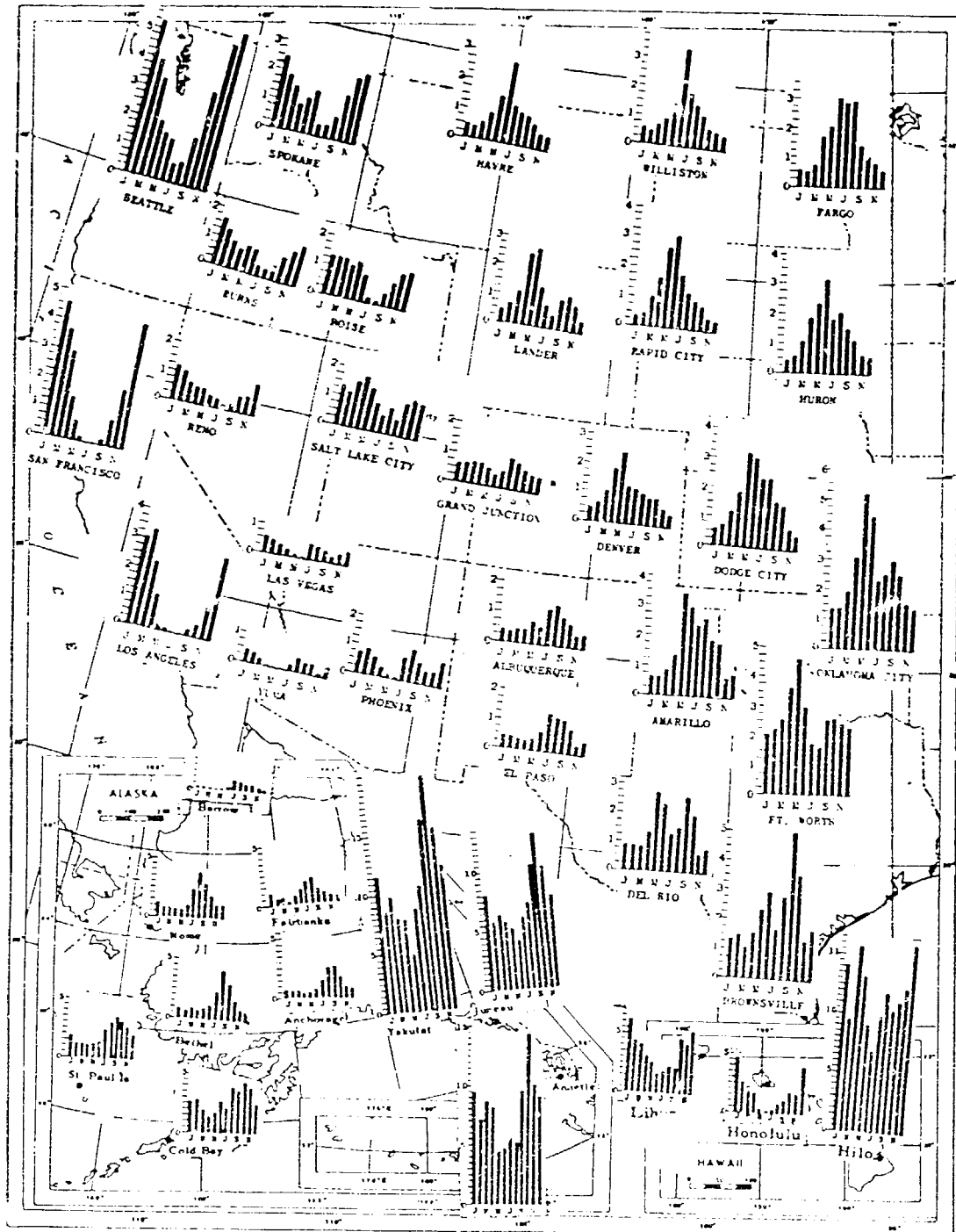
Based on 30-year Period, 1931-60

Figure 7-4

Figure 7-5

MEAN ANNUAL PRECIPITATION

A-82

Figure 7-6

MEAN ANNUAL PRECIPITATION

A-83
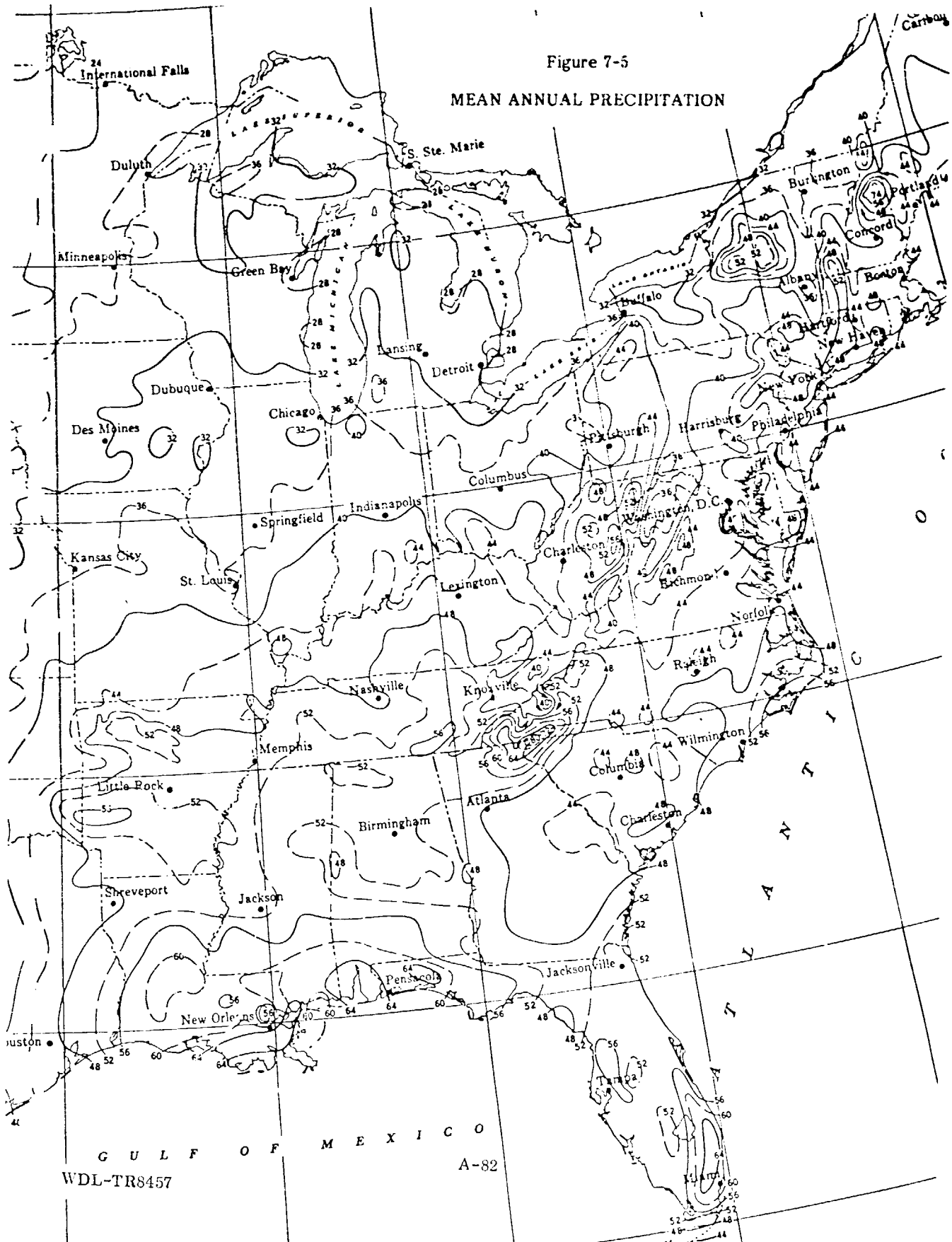
For comparison, it may be of interest to note that the world record rainfall for a 40-year mean of 460 inches or 38 feet per year occurs on Mt. Waialeale on the island of Kauai, Hawaii.

7.2   U. S. Climatological Model Zones

For the purpose of a general satellite system trade-off study it is not practical to select and consider all individual earth station sites. Instead, it is desirable to divide the coverage area into general rain model zones. The model for the cumulative time distribution of rainfall rates that we are using is that due to Rice and Holmberg (Ref. 12). Consistent with this model, we have used the geographical variations of the parameter Beta and the parameter M, the total annual average rainfall, to determine the rain model zones. The division of the United States into these zones is shown in Figure 7-7, and the parameters Beta and M for the zones are given in Table 7-3. The variation of Beta over the United States is shown in Figure 7-8.

Table 7-3

Average Rain Statistics for U. S. Rain Model Zones

Rain Zone Number	Average Annual Rainfall Inches	Thunderstorm Rain to Total Rain Ratio
1	10	0.20
2	24	0.20
3	40	0.25
4	56	0.40
5	64	0.50
6	100	0.07
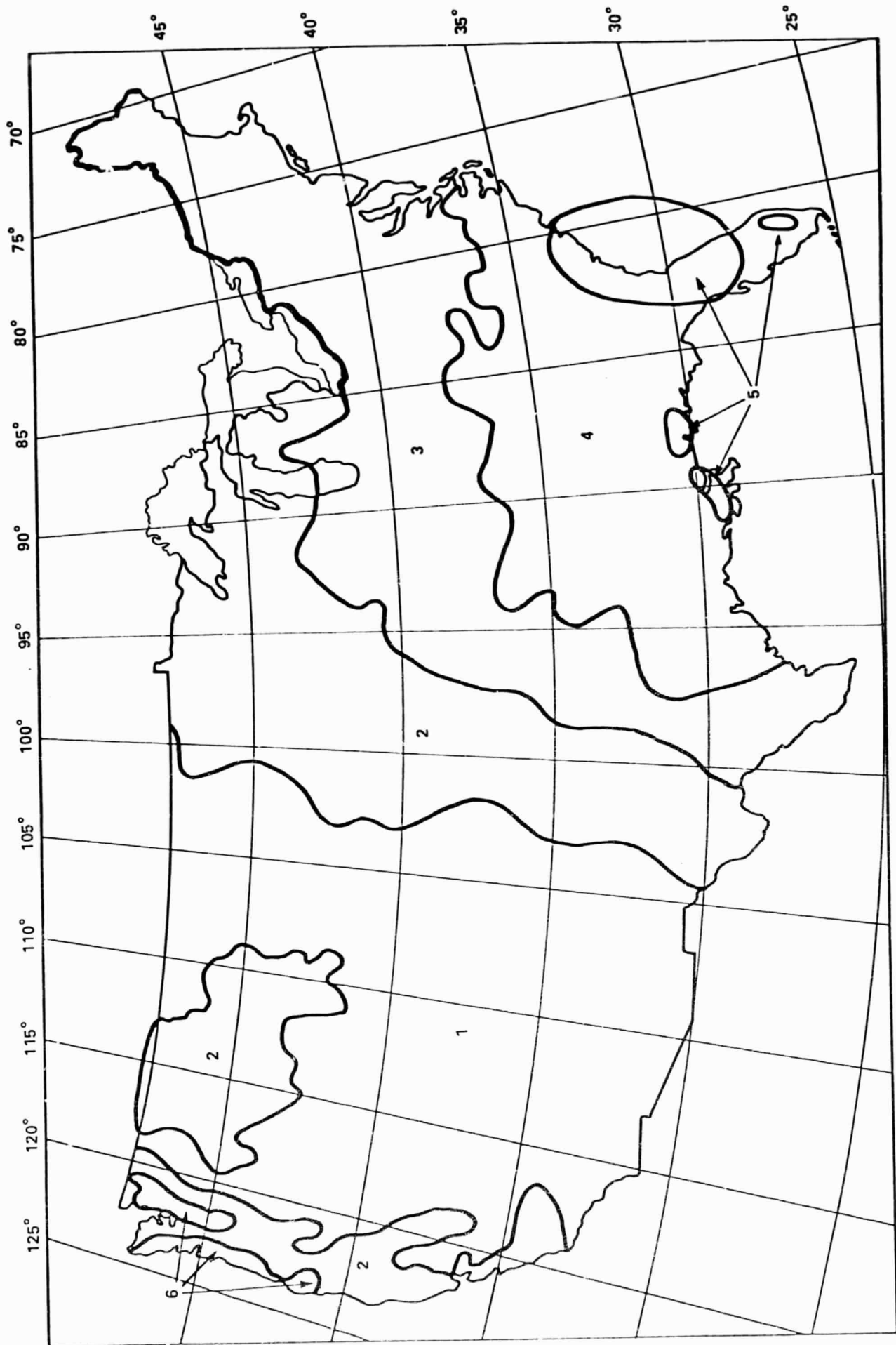
Figure 7-7

CLIMATOLOGICAL ZONES FOR CONUS

WDL-TR8457
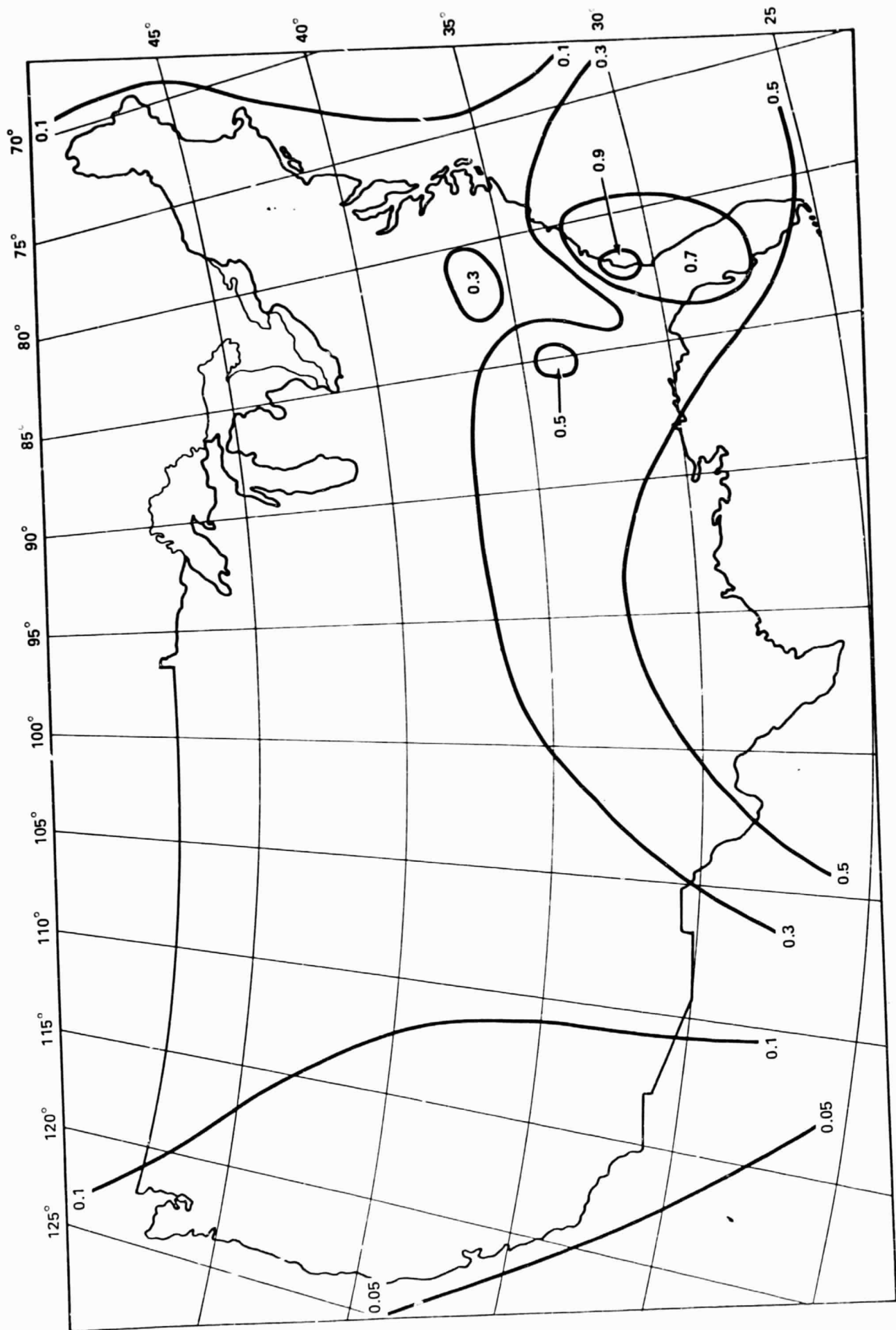
Figure 7-8

THE PARAMETER BETA IN
RICE-HOLMBERG CLIMATE MODEL

Please note that Rain Zone 1 has mountain areas with pockets of much higher precipitation than the average of 10 inches per year. This will have to be considered when individual earth station sites are selected. Also noteworthy is the fact that the high rain rates in the Northwest produce a different attenuation distribution from the equally high annual rates in the Southeast, since the thunderstorm to total rainfall ratio in the Northwest is much lower than in the Southeast.

The resulting cumulative time distributions of rainfall rates are shown in Figures 7-9 and 7-10.

The relation between rain rate and specific attenuation is that given by Olsen, et. al. (ref. 4). The values used are given in Table 7-4.

Table 7-4
Values of a and b in aR^b
(Laws and Parsons Rain)

Frequency	LP_l		LP_h	
GHz	a	b	a	b
18	0.0474	1.129	0.0545	1.096
30	0.162	1.061	0.226	0.964
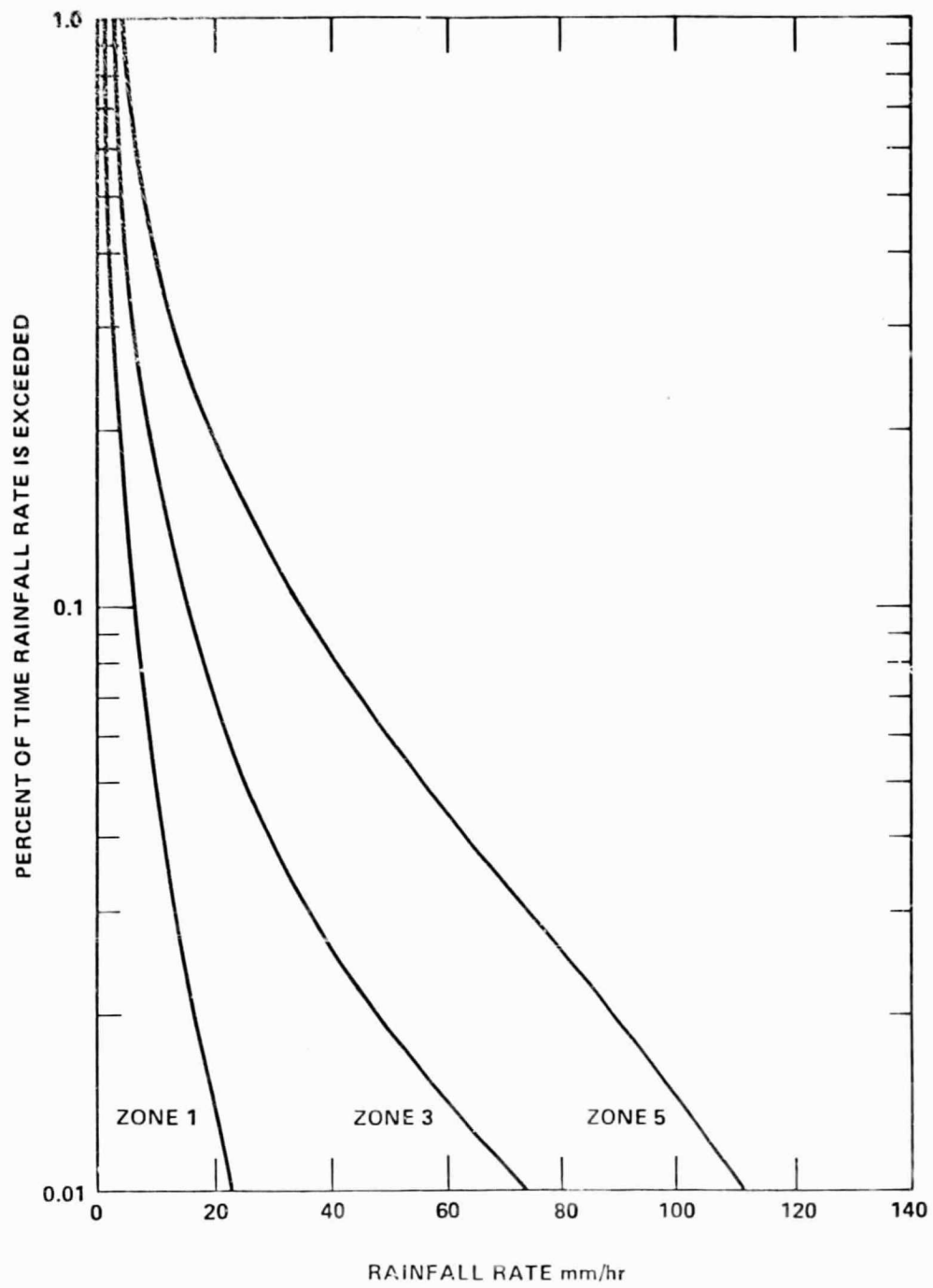
Figure 7-9

CUMULATIVE TIME

DISTRIBUTION OF RAINFALL RATE
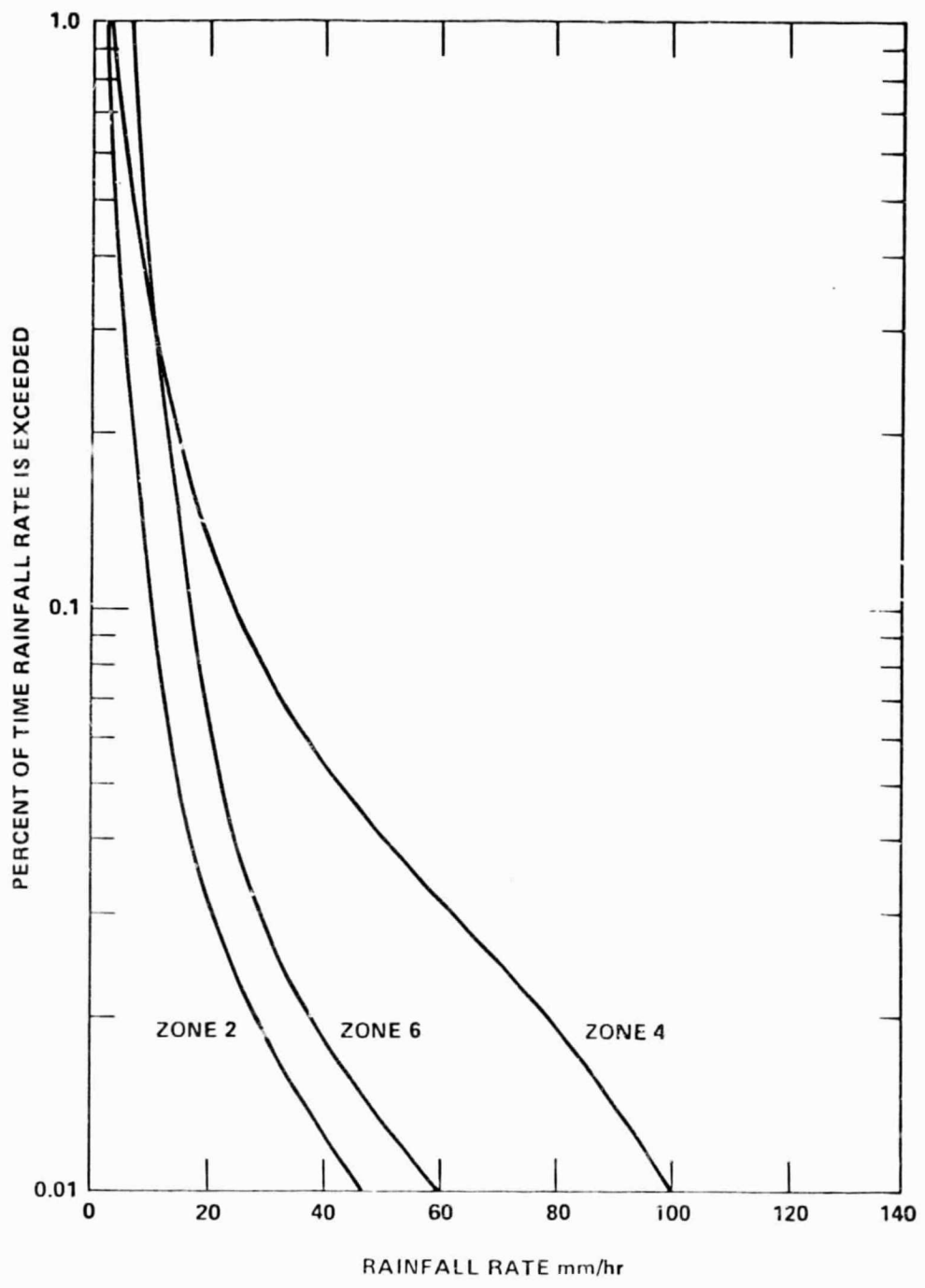
Figure 7-10

CUMULATIVE TIME

DISTRIBUTIONS OF RAINFALL RATE

The final factor in converting from a distribution of rainfall rates to a distribution of attenuation is a function yielding values for the mean effective path length through rain. This poses a rather difficult choice, due primarily to the large variations between the results of different experimenters. We have chosen for this report to use the method disclosed in CCIR Document F5/003. This method involves several components, among them the height of the zero-degree isotherm, the elevation angle at the earth station and the rainfall rate.

The complete model produces cumulative time distributions of attenuation. These are shown in Figures 7-11 through 7-22 for the six climate zones. These climate zones do not coincide with those in CCIR F5/003; we have combined our division into climate zones with the CCIR method for estimating attenuation from rainfall rate. An elevation angle of 35 degrees was assumed. This is a fairly pessimistic value for the Southern U.S. Somewhat pessimistic values were also chosen for the melting-layer altitude.

Also shown in the Figures are curves of attenuation distribution produced by other expressions for mean effective path length. The curves marked "B" are based on the expression cited previously from Reference 13. This expression was derived from data taken at Clarksburg, Maryland using the Comstar beacon. The curves marked "A" are based on data presented in Reference 33. The latter is very close to a function derived by Ippolito from data taken using ATS-5. In the latter two cases, the elevation angle at the earth station is not explicitly taken into account.

Several points of measured data are also shown in the Figures for climate zones where measurements were taken. Particularly in Zones 4 and 5, but also in Zone 3, the measurements tend to lie below the curve computed using the CCIR formula. It is likely that the CCIR formula for mean effective path length tends to overestimate the path length or the path average rain rate at the higher rainfall rates that are significant in Zones 4 and 5. We are of the opinion that further careful investigation will show that the CCIR estimate is too conservative for high rain rates, and that the best estimate for the attenuation distribution will lie between the CCIR values and those of the other curves. However, in order to be conservative we have used the estimate from the CCIR paper in thi report to specify the link margins.

An additional source of degradation on the downlink at 18 GHz is the increase in sky noise during periods of attenuation due to rain. This degradation is dependent on the clear sky system noise temperature and is added directly to the required system margin, since it lowers the G/T ratio of the earth station. The increase in system noise temperature is computed as follows:

$$M = A + 10 \log \left[\frac{Tsys + Tsky}{Tsys} \right]$$

where

M = The total downlink degradation in dB

A = The downlink attenuation in dB

$Tsys$ = The clear weather system noise temperature in degrees Kelvin

Tsky is computed as follows:

$$Tsky = \left[1 - 10^{-A/10} \right] T_r$$

Tr is the physical temperature of the clouds and rain, generally about 273 K.
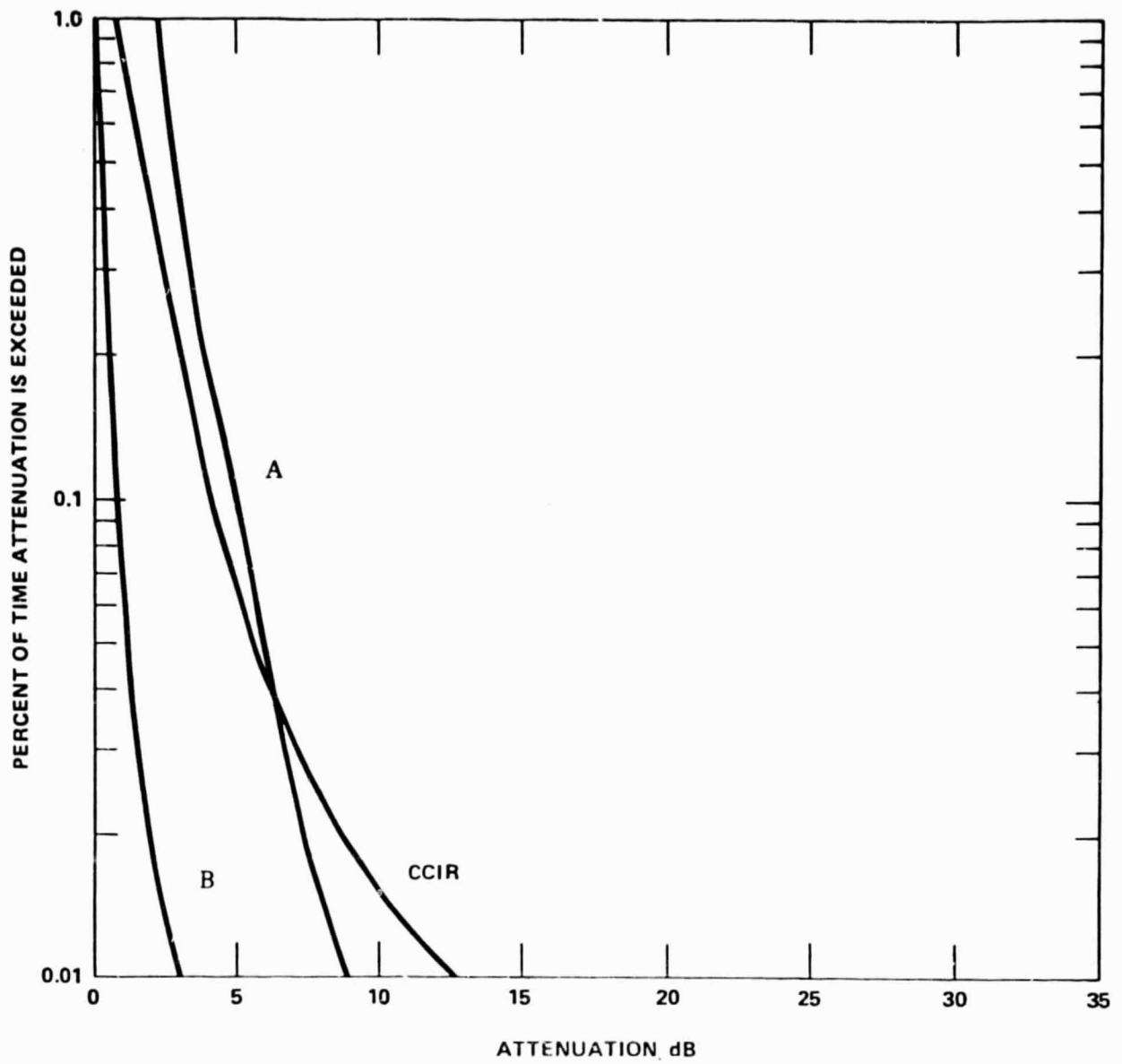
Figure 7-11

CUMULATIVE TIME
DISTRIBUTIONS OF ATTENUATION FOR ZONE # 1
18 GHz
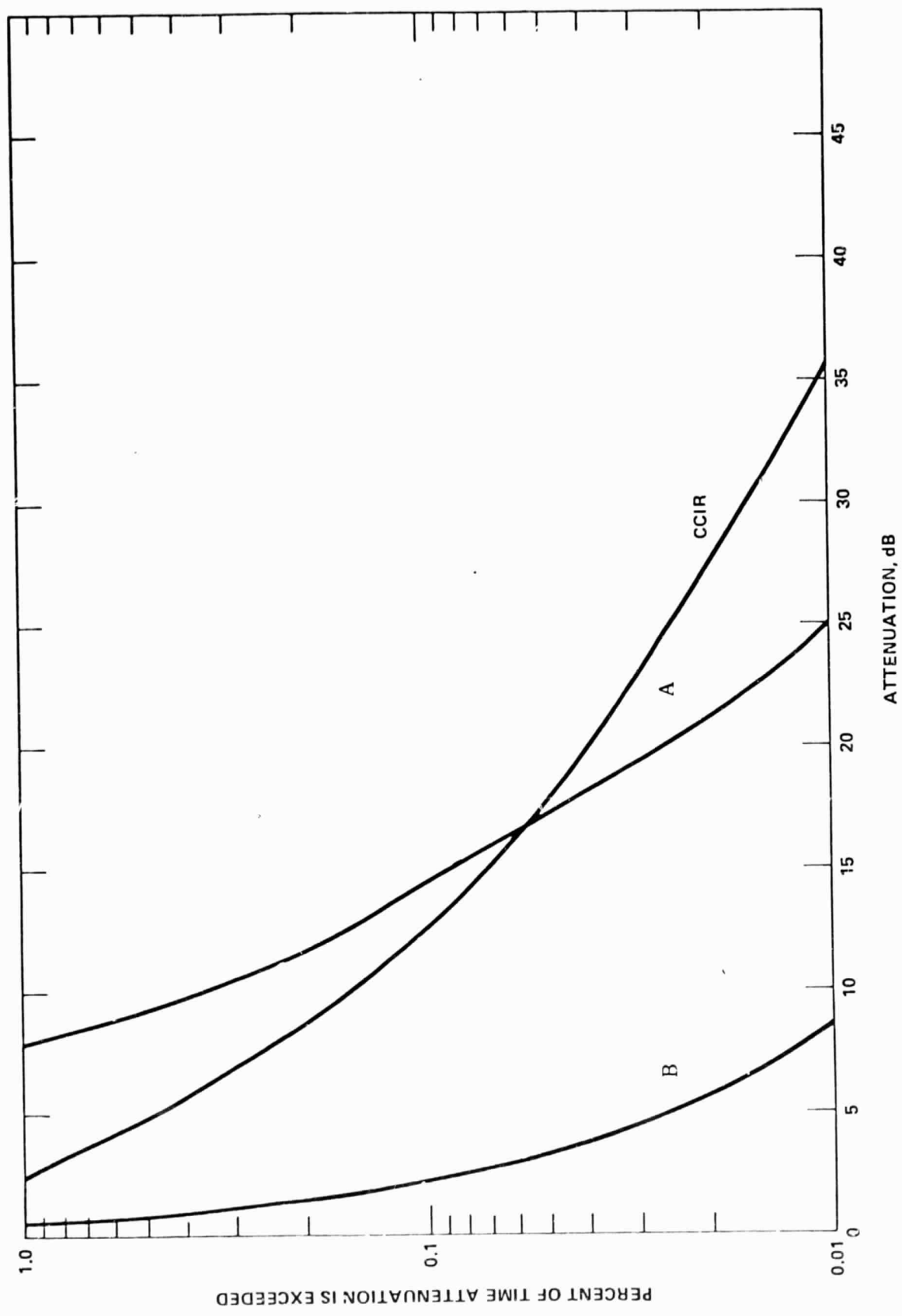
Figure 7-12
CUMULATIVE TIME
DISTRIBUTIONS OF ATTENUATION FOR ZONE # 1
30 GHz

C-2
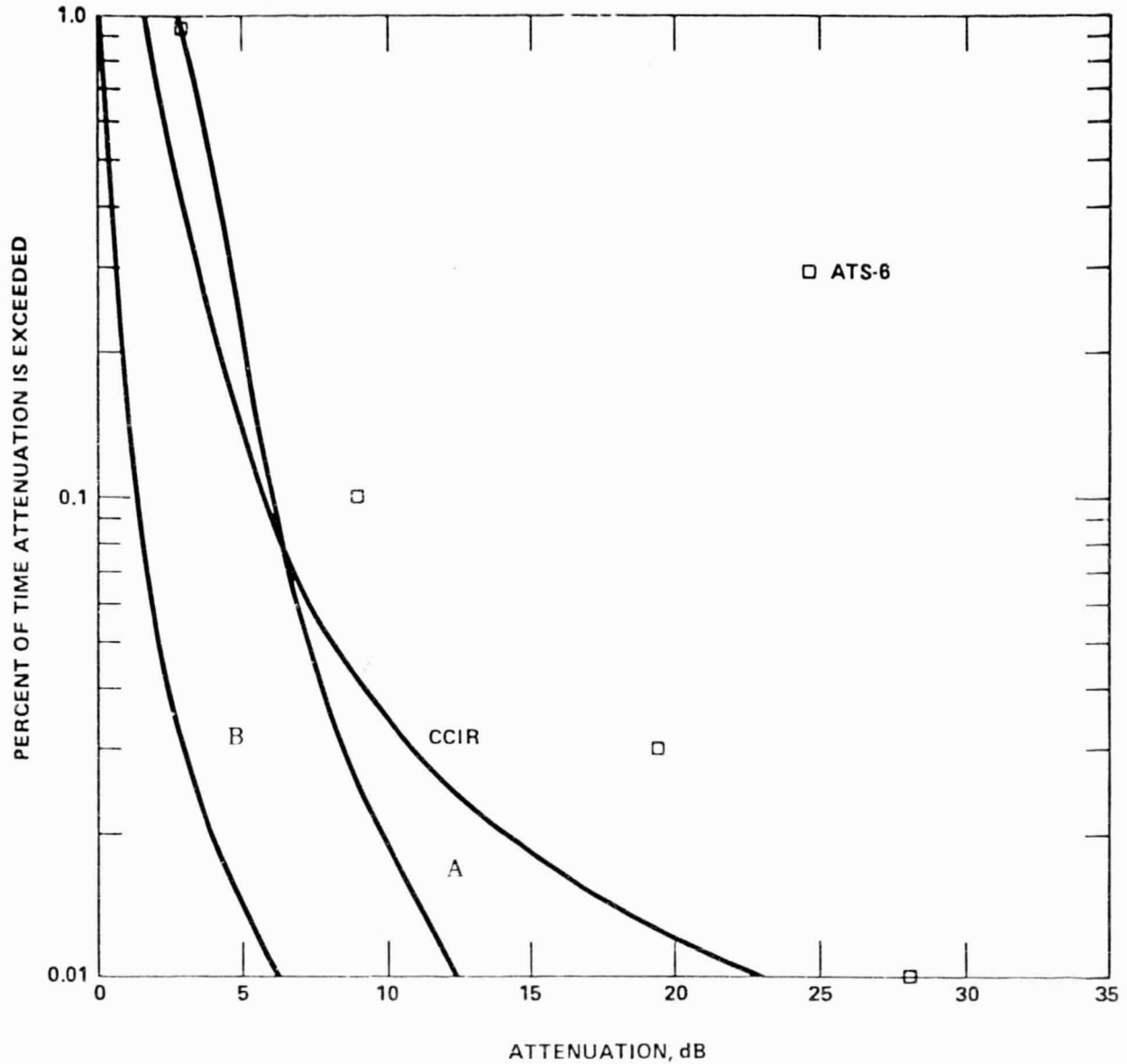
Figure 7-13

CUMULATIVE TIME
DISTRIBUTIONS OF ATTENUATION FOR ZONE # 2
18 GHz
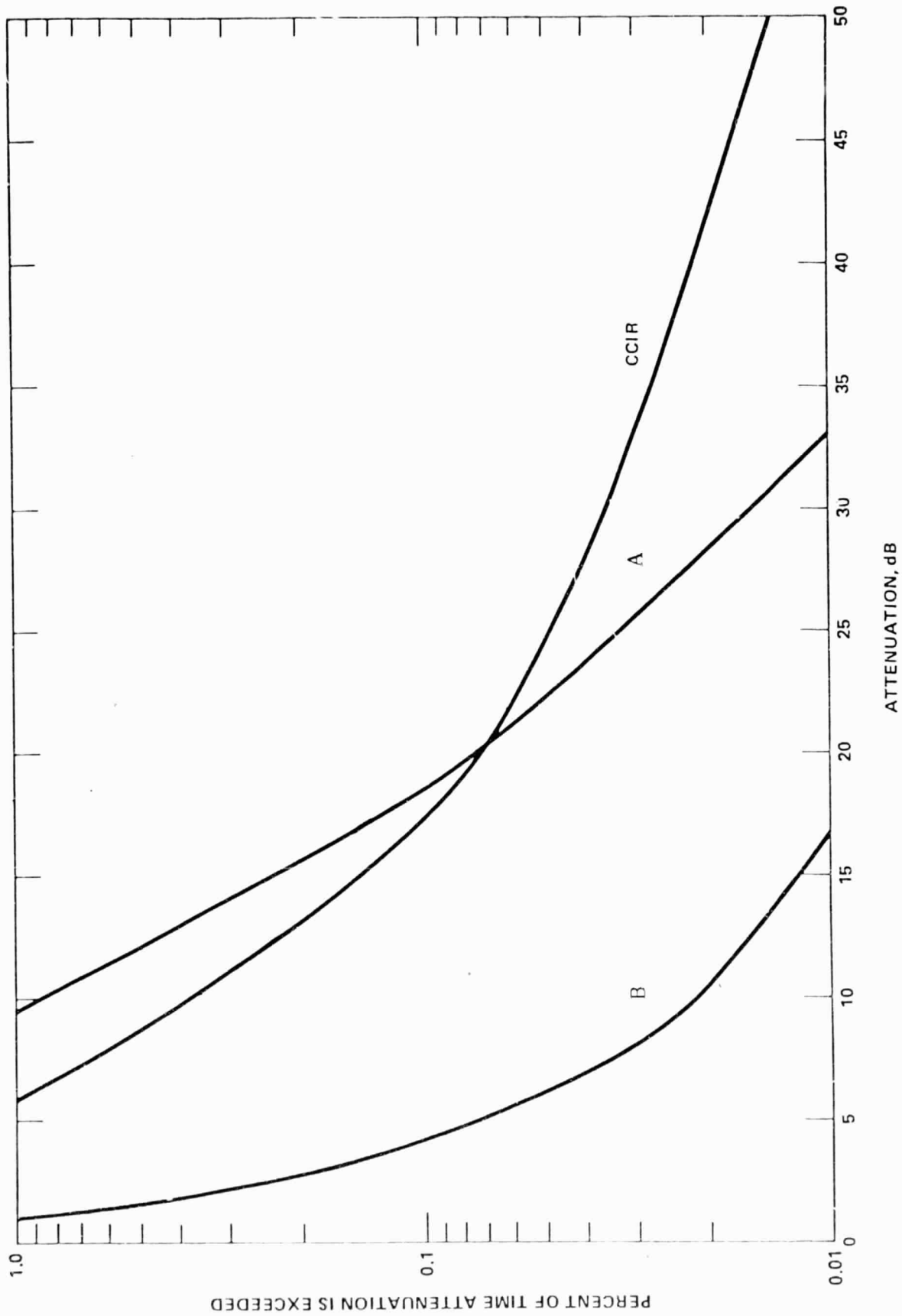
Figure 7-14
CUMULATIVE TIME
DISTRIBUTIONS OF ATTENUATION FOR ZONE # 2
30 GHz
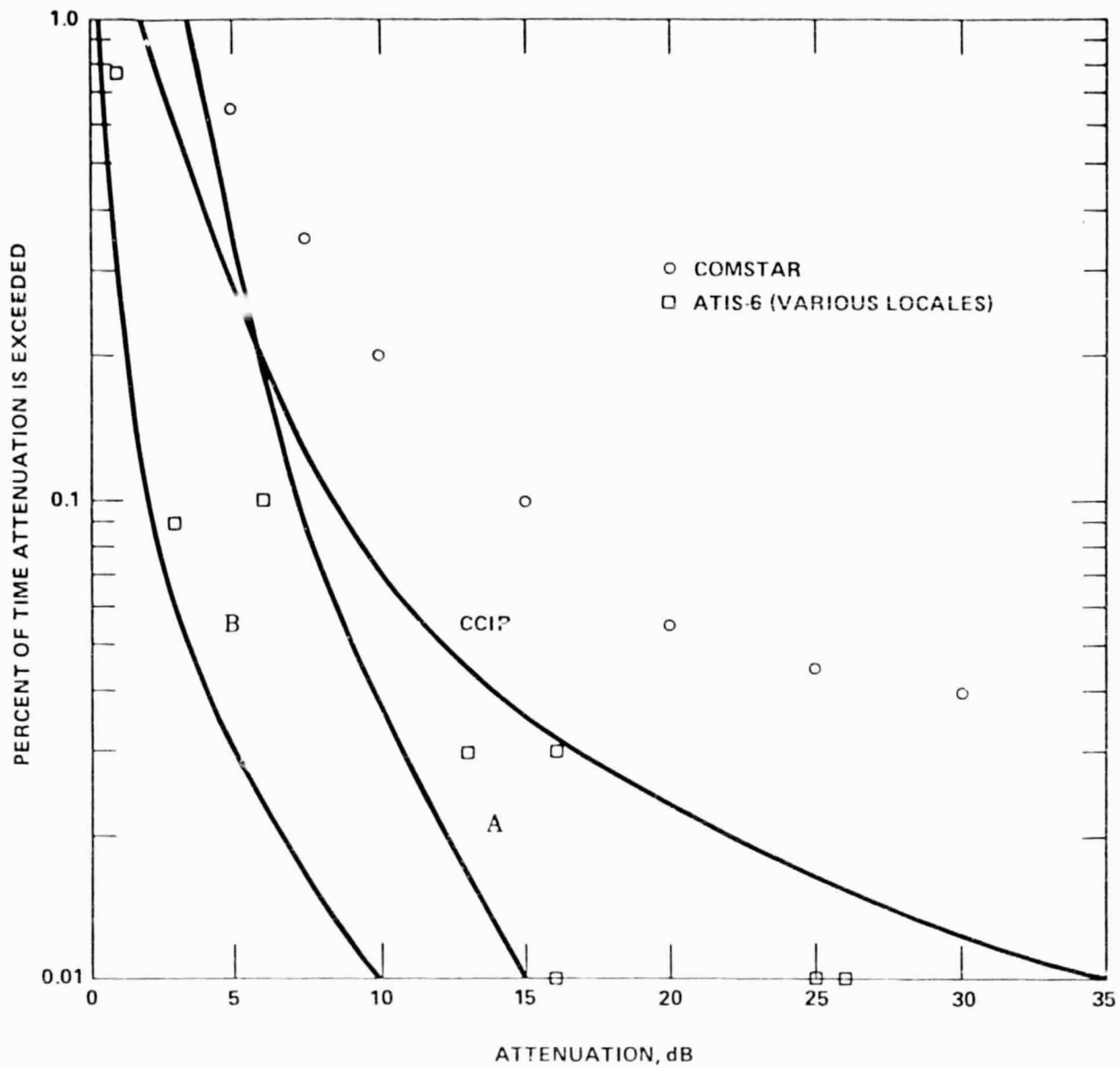
Figure 7-15

CUMULATIVE TIME
DISTRIBUTIONS OF ATTENUATION FOR ZONE # 3
18 GHz
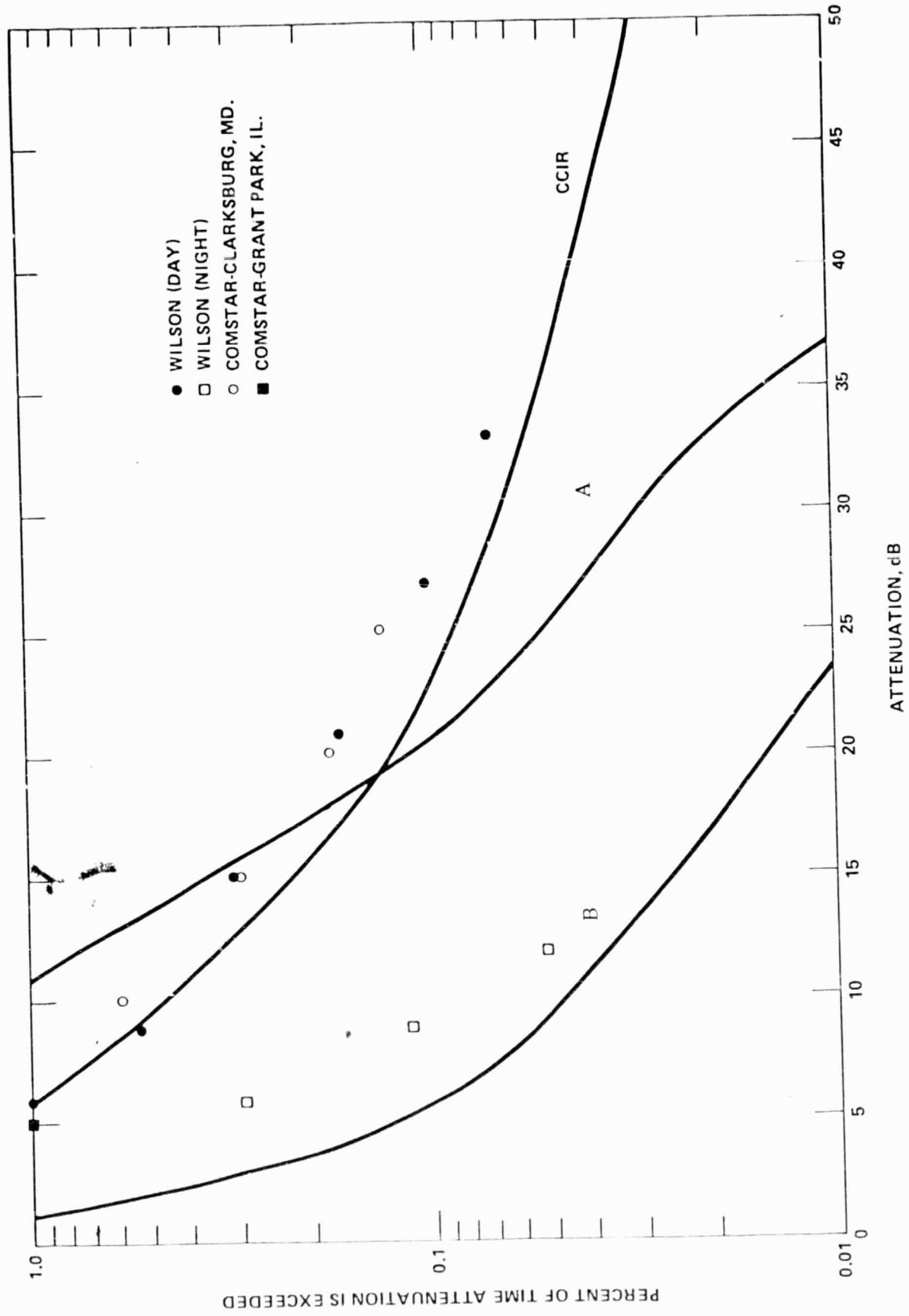
Figure 7-16
CUMULATIVE TIME
DISTRIBUTIONS OF ATTENUATION FOR ZONE # 3
30 GHz
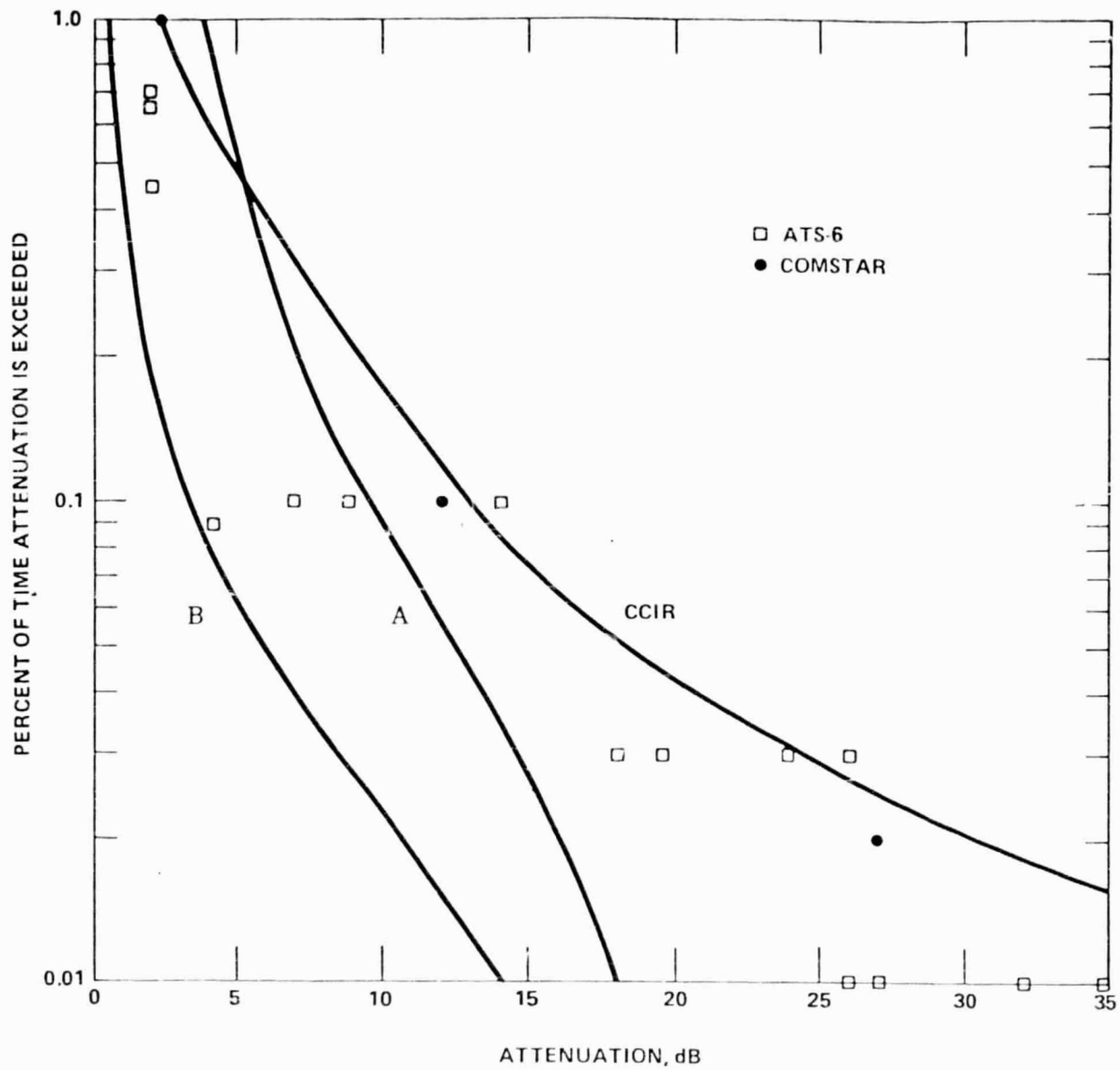
Figure 7-17
CUMULATIVE TIME
DISTRIBUTIONS OF ATTENUATION FOR ZONE # 4
18 GHz
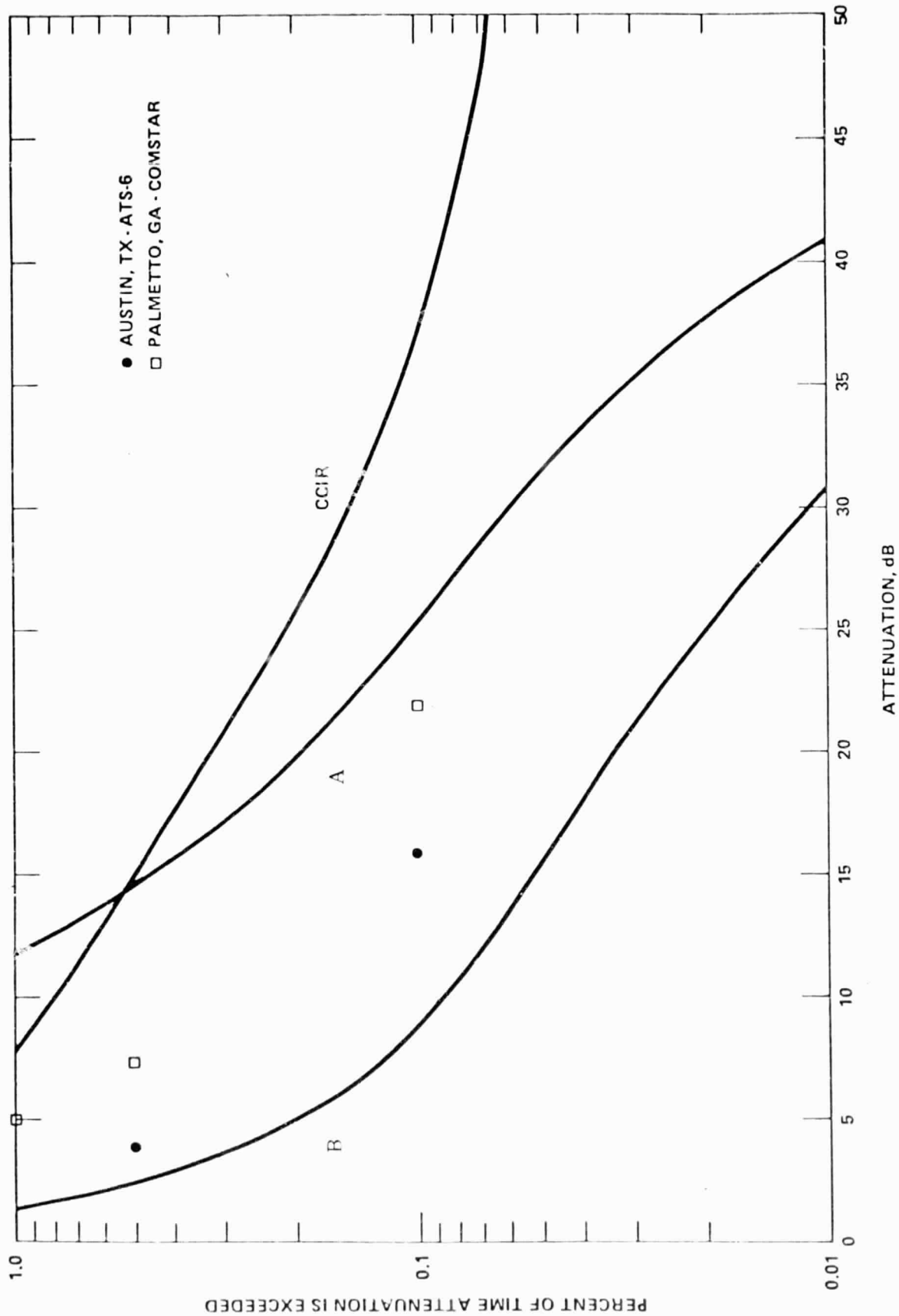
Figure 7-18
CUMULATIVE TIME
DISTRIBUTIONS OF ATTENUATION FOR ZONE # 4
30 GHz
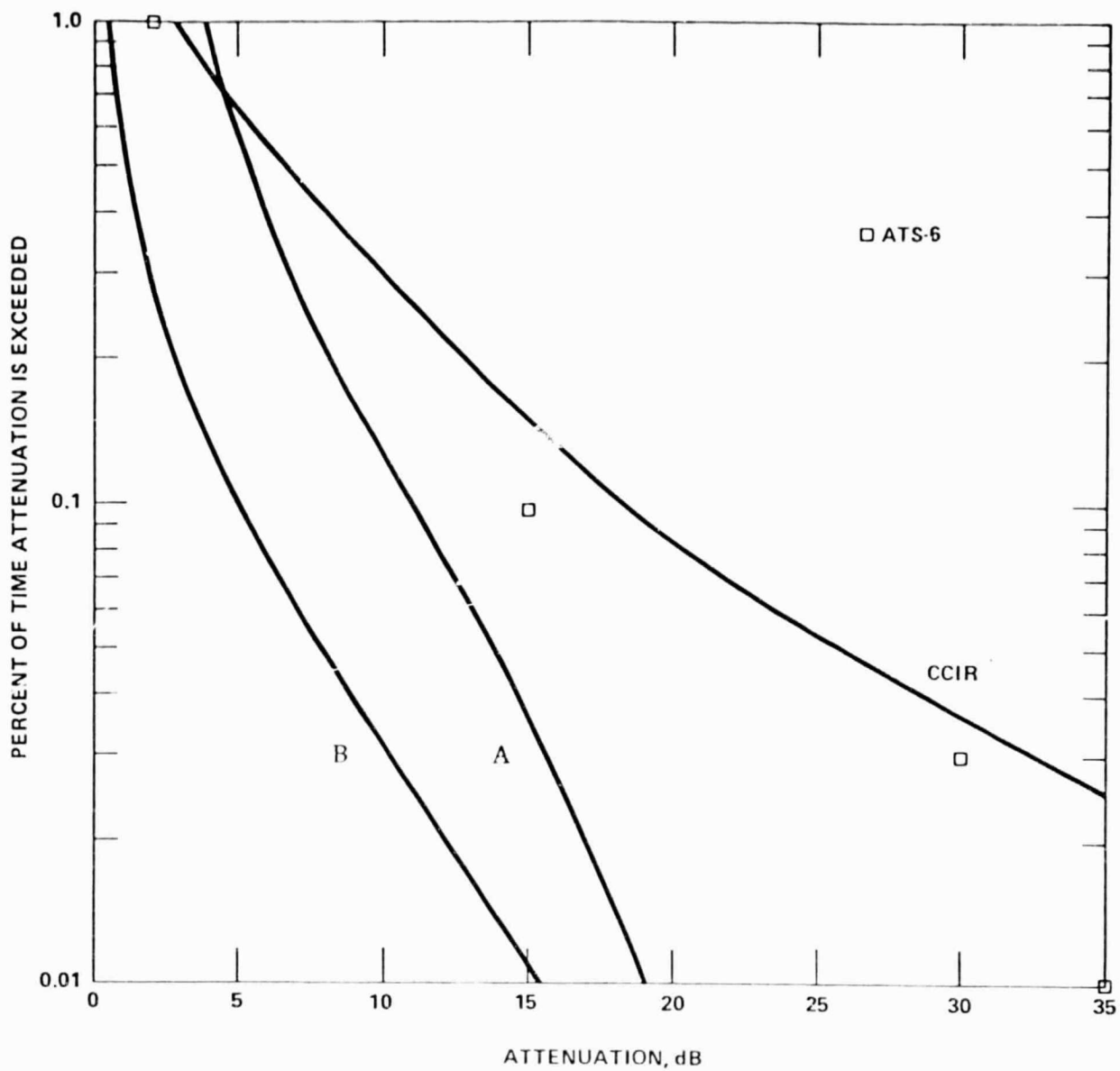
Figure 7-19
CUMULATIVE TIME
DISTRIBUTIONS OF ATTENUATION FOR ZONE # 5
18 GHz
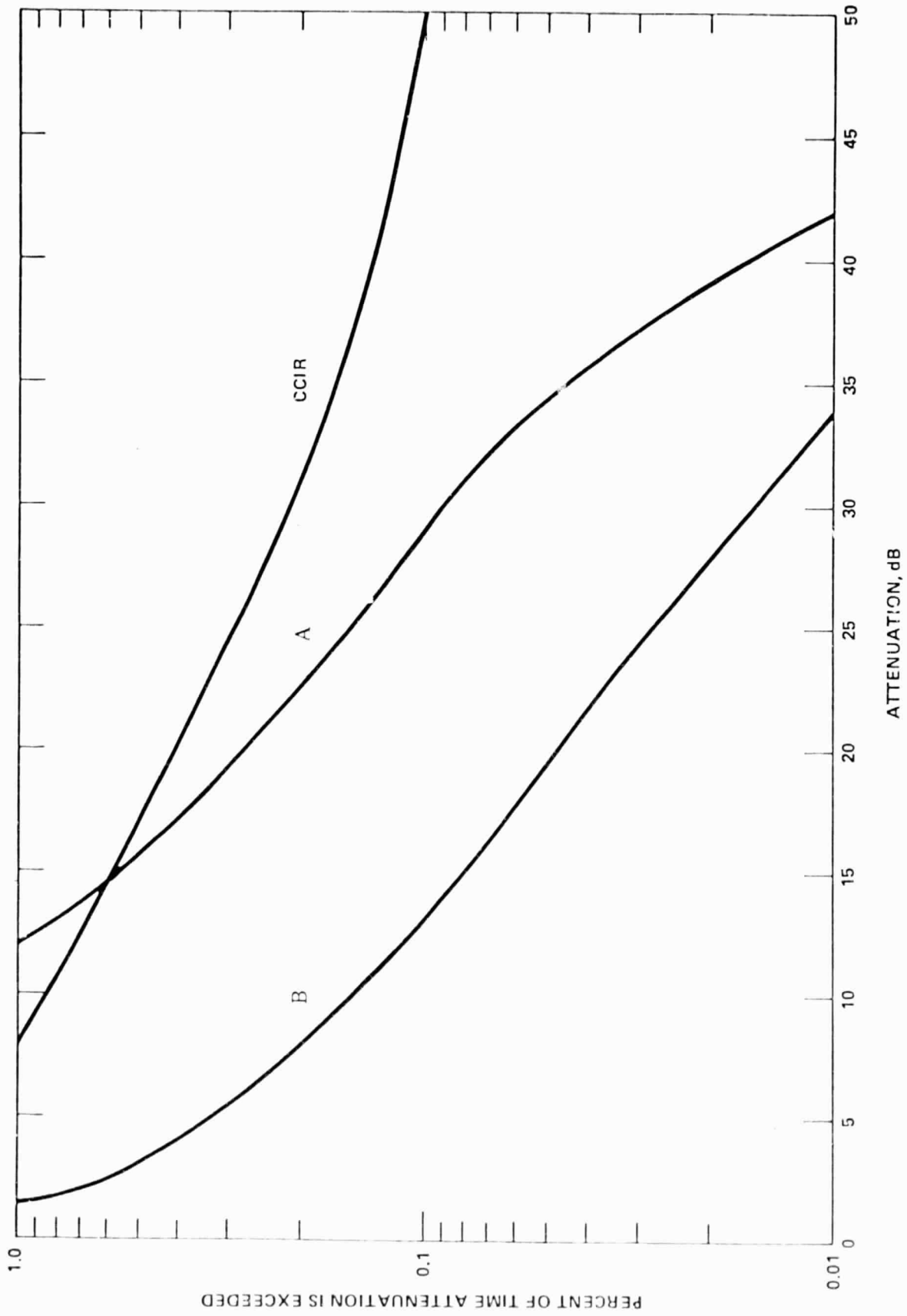
Figure 7-20
CUMULATIVE TIME
DISTRIBUTIONS OF ATTENUATION FOR ZONE # 5
30 GHz
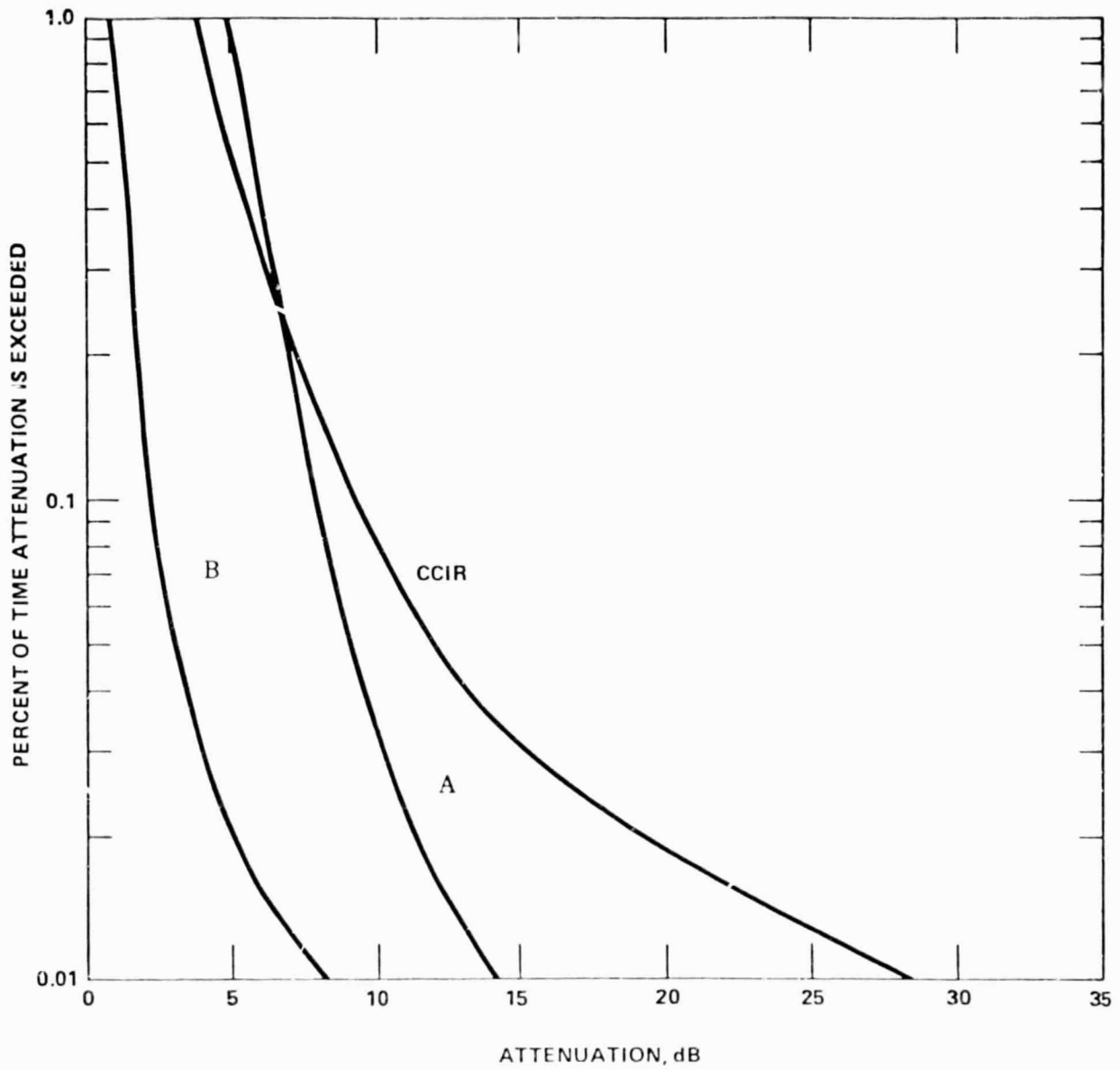
Figure 7-21
CUMULATIVE TIME
DISTRIBUTIONS OF ATTENUATION FOR ZONE # 6
18 GHz
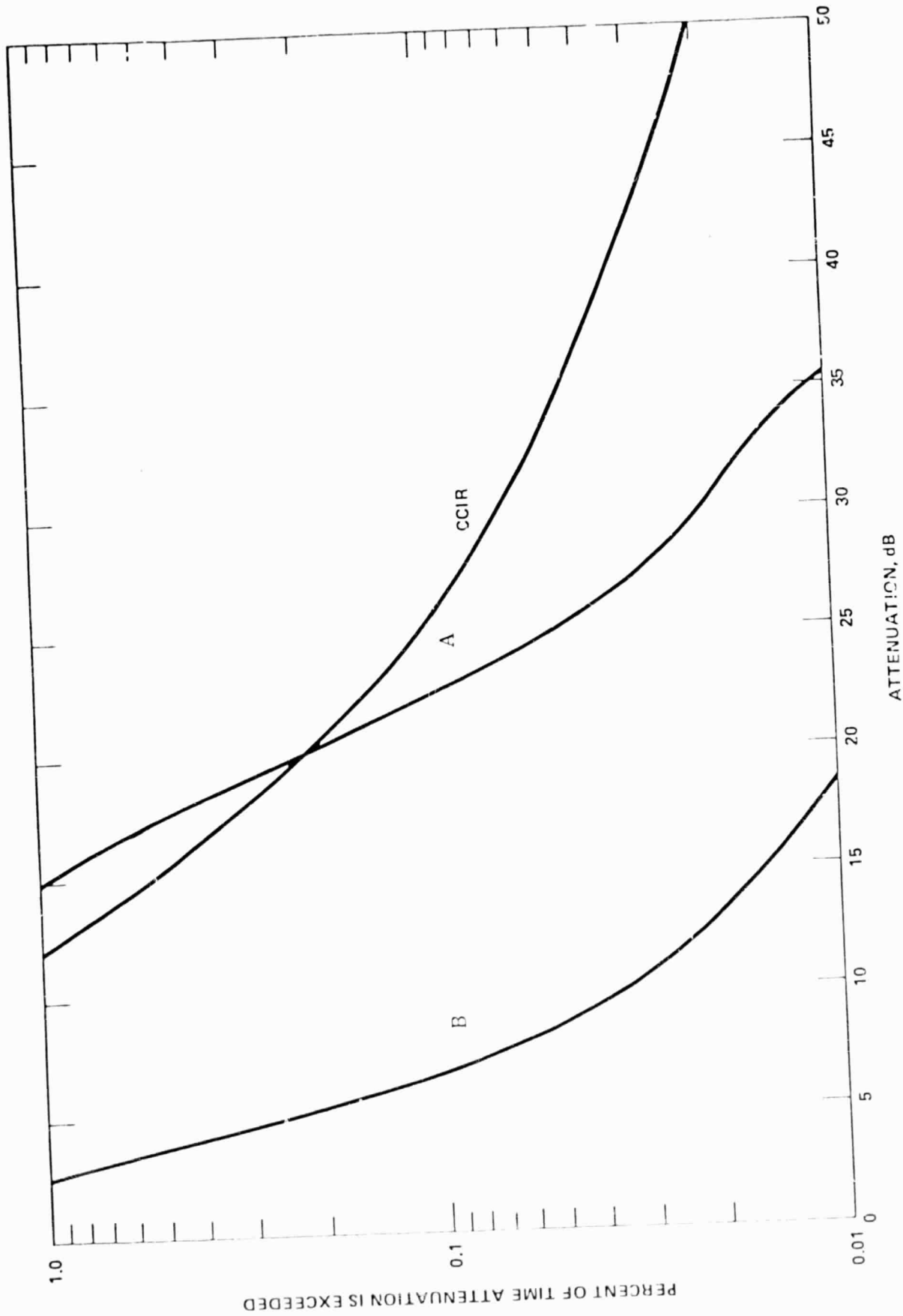
Figure 7-22
CUMULATIVE TIME
DISTRIBUTIONS OF ATTENUATION FOR ZONE # 6
30 GHz

A-103

SECTION 8
SPACE DIVERSITY

8.1   Introduction

Space diversity has been used for a number of years in terrestrial microwave systems. In such systems it is generally used to combat degradations due to ducting, multipath and other phenomena characteristic of paths near and parallel to the earth's surface. The use of space (or "separation") diversity with satellite links is primarily intended to combat high attenuation due to intense precipitation. The basis on which the method rests is the observation that regions of intense rainfall are generally limited in geographic extent. This is true for temperate climates. The physical separation of the satellite earth stations then serves to reduce the correlation of such heavy rainfall at the sites. Some simple means of choosing the better of the sites at any instant then completes the diversity system.

8.2   Background

A useful tool in the study of diversity systems is the concept of "diversity gain", as developed by D. Hodge of Ohio State University (ref. 23). The derivation of diversity gain is best illustrated by a figure. In Figure 8-1 the two curves to the right are the individual cumulative time distributions of attenuation for the two sites operating individually. The single curve to the left is the cumulative time distribution for diversity operation; that is, the better of the two stations at any instant. As shown, the distance between the curves for the same percentage time is the diversity gain in decibels. Figure 8-2 shows some plots of actual diversity gain as measured using ATS-6 (ref. 24).
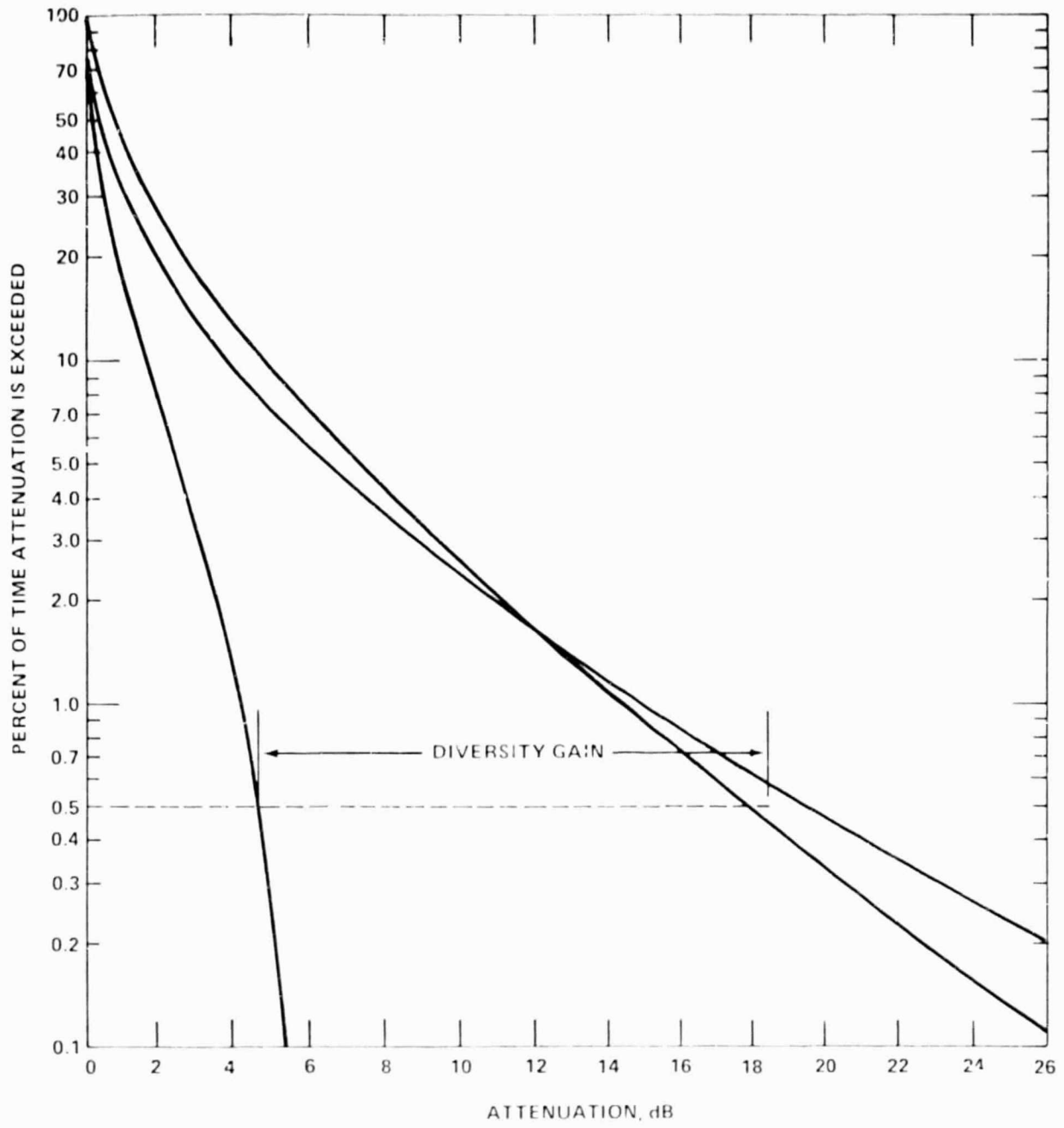
Figure 8-1

DIVERSITY GAIN CALCULATION

Figure 8-2
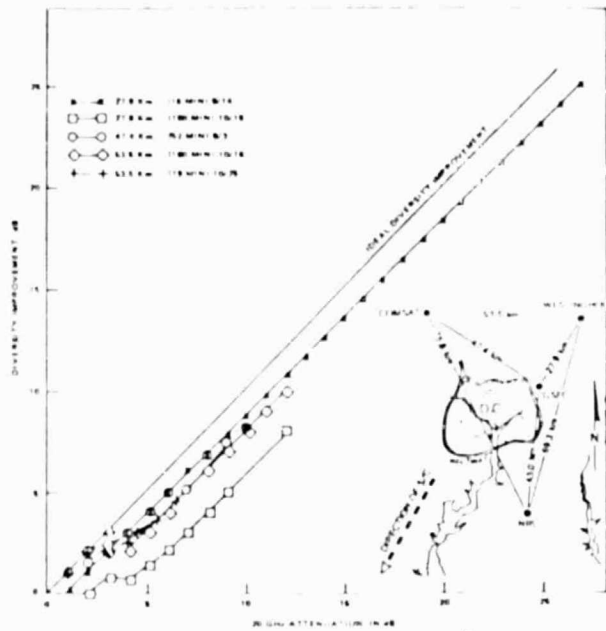
Source: NASA Technical Note (ref. 10)

While a complete theoretical analysis of space diversity would require a much better description of intense rainstorms than we now have, several relationships can be deduced. The degree to which space diversity is useful depends on the frequency. For example, diversity is very rarely needed at 4 GHz for the reason that the attenuation due to rainfall is low enough that significant impairments of the link are very rare. At the higher frequencies, attenuations due to cloud cover and low intensity rain will be rather high and will occur quite often. Against these space diversity is of no avail due to their widespread nature. The designer must consider these levels of precipitation (those occurring more than about 5 percent of the time) to be simply a part of the basic transmission losses.

The diversity gain or advantage will depend to some extent on the physical separation between the stations. At small distances, about 0.5 km, the degree of correlation of rain intensity between the sites will be too high for diversity to be of help. Beyond a certain maximum distance, the correlation will be nearly zero, and the cost of interconnecting the sites for diversity operation will become prohibitive.

Some experimenters have examined these aspects of space diversity and have derived empirical expressions for the relationships.

8.3 Diversity Experiments

A number of experiments have been performed to gain further information about diversity operation at frequencies above 10 GHz. One of the early attempts to quantify the benefits from diversity was that of Hogg (ref. 25). The method used was indirect, in that instead of attenuation measurements, a set of extensive point rainfall measurements were taken and transformed to attenuation figures. The more important data is that which characterizes the rainstorms themselves. The correlation between paths at right angles was found to be low at the higher (above 20 mm/hr) rainfall rates. The size of rain cells varied from about 0.5 km diameter at 100 mm/hr to 1.5 - 2.0 km diameter at 60 mm/hr, thus tending to confirm the hypothesis about regions of intense rainfall.

Freeny and Gabbe (ref. 9) also found that the regions of high rainfall were physically limited. Reference 9 includes several isometric time plots of rainstorms passing through the Bell Labs rain gauge field. These show that although correlation of rainfall at right angles to the storm's direction is relatively high, the correlation along the direction of the storm's travel is very low. This would seem to indicate that the diversity stations should be located along a line in the direction of the prevailing winds. A more important consideration is that the stations be located along a line nearly at a right angle to the path toward the satellite. This provides that the paths from the earth stations to the satellite will traverse physically separate regions of the atmosphere. If the two considerations can be combined, so much the better.

A 16 GHz, 3-radiometer diversity experiment (ref. 16) found that a separation of 2 miles was not sufficient to give a worthwhile diversity gain at this frequency. However, separations of 7 and 9 miles gave good results on the order of 5 dB at a single-site fade depth of 8 dB. See Figure 8-3.

Hodge of Ohio State University has determined an empirical relationship between the separation distance, fade depth and diversity gain based on measurements made using ATS-V. These measurements were taken at 15.3 GHz (ref. 23) and are shown in Figure 8-4. This relation is as follows:

$$G = a(1-e^{-bD})$$

where

$$G = \text{Diversity gain in dB}$$
$$D = \text{The site separation distance in km}$$
$$a = A-3.6(1-e^{-0.24A})$$
$$A = \text{The single site attenuation in dB}$$
$$b = 0.46(1-e^{-0.26A})$$

Data taken using ATS-6 indicated that the diversity gain was not strongly dependent on frequency. The optimum separation for the diversity sites seems to be about 8 to 10 km. This is consistent with the rainfall data recorded by Freeny and Gabbe. In their analysis they found that the empirical probability of simultaneous rainfall at a given rate at two stations reached a minimum at about 8 to 12 km separation. In particular, the minimum was lowest and most pronounced at the higher rainfall rates. See Figure 8-5.

Data taken at the University of Texas (ref. 10) using ATS-6 are shown in Figure 8-7. These were measured at 30 GHz. The diversity gain is calculated in the manner already presented. The results are fairly consistent with those of Hodge.
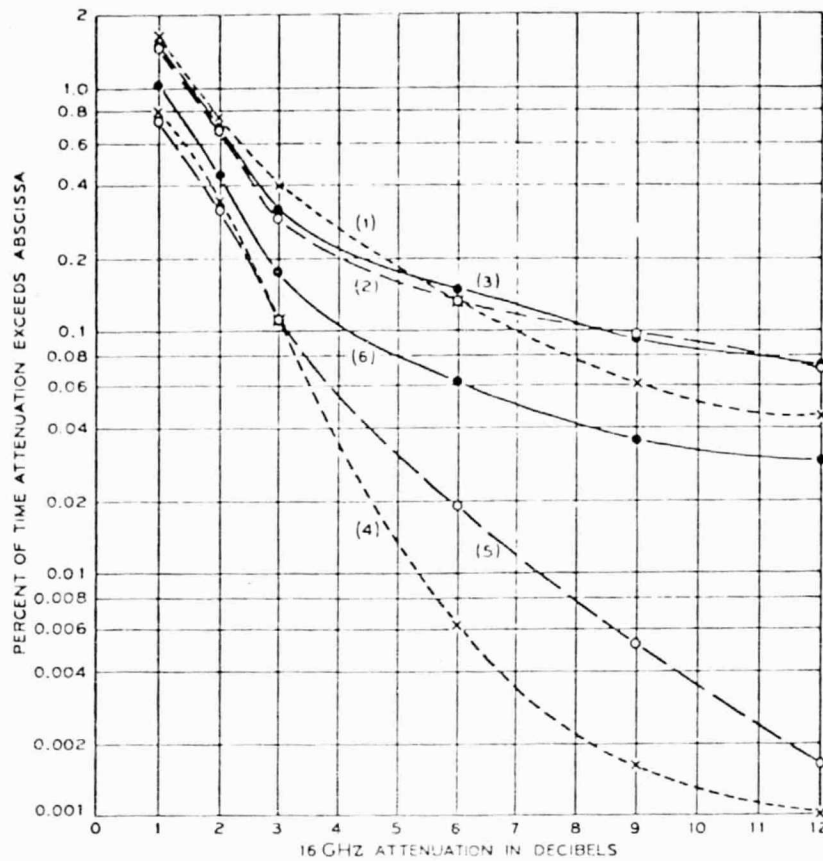
Fig. 1—16 GHz radiometer rain data, April 1, 1969 through August 7, 1969; total time 3081 hrs. Distributions of attenuation for the individual stations: (1) x- - - -x Sayreville; (2) o— — ——o Crawford Hill (3) o————o Parkway. Distributions of attenuation for pairs of stations in diversity: (4) x- - - -x Crawford Hill to Sayreville, 7 miles; (5) o— — ——o Parkway to Sayreville, 9 miles; (6) o————o Parkway to Crawford Hill, 2 miles.

Figure 8-3

Source: A Three-Radiometer Path-Diversity
Experiment
R. W. Wilson (ref. 26)

SITE DIVERSITY MEASUREMENTS AT COLUMBUS, OHIO

UTILIZING THE ATS-5 SATELLITE
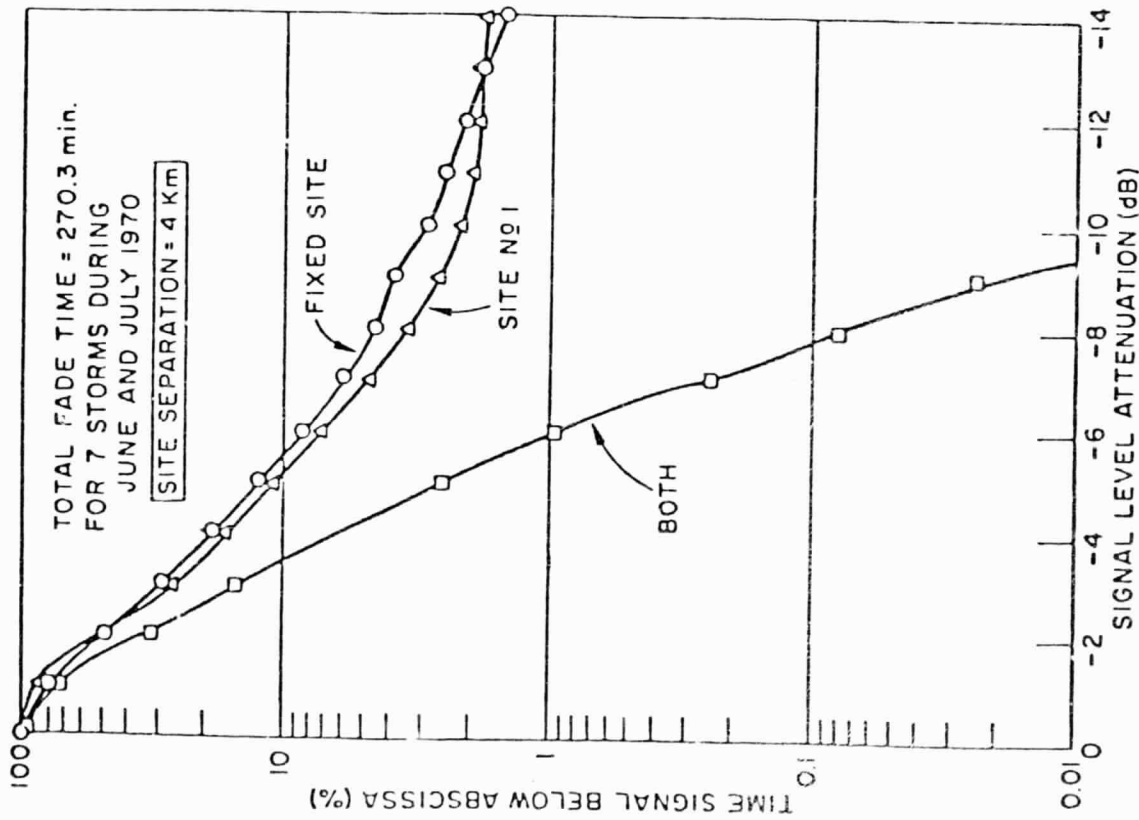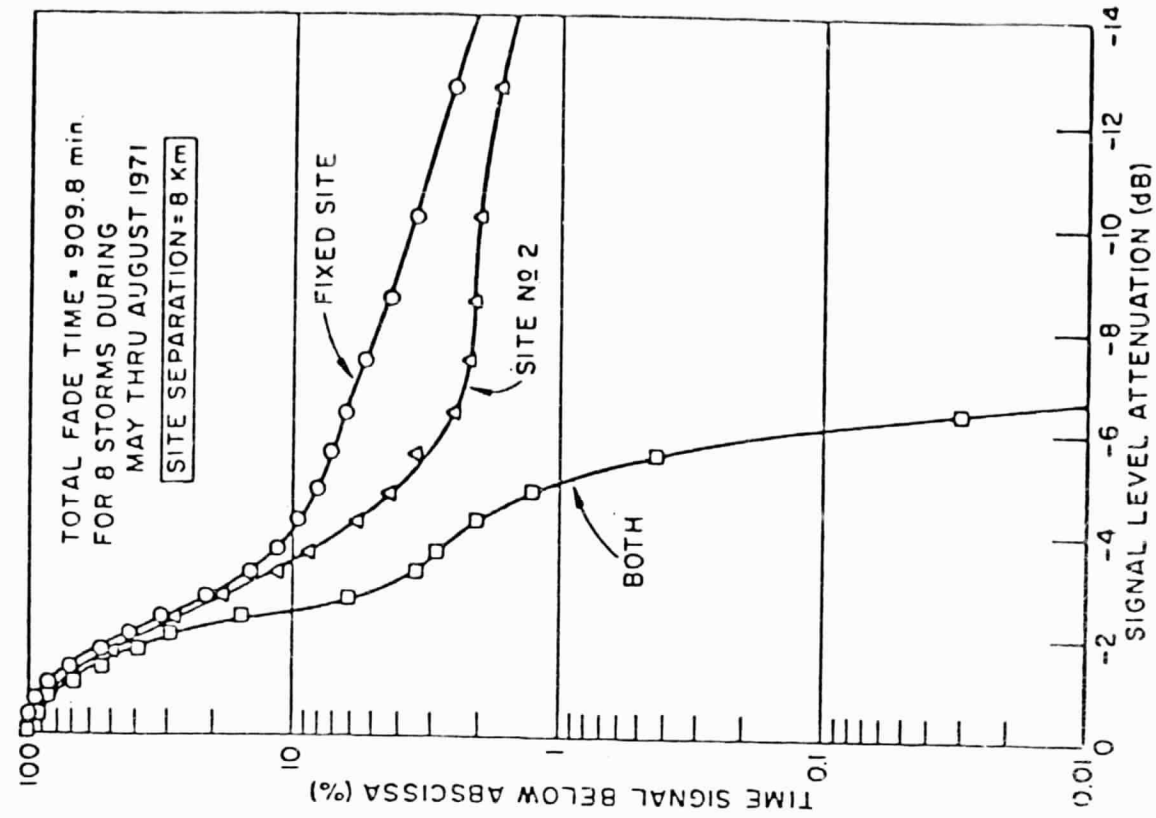
Figure 8-4
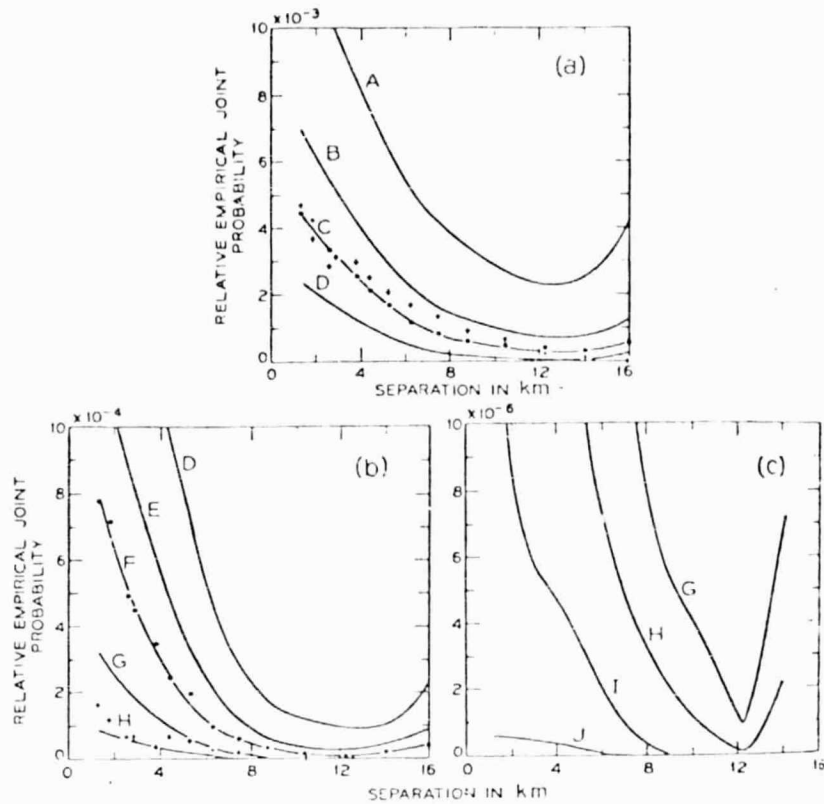
Fig. 23 — Relative empirical joint probability that the rain rate at both stations exceeds the value with which the curve is labeled versus separation in kilometers. Crosses in (a) and (b) indicate the upper quartiles of the distributions of joint probabilities that the rain rate is greater than 50 and 110 mm per hour, respectively, when the 27 rainfalls are considered separately.

Minimum Rain Rate (mm per hour)

A	B	C	D	E	F	G	H	I	J
30	40	50	70	90	110	140	170	200	240

Figure 8-5

Source: (ref. 9)

Figure 8-7
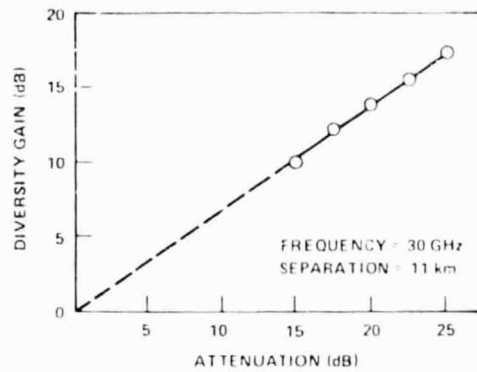
Figure 17. Diversity gain as a function of single
site attenuation.

Source: (ref. 10)

8.4   Diversity Model

Judging from the time distributions of attenuation at 18 and 30 GHz, it
is apparent that space diversity will be needed in order to use these frequency
bands.   There is still a lack of experimental data; however, that which has been
taken tends to be quite consistent.   The relation derived by Hodge is probably the
best working formula currently available.   A family of curves for diversity gain as a
function of single-site fade depth is shown in Figure 8-8.   The separation distance is
the parameter varied.
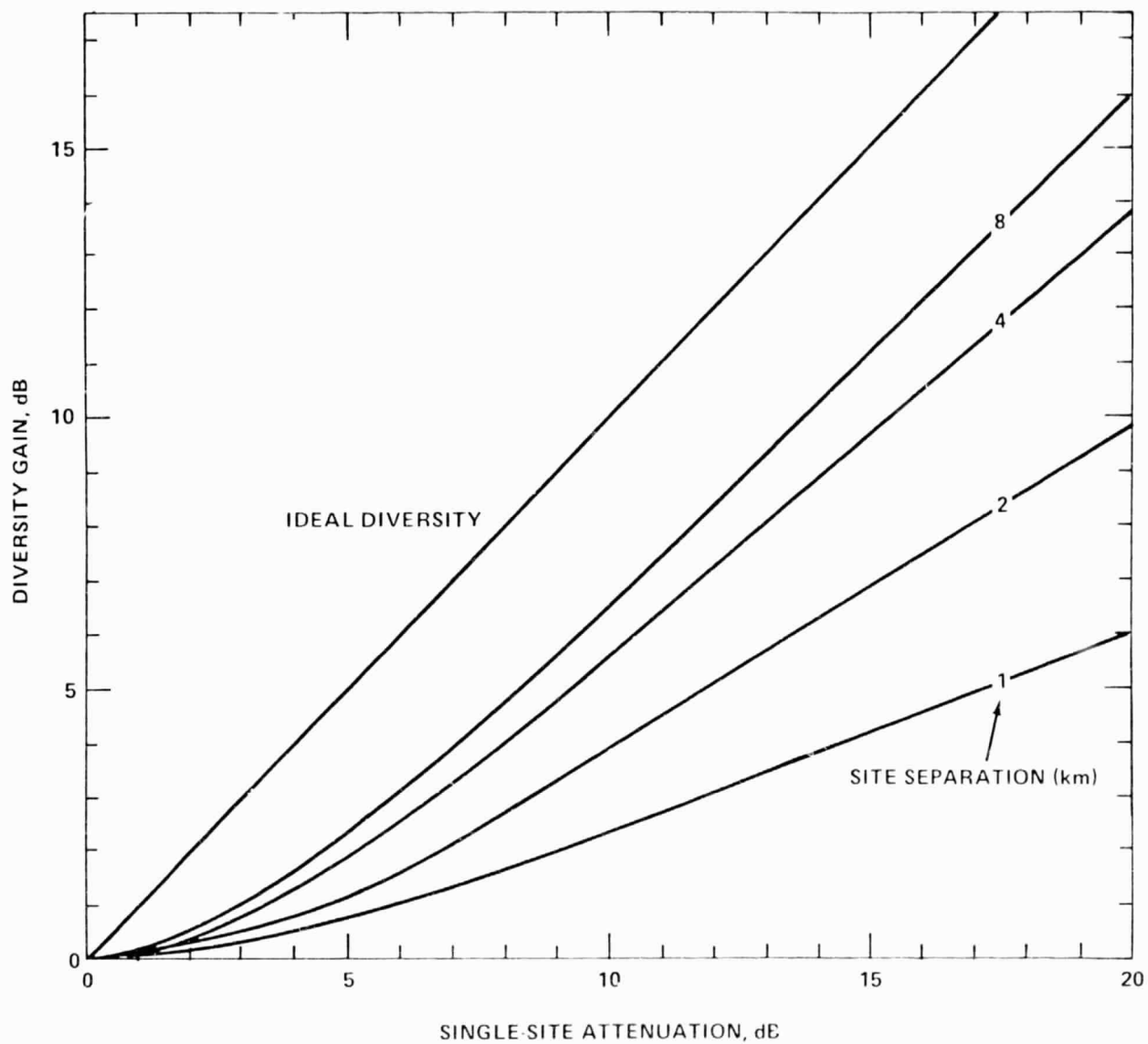
Figure 8-8

DIVERSITY GAIN FOR VARIOUS SEPARATIONS

8.5   Discussion of Diversity Model

The diversity model presented in Section 8.4 should be used with caution for the reasons stated below:

Firstly, the data from which the model is developed does not include (as far as we are aware) any extensive measurements from regions which experience primarily the "widespread" type of rain. The Pacific Northwest is one such area. Little or no work has been done in such regions, insofar as actual measurements are concerned. Generally speaking, this may mean that the model is not appropriate for such a region; we have no firm indication. However, a comparison of the values given by the Hodge model with those given by the "squaring of probabilities", or completely uncorrelated rainfall analysis, shows that for such a region, the Hodge model is somewhat optimistic at 30 GHz. Tables 5 and 6 show this comparison for the six rain model zones. Zone 6 is the region of interest.

Secondly, the model yields rather low values for diversity attenuation even for quite high values of single-site attenuation. Typically, values of single-site fading of more than 100 dB are reduced to less than 10 dB. While it is quite likely that the area of precipitation that produces a 100 dB fade is very small (much less than 1 kilometer in diameter), it seems somewhat less likely that the storm producing such precipitation would have a range of significant heavy rain that is much less than 10 to 15 km in diameter. However, this is somewhat conjectural, since no 100 dB fades have been measured that we are aware of. Additionally, the plots of diversity gain made from actual diversity experiments, where the data is known to be free from artifacts, do show the unbounded increase of diversity gain as the single-site fading increases. Several studies of thunderstorm size have found the sizes to be quite small. One study concluded that 84 percent were less than 7 miles in diameter and that the largest observed was only 9 to 10 miles across. The existence of large "general rain" storms consisting of a large number of intense cells were discovered in a study of New England storms. This effect would likely limit the possible diversity well below the theoretical maximum.

Our conclusion is that the Hodge model is usable for single-site attenuations of 20 to 25 dB or less, with some precautions in areas such as the Pacific Northwest. The values given for single-site fades above this level are not confirmed; however, no model exists which has any more validity.

It will be necessary to obtain additional diversity measurements over longer periods of time, before transmission margins with site diversity operation can be determined with certainty. Of particular interest is the question of diversity gain under conditions of widespread rain in various rain zones. Until additional diversity data is obtained, it is recommended to increase propagation margins in satellite systems design by several dB relative to the calculated margins.

Table 8-1

Comparison of Diversity Models at 18 GHz

Rain Zone	99%		99.5%		99.9%		99.95%		99.99%	
	Hodge	P^2	Hodge	P^2	Hodge	P^2	Hodge	P^2	Hodge	P^2
1	0.2	0	0.6	0	2.1	0	2.6	0	3.5	0.2
2	0.7	0	1.4	0	2.8	0	3.1	0.3	4.0	0.9
3	1.1	0	1.9	0	3.1	0.3	3.5	0.6	4.3	1.6
4	1.5	0	2.3	0	3.7	0.4	4.0	0.8	4.6	2.1
5	1.6	0	2.4	0	3.9	0.4	4.2	0.7	4.8	2.2
6	2.1	0.3	2.6	0.6	3.3	1.5	3.5	2.2	4.2	4.1

Table 8-2

Comparison of Diversity Models at 30 GHz

Rain Zone	99% Hodge	P^2	99.5% Hodge	P^2	99.9% Hodge	P^2	99.95% Hodge	P^2	99.99% Hodge	P^2
1	0.6	0	1.6	0	3.5	0	3.8	0	4.2	0.8
2	1.9	0	2.9	0	3.8	0	4.0	1.1	4.9	3.1
3	2.5	0	3.3	0	4.0	1.1	4.2	2.1	5.4	5.2
4	3.0	0	3.6	0	4.3	1.5	5.0	2.7	6.0	6.6
5	3.0	0	3.7	0	4.7	1.5	5.2	2.5	6.3	6.9
6	3.5	1.1	3.7	1.9	4.1	4.9	4.2	6.9	5.1	12.1

SECTION 9

VALUES OF ATTENUATION FOR SELECTED U.S. CITIES

We have computed the attenuation values for a list of selected U.S. cities. A computer program was written for this purpose; the values are printed in the format illustrated in Figure 9-1. The actual values predicted by the model are shown in Table 9-1 for a satellite position of 100 degrees West longitude, and in Table 9-2 for a satellite position of 80 degrees West.

The predicted values of attenuation using space diversity operation were also computed for the same locations. These are presented in Tables 9-3 and 9-4 for satellite positions of 100 degrees and 80 degrees, respectively. As pointed out in Section 8.5, it is recommended to add an additional transmission margin of several dB, in order to allow for present uncertainties in the diversity model in a conservative manner.

The calculations are based on the CCIR model, with the relevant parameters properly adjusted for each city. The diversity values are computed using the model of Section 8, with an assumed separation of 8 km between diversity locations.

Figure 9-1

SAMPLE OUTPUT OF 18/30 GHz ATTENUATION ANALYSIS PROGRAM

| Satellite Longitude | Elevation Angle to Satellite | Percent of Time Values | | | | Availabilities Outage |
		99.0% 1.000%	99.5% 0.500%	99.9% 0.100%	99.95% 0.050%	99.99% 0.010%
Satellite Location of 100.0 degrees						
New York	35.7					
Rain Rate (mm/hr)		3.0	5.7	13.2	17.6	53.1
18 GHz Attenuation (dB)		1.6	2.9	6.3	8.2	23.5
30 GHz Attenuation (dB)		4.9	8.7	18.0	23.1	57.6

Table 9-1

Attenuation Values for Satellite at 100 Degrees West

SATELLITE LOCATION OF 100.0 DEGREES

		99.000%	99.500%	99.900%	99.950%	99.990%
		1.000%	0.500%	0.100%	0.050%	0.010%
NEW YORK	35.7	3.0	5.7	13.2	17.6	53.1
		1.6	2.9	6.3	8.2	23.5
		4.9	8.7	18.0	23.1	57.6
LOS ANGELES	45.0	0.6	1.5	7.3	10.2	17.7
		0.3	0.9	3.4	4.6	7.9
		1.0	2.6	10.0	13.5	22.3
CHICAGO	40.0	2.3	4.9	12.8	18.0	59.9
		1.0	2.2	5.4	7.5	24.1
		3.4	6.6	15.5	21.1	58.3
PHILADELPHIA	37.0	2.9	5.7	13.2	17.9	55.2
		1.5	2.8	6.3	8.3	24.3
		4.8	8.6	18.0	23.4	59.3
DETROIT	38.0	2.1	4.6	12.0	16.3	50.9
		1.0	2.1	5.2	7.0	21.1
		3.2	6.4	15.1	19.3	52.0
SAN FRANCISCO	40.3	1.3	3.1	9.5	12.5	21.1
		0.7	1.5	4.5	5.8	9.6
		2.3	4.8	13.1	16.7	26.6
WASHINGTON	38.9	2.7	5.5	13.4	18.0	62.3
		1.4	2.7	6.2	8.7	26.9
		4.4	8.1	17.9	24.3	64.7
BOSTON	32.9	3.3	6.0	13.2	17.0	43.8
		1.8	3.1	6.4	8.1	19.7
		5.5	9.4	18.5	23.0	52.1
HOUSTON	54.6	2.2	5.5	28.2	51.1	105.0
		1.0	2.4	12.4	22.6	45.2
		3.1	7.4	33.7	55.3	101.5
DALLAS FT. WORTH	50.3	1.3	3.5	16.3	34.6	88.4
		0.6	1.7	7.3	15.3	38.1
		2.1	5.2	20.6	41.0	87.4

Table 9-1, Continued
Attenuation Values for Satellite at 100 Degrees West

SATELLITE LOCATION OF 100.0 DEGREES

| | | 99.000% | 99.500% | 99.900% | 99.950% | 99.990% |
		1.000%	0.500%	0.100%	0.050%	0.010%
ATLANTA	47.4	2.3	6.0	20.4	40.6	94.5
		1.4	2.9	9.5	13.5	41.5
		4.5	3.3	26.5	49.2	94.4
NEWARK	35.7	3.1	5.3	13.3	17.9	54.2
		1.6	2.9	6.3	3.4	23.9
		5.1	3.3	13.2	23.5	53.5
ANAHEIM	46.0	0.5	1.4	6.9	9.6	17.1
		0.2	0.7	3.2	4.4	7.7
		0.3	2.3	9.5	12.9	21.6
PITTSBURGH	37.9	2.5	5.2	12.9	17.9	58.1
		1.2	2.4	5.3	7.9	24.4
		3.9	7.4	16.6	22.2	59.2
ST. LOUIS	44.2	2.3	5.0	13.5	20.5	68.8
		1.0	2.2	5.7	3.6	29.0
		3.3	6.7	16.4	24.0	66.5
DENVER	48.4	0.3	2.1	3.6	12.1	30.6
		0.4	0.9	3.6	5.0	18.5
		1.2	2.9	10.6	14.5	33.3
SAN JOSE	41.2	1.4	3.3	9.7	12.7	21.6
		0.7	1.6	4.6	5.9	9.3
		2.4	5.2	13.4	17.0	27.2
MIAMI	52.3	3.3	6.9	32.0	55.2	109.0
		1.6	3.3	14.7	25.2	48.2
		4.9	9.3	39.6	61.7	107.6
CINCINATTI	42.0	2.6	5.4	14.4	23.0	73.7
		1.2	2.5	6.3	9.9	30.3
		3.9	7.5	17.9	37.2	71.3
MILWAUKEE	33.9	1.9	4.3	11.6	15.9	48.8
		0.9	1.9	4.9	6.6	19.5
		2.3	5.3	14.1	18.7	51.2

SATELLITE LOCATION OF 100.0 DEGREES

		99.000% 1.000%	99.500% 0.500%	99.900% 0.100%	99.950% 0.050%	99.990% 0.010%
MINNEAPOLIS	37.7	1.7	3.9	11.0	14.8	40.8
		0.7	1.6	4.5	6.0	15.9
		2.4	5.1	12.9	16.9	42.2
BALTIMORE	38.2	2.9	5.7	13.6	19.1	61.8
		1.5	2.8	6.3	8.7	26.7
		4.7	8.4	18.1	24.5	64.3
CLEVELAND	38.6	2.4	5.1	12.7	17.7	56.9
		1.1	2.3	5.6	7.7	23.7
		3.7	7.1	16.1	21.6	57.6
KANSAS CITY	44.5	2.4	5.1	13.7	21.0	69.8
		1.0	2.2	5.7	8.7	28.1
		3.4	6.7	16.4	24.2	66.5
SAN DIEGO	47.9	0.4	1.2	6.5	9.3	17.0
		0.2	0.6	3.0	4.2	7.5
		0.6	2.0	8.9	12.4	21.3
SEATTLE	31.4	0.7	1.8	7.8	10.7	19.6
		0.3	0.9	3.4	4.7	8.3
		1.2	2.9	10.3	13.7	23.2
NEW ORLEANS	53.3	2.8	6.5	33.4	56.6	110.5
		1.3	2.9	14.9	25.2	47.8
		4.0	8.8	40.0	61.3	106.4
PHOENIX	49.0	0.1	0.8	5.3	8.2	15.7
		0.0	0.4	2.8	3.6	6.8
		0.1	1.2	7.1	10.6	19.2

Table 9-2
Attenuation Values for Satellite at 80 Degrees West

SATELLITE LOCATION OF 80.0 DEGREES

| | | 99.000% | 99.500% | 99.900% | 99.950% | 99.990% |
		1.000%	0.500%	0.100%	0.050%	0.010%
NEW YORK	42.2	3.0	5.7	13.2	17.6	53.1
		1.3	2.4	5.5	7.2	21.4
		4.1	7.4	15.7	20.3	52.5
LOS ANGELES	33.5	0.6	1.6	7.3	10.2	17.7
		0.5	1.2	4.5	6.0	10.0
		1.6	3.8	13.4	17.6	28.0
CHICAGO	40.8	2.3	4.9	12.8	18.0	59.9
		1.0	2.1	5.3	7.4	23.9
		3.3	6.5	15.2	20.8	57.6
PHILADELPHIA	43.4	2.9	5.7	13.2	17.9	55.2
		1.3	2.4	5.5	7.4	22.3
		4.0	7.3	15.8	20.8	54.5
DETROIT	40.8	2.1	4.6	12.0	16.3	50.9
		0.9	1.9	4.9	6.6	20.2
		2.9	5.9	14.2	18.7	49.9
SAN FRANCISCO	28.2	1.3	3.1	9.5	12.5	21.1
		1.1	2.3	6.1	7.7	12.3
		3.6	7.2	17.9	22.3	34.3
WASHINGTON	44.7	2.7	5.5	13.4	19.0	62.3
		1.2	2.3	5.6	7.9	25.1
		3.8	7.1	16.0	22.0	60.4
BOSTON	40.1	3.3	6.0	13.2	17.0	43.8
		1.4	2.6	5.5	7.0	17.5
		4.5	7.8	15.7	19.7	46.2
HOUSTON	51.4	2.2	5.5	23.2	51.1	105.0
		1.0	2.6	12.8	23.2	45.9
		3.4	7.8	34.9	57.3	103.0
DALLAS/FT. WORTH	46.5	1.3	3.6	16.3	34.6	93.4
		0.7	1.8	7.7	15.9	39.1
		2.3	5.6	21.3	42.8	93.7

Table 9-2, Continued

Attenuation Values for Satellite at 80 Degrees West

SATELLITE LOCATION OF 80.0 DEGREES

| | | 99.000% | 99.500% | 99.900% | 99.950% | 99.990% |
		1.000%	0.500%	0.100%	0.050%	0.010%
ATLANTA	50.3	2.3	6.0	20.4	40.6	94.5
		1.3	2.7	9.1	17.9	40.6
		4.1	8.3	25.3	47.5	92.4
NEWARK	42.2	3.1	5.9	13.3	17.9	54.2
		1.3	2.5	5.5	7.3	21.3
		4.2	7.5	15.9	20.6	53.4
ANAHEIM	33.5	0.5	1.4	6.9	9.6	17.1
		0.4	1.0	4.2	5.7	9.6
		1.3	3.4	12.6	16.9	27.2
PITTSBURGH	42.1	2.5	5.2	12.9	17.9	53.1
		1.1	2.2	5.3	7.3	23.1
		3.5	6.7	15.2	20.5	55.9
ST. LOUIS	44.2	2.3	5.0	13.5	20.5	63.3
		1.0	2.2	5.7	8.6	29.0
		3.3	6.7	16.4	24.0	66.5
DENVER	37.0	0.8	2.1	9.6	12.1	30.6
		0.4	1.1	4.1	5.7	13.3
		1.5	3.5	12.2	16.6	37.4
SAN JOSE	29.8	1.4	3.3	9.7	12.7	21.6
		1.1	2.4	6.2	7.9	12.5
		3.8	7.6	18.3	22.7	34.9
MIAMI	59.6	3.3	6.9	32.0	55.2	109.0
		1.4	2.9	13.8	24.1	47.0
		4.8	8.7	37.1	59.8	104.8
CINCINATTI	44.6	2.6	5.4	14.4	23.0	73.7
		1.1	2.3	6.0	9.5	29.5
		3.6	7.1	17.1	26.1	69.4
MILWAUKEE	38.7	1.9	4.3	11.6	15.9	43.8
		0.8	1.9	4.9	6.5	19.8
		2.8	5.7	13.9	18.4	50.6

Table 9-2, Continued

Attenuation Values for Satellite at 80 Degrees West

SATELLITE LOCATION OF 80.0 DEGREES

		99.000% 1.000%	99.500% 0.500%	99.900% 0.100%	99.950% 0.050%	99.990% 0.010%
MINNEAPOLIS	36.6	1.7	3.9	11.0	14.8	40.8
		0.8	1.7	4.6	6.1	16.2
		2.5	5.3	13.3	17.4	43.0
BALTIMORE	44.1	2.9	5.7	13.6	19.1	61.8
		1.2	2.4	5.6	7.9	24.9
		4.0	7.3	16.1	22.0	59.9
CLEVELAND	42.0	2.4	5.1	12.7	17.7	56.9
		1.0	2.1	5.2	7.2	22.6
		3.4	6.5	15.0	20.3	55.1
KANSAS CITY	42.4	2.4	5.1	13.7	21.0	69.8
		1.1	2.3	6.0	9.0	29.7
		3.6	7.0	17.0	25.0	68.0
SAN DIEGO	35.2	0.4	1.2	6.5	9.3	17.0
		0.3	0.9	3.9	5.5	9.4
		1.0	2.9	11.8	16.1	26.6
SEATTLE	22.1	0.7	1.8	7.8	10.7	19.6
		0.6	1.3	4.8	6.4	10.9
		2.0	4.4	14.3	18.7	30.5
NEW ORLEANS	53.3	2.8	6.5	33.4	56.6	110.5
		1.3	2.9	14.9	25.2	47.8
		4.0	8.8	40.0	61.3	105.4
PHOENIX	33.2	0.1	0.8	5.3	8.2	15.7
		0.9	0.5	3.0	4.4	8.2
		0.2	1.8	9.1	13.2	23.1

Table 9-3

Attenuation Values Using Diversity for Satellite at 100 Degrees West

SATELLITE LOCATION OF 100.0 DEGREES
DIVERSITY OPERATION - HODGE

		99.000%	99.500%	99.900%	99.950%	99.990%
		1.000%	0.500%	0.100%	0.050%	0.010%
NEW YORK	35.7	3.0	5.7	13.2	17.6	53.1
		1.3	1.9	3.0	3.3	4.1
		2.7	3.4	3.9	4.1	5.0
LOS ANGELES	46.0	0.6	1.6	7.3	10.2	17.7
		0.3	0.7	2.2	2.6	3.3
		0.9	1.8	3.5	3.7	4.1
CHICAGO	40.0	2.3	4.9	12.8	18.0	58.9
		0.9	1.6	2.8	3.2	4.1
		2.2	3.0	3.8	4.0	5.0
PHILADELPHIA	37.0	2.9	5.7	13.2	17.9	55.2
		1.2	1.9	3.0	3.3	4.1
		2.6	3.3	3.9	4.1	5.0
DETROIT	38.0	2.1	4.6	12.0	16.3	50.9
		0.9	1.5	2.7	3.1	4.0
		2.1	3.0	3.8	4.0	4.8
SAN FRANCISCO	40.3	1.3	3.1	9.5	12.5	21.1
		0.6	1.2	2.5	2.9	3.5
		1.7	2.6	3.7	3.9	4.2
WASHINGTON	38.9	2.7	5.5	13.4	19.0	62.3
		1.1	1.9	3.0	3.4	4.2
		2.5	3.3	3.9	4.1	5.1
BOSTON	32.9	3.3	6.0	13.2	17.0	43.8
		1.4	2.1	3.0	3.3	4.0
		2.8	3.4	3.9	4.1	4.8
HOUSTON	54.6	2.2	5.5	28.2	51.1	105.0
		0.8	1.7	3.7	4.1	4.7
		2.1	3.2	4.4	4.9	6.1
DALLAS/FT. WORTH	50.3	1.3	3.6	16.3	34.6	88.4
		0.6	1.3	3.2	3.8	4.5
		1.6	2.7	4.0	4.5	5.7

Table 9-3, Continued

Attenuation Values Using Diversity for Satellite at 100 Degrees West

SATELLITE LOCATION OF 100.0 DEGREES
DIVERSITY OPERATION - HODGE

		99.000% 1.000%	99.500% 0.500%	99.900% 0.100%	99.950% 0.050%	99.990% 0.010%
ATLANTA	47.4	2.3	6.0	20.4	49.6	94.5
		1.2	2.0	3.4	3.9	4.6
		2.5	3.4	4.2	4.7	5.9
NEWARK	35.7	3.1	5.3	13.3	17.9	54.2
		1.3	2.0	3.0	3.3	4.1
		2.7	3.4	3.9	4.1	5.0
ANAHEIM	46.0	0.5	1.4	6.9	9.6	17.1
		0.2	0.6	2.1	2.5	3.2
		0.7	1.7	3.4	3.7	4.0
PITTSBURGH	37.9	2.5	5.2	12.9	17.9	53.1
		1.0	1.7	2.9	3.3	4.1
		2.4	3.2	3.9	4.1	5.0
ST. LOUIS	44.2	2.3	5.0	13.5	20.5	63.3
		0.9	1.6	2.9	3.3	4.2
		2.1	3.1	3.9	4.1	5.2
DENVER	43.4	0.8	2.1	8.6	12.1	30.6
		0.3	0.9	2.2	2.7	3.7
		1.0	2.0	3.6	3.8	4.4
SAN JOSE	41.2	1.4	3.2	9.7	12.7	21.6
		0.7	1.3	2.6	2.9	3.5
		1.7	2.7	3.7	3.9	4.2
MIAMI	52.3	3.3	6.9	32.0	55.2	109.0
		1.2	2.1	3.3	4.1	4.7
		2.7	3.5	4.5	5.1	6.2
CINCINATTI	42.0	2.6	5.4	14.4	23.0	73.7
		1.0	1.8	3.0	3.5	4.3
		2.3	3.2	3.9	4.2	5.3
MILWAUKEE	33.9	1.9	4.3	11.6	15.9	48.0
		0.8	1.4	2.7	3.0	4.0
		1.9	2.9	3.3	4.0	4.8

Table 9-3, Continued

Attenuation Values Using Diversity for Satellite at 100 Degrees West

SATELLITE LOCATION OF 100.0 DEGREES
DIVERSITY OPERATION - HODGE

		99.900% 1.000%	99.500% 0.500%	99.900% 0.100%	99.950% 0.050%	99.990% 0.010%
MINNEAPOLIS	37.7	1.7	3.9	11.0	14.3	40.3
		0.7	1.3	2.5	2.9	3.9
		1.7	2.7	3.7	3.9	4.6
BALTIMORE	33.2	2.9	5.7	13.6	19.1	61.3
		1.2	1.9	3.0	3.4	4.2
		2.6	3.3	3.9	4.1	5.1
CLEVELAND	33.6	2.4	5.1	12.7	17.7	56.9
		1.0	1.7	2.8	3.2	4.1
		2.3	3.1	3.9	4.0	5.0
KANSAS CITY	44.5	2.4	5.1	13.7	21.0	69.3
		0.9	1.6	2.9	3.4	4.2
		2.2	3.1	3.9	4.1	5.2
SAN DIEGO	47.9	0.4	1.2	6.5	9.3	17.0
		0.2	0.5	2.0	2.5	3.2
		0.6	1.5	3.4	3.7	4.0
SEATTLE	31.4	0.7	1.3	7.3	10.7	19.6
		0.3	0.8	2.2	2.6	3.3
		1.0	1.9	3.5	3.8	4.1
NEW ORLEANS	53.3	2.3	6.5	33.4	56.6	110.5
		1.1	2.0	3.8	4.1	4.7
		2.4	3.4	4.5	5.1	6.2
PHOENIX	49.0	0.1	0.3	5.3	8.2	15.7
		0.0	0.3	1.7	2.2	3.1
		0.1	1.0	3.1	3.5	4.0

Table 9-4

Attenuation Values Using Diversity for Satellite at 80 Degrees West

```
SATELLITE LOCATION OF  80.0 DEGREES
DIVERSITY OPERATION - HODGE
```

		99.000%	99.500%	99.900%	99.950%	99.990%
		1.000%	0.500%	0.100%	0.050%	0.010%
NEW YORK	42.2	3.0	5.7	13.2	17.6	53.1
		1.1	1.7	2.8	3.2	4.0
		2.4	3.2	3.8	4.0	4.8
LOS ANGELES	33.5	0.6	1.6	7.3	10.2	17.7
		0.4	1.0	2.5	2.9	3.5
		1.3	2.3	3.7	3.9	4.2
CHICAGO	40.8	2.3	4.9	12.8	18.0	59.9
		0.9	1.6	2.8	3.2	4.1
		2.1	3.0	3.8	4.0	5.0
PHILADELPHIA	43.4	2.9	5.7	13.2	17.9	55.2
		1.1	1.7	2.8	3.2	4.1
		2.4	3.2	3.8	4.0	4.9
DETROIT	40.8	2.1	4.6	12.0	16.3	50.9
		0.8	1.5	2.7	3.0	4.0
		2.0	2.9	3.8	4.0	4.8
SAN FRANCISCO	28.2	1.8	3.1	9.5	12.5	21.1
		0.9	1.7	2.9	3.2	3.7
		2.2	3.1	3.9	4.1	4.4
WASHINGTON	44.7	2.7	5.5	13.4	19.0	62.3
		1.0	1.7	2.8	3.2	4.1
		2.3	3.1	3.9	4.1	5.0
BOSTON	40.1	3.3	6.0	13.2	17.0	43.8
		1.2	1.8	2.8	3.1	3.9
		2.5	3.2	3.8	4.0	4.7
HOUSTON	51.4	2.2	5.5	23.2	51.1	105.0
		0.9	1.8	3.7	4.1	4.7
		2.2	3.2	4.4	5.0	6.1
DALLAS FT. WORTH	46.5	1.8	3.6	16.3	34.6	93.4
		0.6	1.4	3.2	3.9	4.5
		1.7	2.8	4.0	4.6	5.3

Table 9-4, Continued

Attenuation Values Using Diversity for Satellite at 80 Degrees West

```
SATELLITE LOCATION OF  80.0 DEGREES
DIVERSITY OPERATION - HODGE
```

		99.000%	99.500%	99.900%	99.950%	99.990%
		1.000%	0.500%	0.100%	0.050%	0.010%
ATLANTA	50.8	2.3	6.0	20.4	40.6	94.5
		1.1	1.9	3.4	3.9	4.5
		2.4	3.3	4.1	4.7	5.3
NEWARK	42.2	3.1	5.8	13.3	17.9	54.2
		1.1	1.8	2.8	3.2	4.0
		2.5	3.2	3.9	4.0	4.9
ANAHEIM	33.5	0.5	1.4	6.9	9.6	17.1
		0.3	0.9	2.5	2.9	3.5
		1.1	2.1	3.7	3.9	4.2
PITTSBURGH	42.1	2.5	5.2	12.9	17.9	53.1
		0.9	1.6	2.8	3.2	4.1
		2.2	3.1	3.8	4.0	4.9
ST. LOUIS	44.2	2.3	5.0	13.5	20.5	68.8
		0.9	1.6	2.9	3.3	4.2
		2.1	3.1	3.9	4.1	5.2
DENVER	37.0	0.8	2.1	8.6	12.1	39.6
		0.4	0.9	2.4	2.9	3.8
		1.2	2.2	3.7	3.9	4.5
SAN JOSE	23.8	1.4	3.3	9.7	12.7	21.6
		1.0	1.7	3.0	3.3	3.7
		2.3	3.2	3.9	4.1	4.4
MIAMI	59.6	3.3	6.9	32.0	55.2	109.0
		1.1	2.0	3.3	4.1	4.7
		2.5	3.4	4.4	5.0	6.2
CINCINATTI	44.6	2.6	5.4	14.4	23.0	73.7
		1.0	1.7	2.9	3.4	4.3
		2.3	3.1	3.9	4.2	5.3
MILWAUKEE	39.7	1.9	4.3	11.6	15.9	49.3
		0.8	1.4	2.6	3.0	4.0
		1.9	2.9	3.3	3.9	4.8

Table 9-4, Continued

Attenuation Values Using Diversity for Satellite at 80 Degrees West

SATELLITE LOCATION OF 80.0 DEGREES
DIVERSITY OPERATION - HODGE

| | | 99.000% | 99.500% | 99.900% | 99.950% | 99.990% |
		1.000%	0.500%	0.100%	0.050%	0.010%
MINNEAPOLIS	36.6	1.7	3.9	11.0	14.8	40.8
		0.7	1.3	2.6	2.9	3.9
		1.8	2.8	3.7	3.9	4.6
BALTIMORE	44.1	2.9	5.7	13.6	19.1	61.8
		1.0	1.7	2.8	3.3	4.1
		2.4	3.2	3.9	4.1	5.0
CLEVELAND	42.0	2.4	5.1	12.7	17.7	56.9
		0.9	1.6	2.7	3.1	4.1
		2.2	3.0	3.8	4.0	4.9
KANSAS CITY	42.4	2.4	5.1	13.7	21.0	69.8
		0.9	1.7	2.9	3.4	4.2
		2.2	3.1	3.9	4.1	5.2
SAN DIEGO	35.2	0.4	1.2	6.5	9.3	17.0
		0.3	0.8	2.4	2.8	3.4
		0.9	2.0	3.6	3.9	4.2
SEATTLE	22.1	0.7	1.8	7.8	10.7	19.6
		0.5	1.1	2.6	3.0	3.6
		1.5	2.5	3.8	4.0	4.3
NEW ORLEANS	53.3	2.8	6.5	33.4	56.6	110.5
		1.1	2.0	3.3	4.1	4.7
		2.4	3.4	4.5	5.1	5.2
PHOENIX	33.2	0.1	0.8	5.3	8.2	15.7
		0.0	0.5	2.0	2.5	3.3
		0.2	1.4	3.4	3.7	4.1

SECTION 10
ADDITIONAL CONSIDERATIONS

10.1   Distribution of Earth Stations Among the Rain Zones

The approximate distribution of potential earth stations among the six rain zones is assumed to be based on the percentage of the U.S. population residing in the various zones. This data is presented in Table 10-1. A more detailed examination could investigate other factors affecting the location of earth stations; such as GNP/Capita and existing terrestrial facilities, however, due to the relatively large size of rain zones, variations in such factors will average out to some degree. Thus, as a first approximation the distribution of earth stations is assumed to be identical to the population distribution.

Table 10-1

Population and Earth Station Distribution

Rain Zone	Percent of Population and Earth Stations
1	9.5
2	21.5
3	47.5
4	16.0
5	3.5
6	2.0

10.2   Comparison of Methods Used for Attenuation Calculations

In Section 7, we presented curves showing the cumulative time distributions of attenuation. These curves were calculated using three different methods which were labeled "A", "B" and CCIR. In addition, measured data points were shown on the graphs. There is a great deal of variation among the three methods, and a discussion of the reasons for these differences is given below.

The primary difference among the three methods is in the computation of the effective path length. In the case of "A" and "B", a simple curve fit of data taken at a single elevation angle was taken, which produces a path length inversely proportional to the rain rate. The coefficients of the equations are quite different in the two cases, however, resulting in substantially different path lengths. Since the total attenuation along a path is directly proportional to the path length, it is obvious that this will result in considerable differences in the attenuation level. The differences are due to different basic data reported in References 33 and 13. The curves labeled CCIR, however, were prepared according to the method outlined in CCIR Document F5/003. This method takes into account not only the elevation angle but the height of the cloud tops at which rain occurs, which generally coincides with the height of the zero degree isotherm or freezing level. In addition there are several other experimentally determined factors which generally result in an increase in path length. The CCIR curves produce larger values of attenuation in almost every case than the values produced by the formula based on Reference 13. In evaluating the CCIR method, several assumptions that were appropriate to the contiguous United States were made, and so the values given for the various rain zones do not coincide precisely with the values given for specific cities, even when those cities may lie within the rain zone. This is due to the effects of differing latitude and elevation angles to the satellite on the parameters of the CCIR method. In summary, the differences can be ascribed to differences in the data leading to the calculation of effective path length.

In several of the rain zones, the CCIR model produces rather high values of 30 GHz attenuation for substantial percentages of the time. In the case of Zone 5, for instance, the 30 GHz attenuation is around 50 dB at one-tenth of one percent of the time. It may justifiably be argued that figures like this do not have much meaning because it is not realistic to provide a 50 dB margin, for instance, in order to make a system that is available for 99. percent of the time. In fact, since the measurements taken by various experimenters do not extend to values of 50 dB and above, it could equally well be argued that the CCIR method is not particularly valid at these high levels of attenuation. In either case, the values serve primarily as an indicator that some means of providing additional availability will have to be found other than merely increasing the system margin, since in the case of such large attenuations this is not practical.

10.3   Variation of Attenuation During the Day, Month and Year

It might be expected that the attenuation experienced due to precipitation would show a cyclical variation depending on the time of day. This is in fact the case; however, the cycle changes from season to season as the predominant type of precipitation changes. In the summer months, the worst time is from mid-afternoon to evening (local time). This is due to the frequent occurances of thunderstorms (with their associated high rain rates) during this time of day.

Figure 10-1 shows the variation of attenuation during some measurements made at Clarksburg, Maryland using the Comstar beacon. The characteristic shows two peaks, one centered at about 5 a.m. local time and the other at about 4 p.m. The author's explanation notes that the morning peak was due primarily to the fall and winter months, while the afternoon one was due to the summer months, as expected.

The U.S. Weather Bureau has published data on the frequencies and intensities of precipitation for each hour of the day and each month of the year. These are available for 138 weather stations in the U.S. It is possible to estimate from them the approximate worst times for precipitation attenuation outages.

As a further step, we have constructed a simulation of precipitation attenuation based on some of the data available to us. The essence of the simulation is as follows. For a given hour of a typical day in a given month, the probability of rainfall is obtained from the aforementioned Weather Bureau data. A random number generator is used to determine whether it is "raining". The probability distribution for rainfall amounts in 1 hour for that hour is also sampled to determine the amount of "rain" that "falls". A simplified "storm profile" is constructed from this sampling. The attenuation is then computed from this profile of rain rates. The "time" in the simulation then advances to the next hour and the process is repeated. The parameters used are adjusted for the particular month under consideration so that the prevailing "weather" conditions will change in a realistic manner throughout the year.

Figure 10-1
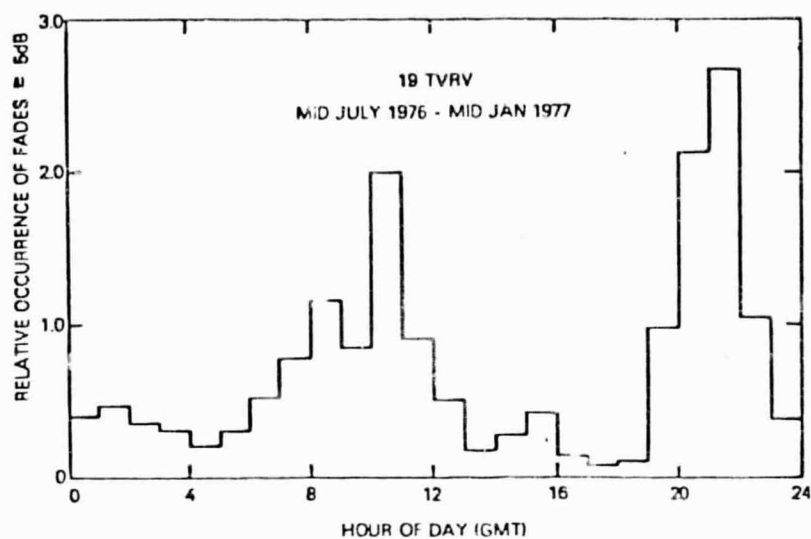
Figure 5a. *Diurnal Distribution of Fades* $\geq$ *5 dB* ϵ *1 04 GHz*
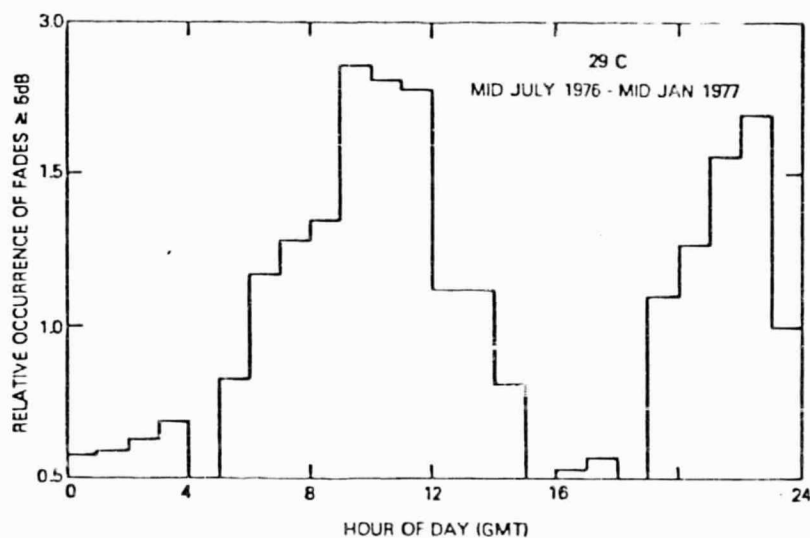
Figure 5b. *Diurnal Distribution of Fades* $\geq$ *5 dB at 28.56 GHz*

Source: Harris, J.M. and G. Hyde. "Preliminary Results of Comstar 19/29 GHz Beacon Measurements at Clarksburg, Maryland," COMSAT Technical Review, Volume 7, No. 2, Fall 1977, pp. 599-624.

The simple "storm profiles" used are shown in Figures 10-2 and 10-3. We did not attempt to use a realistic model for this first approximation. However, models which more closely approach reality are available, and actual data could be used to construct others.
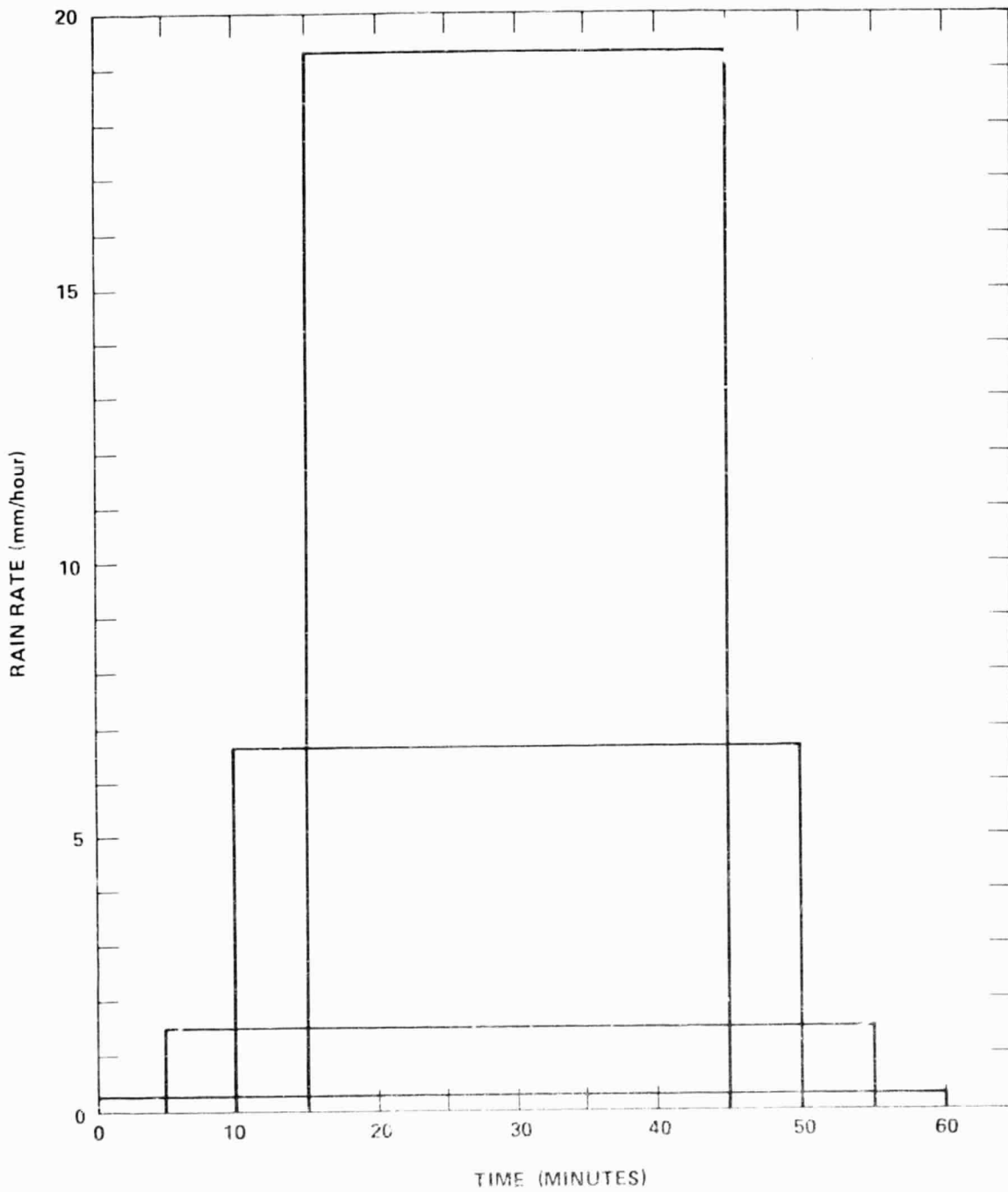
Figure 10-2

LOW RAIN RATE SIMPLIFIED STORM MODELS
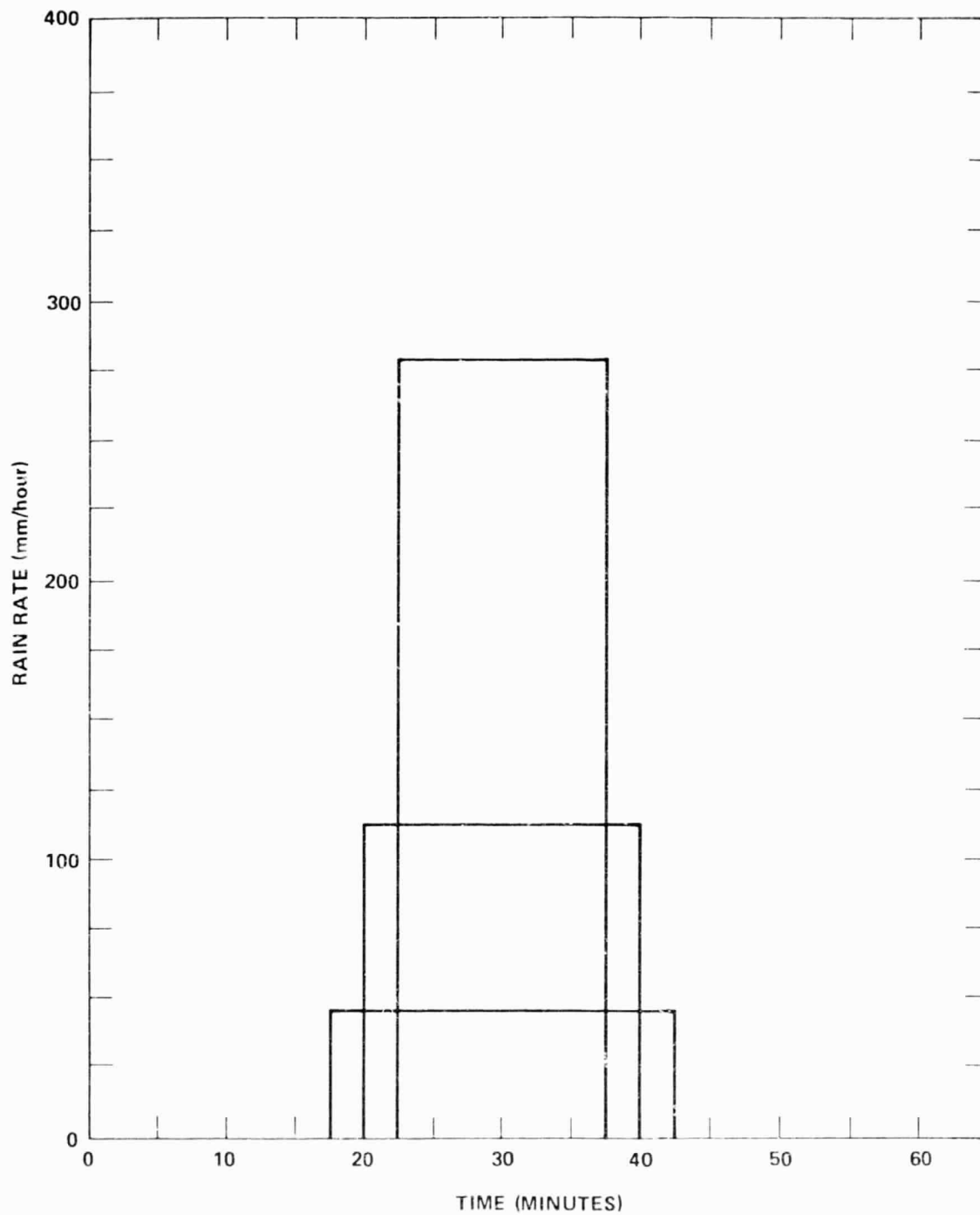
Figure 10-3

HIGH RAIN RATE SIMPLIFIED STORM MODELS

Typical time series plots of the simulation results for Chicago, Illinois are presented in Figures 10-4 and 10-5. Figure 10-4 is for the month of January and Figure 10-5 is for July. The values of maximum attenuation at 18 GHz in each hour of the day are plotted versus time. While it is more likely to rain in Chicago in January, it is more likely to rain heavily in July. This tendency can be seen in the Figures.

This data can be summarized in the form of outages if we select a rain margin, say 5 dB at 18 GHz. In this case our Chicago simulation results are shown in Table 10-2.

The percentage of time figures are rather high, but this can be attributed to the very simple storm models used. Of more significance is the number of occurances. A large number of low level rain events are also indicated, and the attenuation from these is generally less than 3 dB.

A more elaborate storm model is required in order to provide simulation results with more detail. Such a storm model would require considerable study and simulation work.

Table 10-2

Storm Simulation Results for Chicago

18 GHz Margin (dB)	Month	Number of Outages	Total Minutes Outage	Percent of Month Availability
2.5	January	2	70	99.8
	July	18	595	98.7
5	January	1	30	99.93
	July	10	275	99.4
10	January	0	0	100.0
	July	3	65	99.8
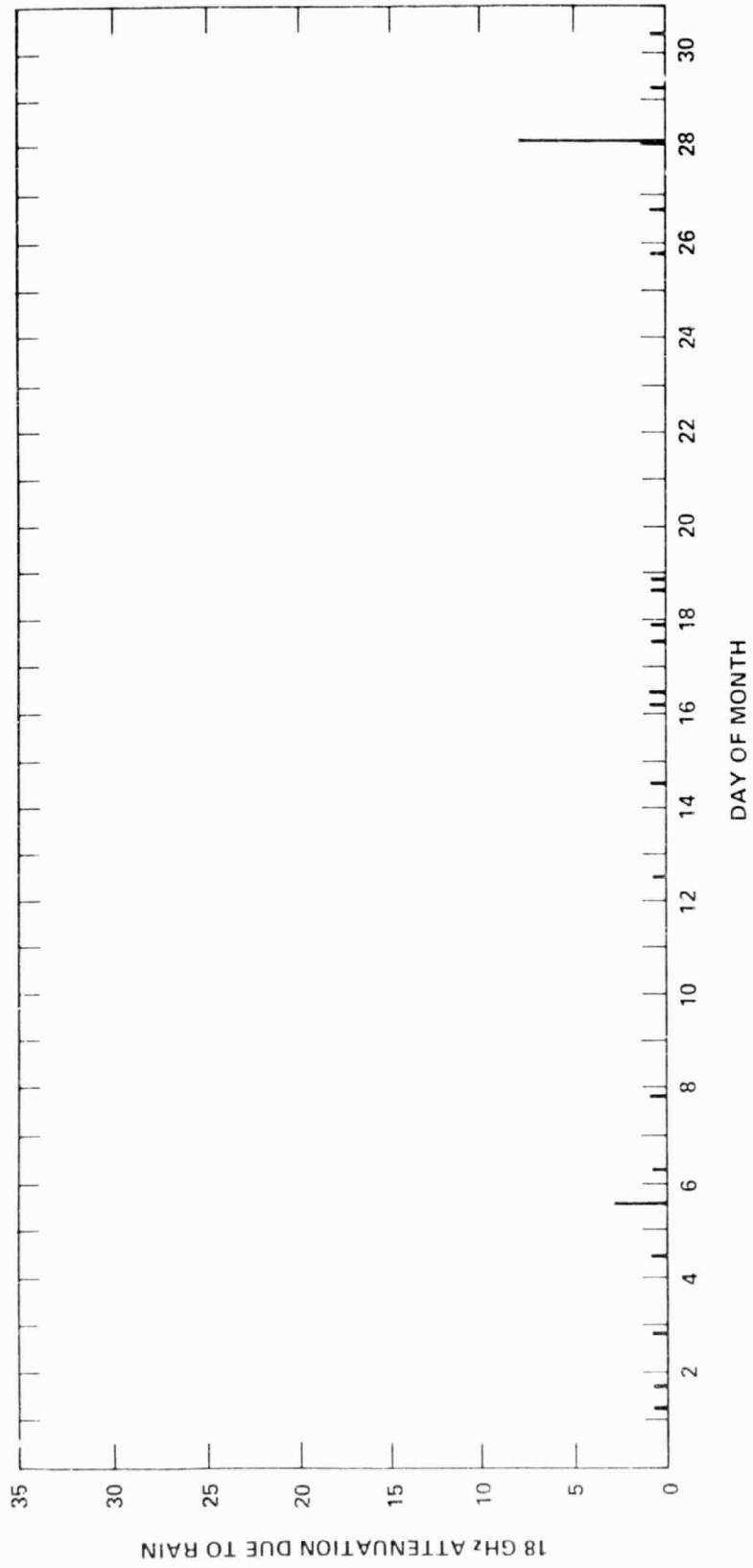
Figure 10-4

TIME SERIES SIMULATION OF 18 GHz ATTENUATION FOR JANUARY
Location: Chicago, Illinois
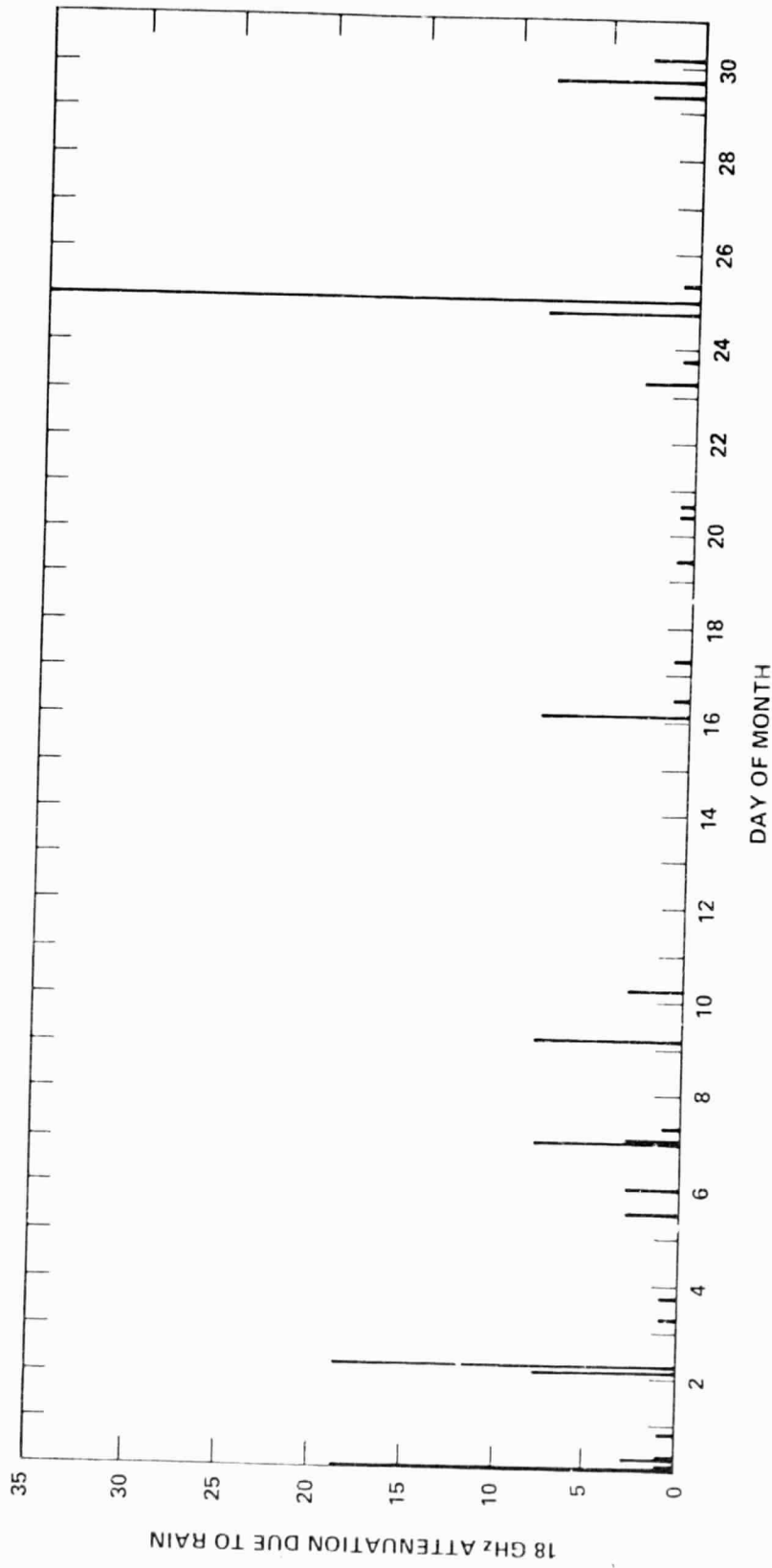
Figure 10-5

TIME SERIES SIMULATION OF 18 GHz ATTENUATION FOR JULY
Location: Chicago, Illinois

LIST OF REFERENCES

1) Setzer, David E. "Computed Transmission Through Rain at Microwave and Visible Frequencies," Bell System Technical Journal, October 1970.

2) Laws, J.O. and D.A. Parsons. "The Relation of Raindrop-Size to Intensity," Trans. American Geophysical Union, 1943.

3) Oguchi, Tomohiro. "Attenuation and Phase Rotation of Radio Waves due to Rain," Radio Science, January 1973.

4) Olsen, R.L., D.V. Rogers and D.B. Hodge. "The aR^b Relation in the Calculation of Rain Attenuation," IEEE Trans. on Antennas and Propagation, March 1978.

5) "Propagation in Non-Ionized Media," CCIR Green Book, Vol. 5, I.T.U., Geneva, 1975.

6) "Five-to-60-Minute Precipitation Frequency for the Eastern and Central United States," National Weather Service, June 1977.

7) Skerjanec, R.E. and C.A. Samson. "Rain Attenuation Study for 15 GHz Relay Design," ESSA, Department of Commerce, May 1970.

8) Semplak, R.A. and H.E. Keller. "A Dense Network for Rapid Measurement of Rainfall Rate," Bell System Technical Journal, July-August 1969.

9) Freeny, A.E. and J.D. Gabbe. "A Statistical Description of Intense Rainfall," Bell System Technical Journal, July-August 1969.

10) Ippolito, Louis J. "20- and 30-GHz Millimeter Wave Experiments with the ATS-6 Satellite," NASA Technical Note TN D-8197.

11)   "Data Analysis Report for ATS-F COMSAT Millimeter Wave Propagation Experiment," COMSAT Laboratories, prepared under NASA Contract NAS 5-21616.

12)   Rice, P.L. and N.R. Holmberg. "Cumulative Time Statistics of Surface-Point Rainfall Rates," IEEE Transactions on Communications, Vol. COM-21, No. 10, October 1973.

13)   Harris, J.M. and G. Hyde.   "Preliminary Results of COMSTAR Beacon Measurements at Clarksburg, Maryland," COMSAT Technical Review, Vol. 7, No. 2, Fall 1977.

14)   Semplak, R.A. and R.H. Turrin.   "Some Measurements of Attenuation by Rainfall at 18.5 GHz," Bell System Technical Journal, July-August 1969.

15)   Wilson, R.W. "Sun Tracker Measurements of Attenuation by Rain at 16 and 30 GHz," Bell System Technical Journal, May-June 1969.

16)   Meyerhoff, H.J., A. Buige and E.A. Robertson.   "15.3 GHz Precipitation Attenuation Measurements at Utibe, Panama," COMSAT Technical Review, Vol. 4, No. 1, Spring 1974.

17)   Crane, R.K.   "Radar Detection of Thunderstorm Hazards for Air Traffic Control, Vol. I, Storm Cell Detection," Lincoln Laboratory, M.I.T., Proj. Rept. ATC-67, Vol.I, October 1976.

18)   Drufuca, G. "Rain Attenuation Statistics for Frequencies Above 10 GHz from Radar Observations," J. Rech. Atmos., Vol. 8, 1974.

19)   Goldhirsh, J. and F.L. Robison.   "Attenuation and Space Diversity Statistics Calculated from Radar Reflectivity Data of Rain," IEEE Trans. on Antennas and Propagation, Vol. AP-23, 1975.

20)   Ippolito, L.J. "Millimeter Wave Propagation Measurements from the Applications Technology Satellite (ATS-V)," IEEE Trans. on Antennas and Propagation, July 1970.

21) Bell System Technical Journal, Vol. 57, No. 5, May-June 1978. (Devoted to articles on COMSTAR Beacon Experiment.)

22) Muller, E.E. "Long-Term Rain Attenuation Observations at 13, 19 and 28 GHz," Proc. of Symposium on Advanced Satellite Communications Systems, Genca, Italy, December 1977.

23) Hodge, D.B. "A 15.3 GHz Satellite-to-Ground Diversity Experiment," Ohio State Electroscience Laboratory Report 2374-11, October 1972.

24) Ippolito, L.J. "Millimeter Wave Propagation and Cummunications Experiments at 20 and 30 GHz," IEEE Transactions on Aerospace and Electronic Systems, Vol. AES-11, No. 6, November 1975.

25) Hogg, D.C. "Path Diversity in Propagation of Millimeter Waves Through Rain," IEEE Trans. on Antennas and Propagation, Vol. AP-15, No. 3, May 1967.

26) Wilson, R.W. "A Three-Radiometer Path-Diversity Experiment," Bell System Technical Journal, July-August 1970.

27) Medhurst, R.G. "Rainfall Attenuation of Centimeter Waves: Comparison of Theory and Measurement," IEEE Trans. on Antennas and Propagation, July 1965.

28) Steinhorn, J.P. and J. Harris. "Effects of Rain on Communications Satellite Systems Trade-offs," International Conference on Communications, Philadelphia, PA, June 1976.

29) Crane, R.K. "Prediction of the Effects of Rain on Satellite Communications Systems," Proceedings of the IEEE, Vol. 65, No. 3, March 1977.

30) Hogg, D.C. and Ta-Shing Chu. "The Role of Rain in Satellite Communications," Proceedings of the IEEE, Vol. 63, No. 9, September 1975.

31) European Space Agency. "Problems of Space and Terrestrial Microwave Propagation." Proceedings of a Symposium held in Graz, Austria, April 7-9, 1975, ESA Document ESA-SP-113.

32) Rice, P.L. et. al. "Transmission Loss Predictions for Tropospheric Communication Circuits: Vol. 1." National Bureau of Standards Technical Note 101, U.S. Department of Commerce Document AD-687-820.

33) Evans, H. W. "Attenuation on Earth-Space Paths at Frequencies up to 30 GHz." International Conference on Communications, Montreal, Canada, June 1971.

34) Fang, D.J. and J.M. Harris. "Precipitation Attenuation Studies Based on Measurements of ATS-6 20/30 GHz Beacon Signals at Clarksburg, MD." IEEE Transactions on Antennas and Propagation, Vol. AP-27, No. 1, January 1979, 1-11.

35) Watson, P.A., N.J. McEwan, A.W. Dissanayake, and D.P. Haworth. "Attenuation and Cross-Polarization Measurements at 20 GHz Using the ATS-6 Satellite with Simultaneous Radar Observations." IEEE Transactions on Antennas and Propagation, Vol. AP-27, No. 1, January 1979, 11-17.

36) Kaul, R., D.B. Hodge and D.M. Theobold. "Prediction of Millimeter Wave Propagation Effects on Earth-Space Paths." Prepared by ORI, Inc., Silver Spring, Maryland for NASA Goddard Space Flight Center, NASA Contract No. NAS5-23438, Mod 68, December 1978.

37) "Earth-Space Attenuation Prediction Procedures at 4 to 6 GHz." U.S. Department of Commerce, Office of Telecommunications, OT Report 77-123, May 1977.

38) Eaton, J.L. "Satellite Broadcasting: Slant Path Attenuation Through Rain Storms." The British Broadcasting Corporation, Document No. BBC RD 1977/7, February 1977.

BIBLIOGRAPHY

Oguchi, T. "Attenuation and Phase Rotation of Radio Waves Due to Rain: Calculations at 19.3 and 34.8 GHz," Radio Science, Vol. 8, No. 1, 1973, 31-38.

Fang, D.J. "Attenuation and Phase Shift of Microwaves Due to Canted Raindrops," COMSAT Technical Review, Vol. 5, No. 1, Spring 1975.

Meyerhoff, H.J., A. Buige and E.A. Robertson. "15.3 GHz Precipitation Attenuation Measurements Using a Transportable Earth Station at Utibe, Panama," COMSAT Technical Review, Vol. 4, No. 1, 1974, 169-186.

Wilson, R.W. "Measurements of Attenuation by Rain at 16 and 30 GHz with a Sun Tracker," Bell System Technical Journal, Vol. 48, 1383-1404.

Hogg, D.C. "The Role of Rain in Satellite Communications," IEEE Proceedings, September 1975.

Crane, R.K. "Prediction of the Effects of Rain on Satellite Communication Systems," IEEE Proceedings, Vol. 65, 1977.

Setzer, D.E. "Computed Transmission Through Rain at Microwave Frequencies," Bell System Technical Journal, Vol. 49, No. 8, October 1970, 1873-1892.

Semplak, R.A. and H.E. Keller. "A Dense Network for Rapid Measurement of Rainfall Rate," Bell System Technical Journal, 1960, 1745-1756.

Freeny, A.E. and J.D. Gabbe. "A Statistical Description of Intense Rainfall," Bell System Technical Journal, 1969, 1789-1851.

Freeny, A.E. and R.A. Semplak. "Measuring Rainfall," Bell Laboratories Record, November 1969, 315-319.

Dougherty, H.T. and E.J. Dutton. "Estimating the Year-to-Year Variability f Rainfall for Microwave Applications," IEEE Transactions on Communications, COM-26, 1978.

Rice, P.L. and N.R. Holmberg. "Cumulative Time Statistics of Surface-Point Rainfall Rates," IEEE Transactions on Communications, COM-21, 1973.

Clsen, R.L., D.W. Rogers and D.B. Hodge. "The aR^b Relation in the Calculation of Rain Attenuation," IEEE Transactions on Antennas and Propagation, AP-26, 1978.

Ippolito, L.J. "Millimeter Wave Propagation Measurements from the Applications Technology Satellite (ATS-V)," IEEE Transactions on Antennas and Propagation, Vol. AP-18, July 1970, 535-552.

Ippolito, L.J. "ATS-6 MM Wave Propagation Experiment," NASA Technical Note TND-8197, April 1976.

Harris, J.M. and G. Hyde. "Preliminary Results of COMSTAR 19/29 GHz Beacon Measurements," COMSAT Technical Review, Fall 1977.

Bergmann, H.J. and E.E. Muller. "A Radiometer Experiment at 13 and 18 GHz to Study Satellite System Site Diversity".

Muller, E.E. "Long-Term Rain Attenuation Observations at 13, 19 and 28 GHz," Paper presented at the Proceeding of the Symposium on Advanced Satellite Communication Systems, Genoa, Italy, December 14 - 16, 1977 (ESA SP-138).

Wulfsberg, K.N. and E.E. Altshuler, "Rain Attenuation at 15 and 33 GHz," IEEE Transactions on Antennas and Propagation, Vol. AP-20, No. 2, March 1972, 181-187.

Semplak, R.A. and R.H. Turrin. "Some Measurements of Attenuation by Rainfall at 18.5 GHz," Bell System Technical Journal, Vol. 48, No. 6, July-August 1968.

Hogg, D.C. "Path Diversity in Propagation of Millimeter Waves Through Rain," IEEE Transactions on Antennas and Propagation, Vol. AP-15, No. 3, May 1967, 410-415.

Wilson, R.W. "A Three-Radiometer Path-Diversity Experiment," Bell System Technical Journal, Vol. 49, No. 6, July-August 1970, 1239-1242.

Final Report on COMSAT 13/18 GHz ATS-6 Propagation Experiment.

Bell System Technical Journal, Vol. 57, No. 5. Articles on COMSTAR 19/28 GHz Beacon.

Carne, R.K. "Propagation Phenomena Affecting Satellite Communication Systems Operating in the Centimeter and Millimeter Wavelength Bands," IEEE Proceedings, Vol. 59, February 1971, 173-188.

Ryde, J.W. and D. Ryde. "Attenuation of Centimetre and Millimetre Waves by Rain, Hail, Fogs and Clouds," Res. Labs. of the General Electric Company, Wembley, England, Rep. 8670, 1945.

Rice, P.L., et. al. "Transmission Loss Predictions for Tropospheric Communication Circuits," U.S. Department of Commerce, Washington, D.C. Technical Note 101, January 1967.

Bradley, J.H.S. "Rainfall Extreme Value Statistics Applied to Microwave Attenuation Climatology," Stormy Weather Group, McGill University, Montreal, Quebec, Canada, Scientific Rep. MW-66, February 1970.

Harrold, T.W. "Attenuation of 8.6 MM Wavelength Radiation in Rain," Proceedings of IEE, Vol. 114, February 1967, 201-203.

Easterbrook, B.J. and D. Turner. "Prediction of Attenuation by Rainfall in the 10.7-11.7 GHz Communication Band," Proceedings of IEE, Vol. 114, May 1967, 557-565.

Norbury, J.R. and W.J.K. White. "Microwave Attenuation at 35.8 GHz Due to Rainfall," Electron. Lett., Vol. 8, February 1972, 91-92.

de Bettencourt, J.T. "Statistics of Millimeter-Wave Rainfall Attenuation," J. Rech. Atmos., Vol. 8, January-June 1974, 89-112.

Laws, J.O. and D.A. Parsons. "The Relation of Raindrop Size to Intensity," Trans. Amer. Geophys. Union, Vol. 24, 1943, 452-460.

Marshall, J.S. and W. McK. Palmer. "The Distribution of Raindrops with Size," J. Meteor., Vol. 5, August 1948, 165-166.

Joss, J., et. al. "The Variation of Raindrop Size Distributions at Locarno," Proc. Int. Conf. Cloud Physics, 1968, 369-373.

Hogg, D.C. and T.S. Chu. "The Role of Rain in Satellite Communications," IEEE Proceedings, Vol. 63, September 1975, 1308-1331.

Rogers, R.R. "Statistical Rainstorm Models: Their Theoretical and Physical Foundations," IEEE Transactions on Antennas and Propagation, Vol. AP-24, July 1976, 547-566.

Al'pert, Y.L. Radio Wave Propagation and the Ionosphere New York, 1974.

Rosenblum, E.S. "Atmospheric Absorption of 10-400 kmcps Radiation: Summary and Bibliography to 1969," Microwave Journal, Vol. 4, 1971, 91-96.

Pruppacher, H.R. and K. Beard. "A Wind Tunnel Investigation of the Internal Circulation and Shape of Water Drops Falling at Terminal Velocity in Air," Quarterly Journal of the Royal Meteorological Society, Vol. 96, 1970, 247-256.

Saxton, J.A. and J.A. Lane. "Electrical Properties of Sea Water," Wireless Engineering, Vol. 29, No. 349, 1952, 269-275.

Lenard, P. "Veber Regen," Meteor. Z., Vol. 21, 1904, 249-260.

Best, A.C. "The Shape of Raindrops and Mode of Disintegration of Large Drops," Air Ministry, Great Britain, Meteorological Research Commission, Report M.R.P. 330, 1947.

Blanchard, D.C. "Observations on the Behavior of Water Drops at Terminal Velocity in Air," General Electric Research Lab, Occasional Report 7, Project Cirrus, 1948.

Blanchard, D.C. "The Behavior of Water Drops at Terminal Velocity," Transactions of the American Geophysical Union, Vol. 31, 1950, 836-844.

Blanchard, D.C. Comments on "The Shape of Water Drops Falling in Stagnant Air," Journal of Meteorology, Vol. 12, 1955, 91-93.

Magono, C. "On the Shape of Water Drops Falling in Stagnant Air," Journal of Meteorology, Vol. 11, 1954, 72-74.

Kumai, M. and K. Itagaki. "Shape and Fall Velocity of Raindrops," Journal of the Meteorological Society of Japan, Vol. 32, 1954, 1-18.

Garner, F.H. and J.J. Lane. "Mass Transfer to Drops of Liquid Suspended in a Gas Stream," Trans. Instr. Chem. Eng., Vol. 37, 1959, 167-172.

Jones, D.M. "The Shape of Raindrops," Journal of Meteorology, Vol. 16, 1959, 504-510.

Spilhaus, A.F. "Raindrop Size, Shape and Falling Speed," Journal of Meteorology, Vol. 5, 1948, 108-110.

Imai, I. "On the Velocity of Falling Raindrops." Geophysical Magazine of Tokyo, Vol. 21, 1950, 244-249.

Taylor, T.D. and A. Acrivos. "The Deformation and Drag on a Falling Viscous Drop at Low Reynolds Numbers," Journal of Fluid Mechanics, Vol. 18, 1964, 446-470.

Medhurst, R.G. "Rainfall Attenuation of Centimeter Waves: Comparison of Theory and Measurements," IEEE Transactions on Antennas and Propagation. Vol. AP-13, July 1965, 550-564.

Marshall, J.S. and W. Palmer. "The Distribution of Raindrops with Size," Journal of Meteorology, Vol. 5, August 1948.

Caton, P.G.F. "A Study of Raindrop Size Distribution in the Free Atmosphere," Quarterly Journal of the Royal Meteorological Society, Vol. 92, 1966, 515-30.

Blanchard, D.C. and A.T. Spencer. "Experiments on the Generation of Raindrop-Size Distributions by Drop Breakup," Journal of Atmospheric Sciences, Vol. 27, No. 1, January 1970.

Strivastava, R.C. "Size Distribution of Raindrops Generated by Their Breakup and Coalescence," Journal of Atmospheric Sciences, Vol. 28, No. 3, April 1971, 410-415.

Brazier-Smith, P.R., S.G. Jennings and J. Latham. "The Influence of Evaporation and Drop Interactions on a Rainshaft," Quarterly Journal of the Royal Meteorological Society, Vol. 99, No. 422, October 1973, 704-722.

Medhurst, R.G. "Rainfall Attenuation of Centimeter Waves: Comparison of Theory and Measurements," IEEE Transactions on Antennas and Propagation, Vol. AP-13, July 1965, 550-564.

Ogura, Y. and T. Takahashi. "The Development of Warm Rain in a Cumulus Model," Journal of Atmospheric Sciences. Vol. 30, No. 2, March 1973, 262-277.

Clark, T.L. "Numerical Modeling of the Dynamics and Micro-physics of Warm Cumulus Convection," Journal of Atmospheric Sciences, Vol. 30, No. 5, July 1973, 857-878.

Sekhon, R.S. and R.C. Strivastava. "Doppler Radar Observations of Drop Size Distribution in a Thunderstorm," Journal of Atmospheric Sciences, September 1971.

Liu, J.Y. and H.P. Orville. "Numerical Modeling of Precipitation Effects on a Cumulus Cloud," Report 68-69, South Dakota School of Mines and Technology, 1968.

Bussey, H.E. "Microwave Attenuation Statistics Estimated from Rainfall and Water Vapour Statistics," Proc. IRE, Vol. 38, 1950, 781-785.

Briggs, J. "Estimating the Duration of High-intensity Rainfall," Meteorology Magazine, Vol. 98, 1969, 289-293.

Briggs, J. and J.A. Harker. "Estimates of the Duration of Short-Period Rainfall Rates Based on Clock-Hour Values," Meteorology Magazine, Vol. 98, 1969, 246-252.

Huff, F.A., W.L. Shipp and P.T. Schickendanz. "Evaluation of Precipitation Modification Experience from Precipitation Rate Measurements," Final Report to the U.S. Department of the Interior, Office of Atmospheric Water Resources, Illinois State Water Survey, 1969.

Beals, G.A. "Estimated Probabilities of Path-Cumulative Rain Intensity for Paths of 10 and 22 Nautical Miles in High Rain-Rate Areas," Report FAA-RD-70-55, U.S.A.F. Environmental Technology Applications Center, Vol. 32, 1970.

Semplak, R.A. "A Rare Event of Intense Rainfall," Mo:.thly Weather Review, Vol. 99, 1971, 155-157.

Lenhard, R.W., A.E. Cole and N. Sissenwine. "Preliminary Models for Determining Instantaneous Precipitation Intensities from Available Climatology," Environmental Research Papers, No. 250, AFCRL, Bedford, Massachusetts, 1971.

Hershfield, D.M. "Estimating the Extreme-Value 1-Minute Rainfall," Journal of Applied Meteorology, Vol. 11, 1972, 936-940.

Briggs, J. "Probabilities of Aircraft Encounters with Heavy Rain," Meteorology Magazine, Vol. 101, 1972, 8-13.

Sissenwine, N. "Extremes of Hydrometeors at Altitude for MIL-STD-210B," Air Force Surveys in Geophysics, No. 242, AFCRL, Bedord, Massachusetts, 1972.

Sims, A.L. and D.M.A. Jones. "Climatology in Instantaneous Rates," Final Report to AFCRL, Bedford, Massachusetts, State Water Survey, Urbana, Illinois, 1973.

British Aircraft Corporation. "Attenuation Prediction Study," COMSAT Contract CSC-15-376, May 1972.

Buige, A. "A Comparison of Precipitation-Scattered Signal Intensities and Surface Rainfall Rates," Fall URSI Meeting, December 1972.

Fang, D.J. and J.M. Harris. "A New Method of Estimating Microwave Attenuation Over a Slant Propagation Path Based on Rain Guage Data," Final Report submitted to NASA on Contract NAS5-20740, October 1975.

Saxton, J.A. "The Anomalous Dispersion of Water at Very High Frequencies," Meteorological Factors in Radiowave Propagation, London: The Physical Society, 1946.

Kerr, D.E. "Propagation of Short Radio Waves," MIT Radiation Laboratory Series, Vol. 13. New York, 1951.

Mie, G. "Optics of Turbid Media," Annalen der Physik, Vol. 25, No. 3, 1908, 377-445.

Stratton, J.A. Electromagnetic Theory. New York, 1941.

Infeld, L. Quarterly Journal of Applied Mathematics, Vol. 5, 1947, 113.

Aden, A.L. "Electromagnetic Scattering from Spheres with Sizes Comparable to Wavelength," Journal of Applied Physics, Vol. 22, No. 5, May 1951, 601-605.

Chu, C.M. and S.W. Churchill. "Representation of the Angular Distribution of Radiation Scattered by a Spheroidal Particle," Journal of the Optical Society of America, Vol. 45, No. 11, November 1955, 958-962.

Lord Rayleigh. "On the Electromagnetic Theory of Light," Phil. Mag., Vol. 12, 1881, Science Papers 64, 81.

Grans, R. "Diagrams of Radiation from Ultra-Microscopic Particles," Annalen der Physik, Vol. 76, No. 1, January 1925, 29-38.

Van De Hulst, H.C. Light Scattering by Small Particles. New York, 1957.

Ryde, J.W. "Echo Intensity and Attenuation Due to Clouds, Rain, Hail, Sand and Duststorms at Centimeter Wavelengths," Report 7831, Gene 1 Electric Company Research Labs, Wembley, England, October 1941.

Ryde and Cooper. Proc. Royal Soc., Vol. A131, 1931, 464.

Oguchi, T. "Attenuation of Electromagnetic Waves Due to Rain with Distorted Raindrops," Journal of the Radio Research Laboratories (Japan), Vol. 11, No. 53, 1964, 19-44.

Oguchi, T. "Attenuation of Electromagnetic Waves Due to Rain with Distorted Raindrops (Part II)," Journal of the Radio Research Laboratories (Japan), Vol. 11, No. 53, 1964, 19-44.

Morrison, J.A. and M.J. Cross. "Scattering of a Plane Electromagnetic Wave by Asymmetric Raindrops," Bell System Technical Journal, Vol. 53, No. 6, 1974, 955-1018.

Oguchi, T. "Scattering Properties of Oblate Raindrops and Cross Polarization of Radio Waves Due to Rain: Calculations at 19.3 and 34.8 GHz," Journal of the Radio Research Laboratories (Japan), Vol. 20, No. 102, 1973, 79-118.

Vogel, W.J., B.M. Fannin and A.W. Straiton. "Polarization Effects for Millimeter Wave Propagation in Rain," Technical Report 73-1, University of Texas, Austin, Texas, December 1973.

Pruppacher, H.R. and R.L. Pittner. "A Semi-Empirical Determination of the Shape of Clouds and Raindrops," Journal of Atmospheric Sciences, Vol. 28, 1971, 86-94.

Ryde, J.W. and D. Ryde. "Attenuation of Centimeter Waves by Rain, Hail, Fogs and Clouds," Report 8670, General Electric Research Labs, Wembley, England, May 1945.

Oguchi, T. "Statistical Fluctuation of Amplitude and Phase of Radio Signals Passing Through the Rain," Journal of the Radio Research Labs (Japan), Vol. 9, No. 41, 1962, 51-72.

Watson, P.A. and M. Arabi. "Rainfall Cross Polarization of Linearly and Circularly Polarized Waves at Microwave Frequencies," Electronic Letters, Vol. 8, No. 11, 1972, 283-285.

Chu, C.M. "Rain Induced Cross-Polarization at Centimeter and Millimeter Wavelengths," Bell System Technical Journal, Vol. 53, No. 8, 1974, 1557-1579.

Wilson, R.W. "Measurements of Attenuation by Rain at 16 and 30 GHz with a Sun Tracker," Bell System Technical Journal, Vol. 48, 1383-1404.

Crane, R.K. "A Comparison Between Monostatic and Bistatic Scattering from Rain and Thin Turbulent Layers," M.I.T. Lincoln Laboratory, Technical Note 1970-29, 1970.

Bartholome, P. "Model of Atmospheric Attenuation for Earth/Satellite Links at 11 and 14 GHz," Report EC/3444/PB/as (Rev. 1), ESRO, the Netherlands, October 1973.

Atlas, D. and A.C. Chmele. "Advances in Radio Meteorology," Proceedings of the 6th Weather Radar Conference. Boston, 1957.

Dennis, A.S. "Measurements of Forward Scatter from Rain at 9.05 GHz," Research Memorandum 4, Project 3773, SRI, Menlo Park, California, 1962.

Culnan, D.E., F.O. Guiraud and R.E. Skerjanec. "Radio Scattering Cross Sections of Thunderstorms," National Bureau of Standards Report 8816, 1965.

Herman, B.M., S.R. Browning and L.S. Battan. Report 9, University of Arizona Institute of Atmospheric Physics, 1961.

Harrold, T.W. "Estimation of Rainfall Using Radar - A Critical Review," Her Majesty's Stationary Office, London, England, 1965.

Joss, J.K. et. al. "On the Quantitative Determination of Precipitation by Radar," Osservatoria Ticinese della Centralle Meterologica Svizzera, Locarno-Monti, 190.

Turner, D. B.J. Easterbrock and J.E. Golding. "Experimental Investigation into Radio Propagation of 11.0 to 11.5 GC/S," Proc. IEE, No. 9, September 1966, 1477-1489.

Joss, J. and A. Waldvogel. "Raindrop Size Distribution and Doppler Velocities," Preprint of the 14th Radar Meteorology Conference, American Meteorological Society, Boston, MA, 1970.

Atlas, D. "Advances in Radar Meteorology," Advances in Geophysics, Vol. 10, edited by H.E. Lansberg and I.V. Mieghem, 1964, 317-478.

Austin, P.M. "Application of Radar to Measurement of Surface Precipitation," Final Report DAAB 07-67-C-0319, U.S. Army Electronics Command, 1969.

Atlas, D., R.C. Strivastava and R.S. Sekhon. "Doppler Radar Characteristics of Precipitation at Vertical Incidence," Technical Report 22, University of Chicago and Illinois Institute of Technology, 1971.

Atlas, D. and C.W. Ulbrich. "The Use of Attenuation and Reflectivity for Improved Measurements of Water Content and Rainfall Rate," I.U.C.R.M. Colloquium on the Fine Scale Structure of Precipitation and EM Wave Propagation, 1973.

Crane, R.K. "Coherent Pulse Transmission Through Rain," IEEE Transactions on Antennas and Propagation, Vol. AP-15, No. 2, 1967, 252-256.

Vogler, L.E. "Pulse Distortion in Resonant and Non-Resonant Gases," Radio Science, Vol. 5, No. 11, 1301-1305.

Anderson, L.J., et. al. "Attenuation of 1.25 Centimeter Radiation Through Rain," Proc. IRE, Vol. 35, April 1947, 351-354.

Gunn, K.L.S. and T.W.R. East. "The Microwave Properties of Precipitation Particles," Journal of the Royal Meteorological Society, Vol. 80, 1954, 522-555.

Hathaway, S.D. and H.W. Evans. "Radio Attenuation at 11 kmc and Some Implications Affecting Relay System Engineering," Bell System Technical Journal, Vol. 38, No. 1, January 1959, 73-97.

APPENDIX B

PROGRAM COSTING AND COSTING METHODOLOGY

CONTENTS

ILLUSTRATIONS

TABLES

APPENDIX B

PROGRAM COSTING AND COSTING METHODOLOGY

1.0 INTRODUCTION

The costs generated during the study and presented herein are based on parametric models developed by FACC. When integrated these models provide:

- Spacecraft and spacecraft subsystem weight
- Spacecraft EOL and BOL power
- Spacecraft on-orbit weight
- Spacecraft launch weight
- Spacecraft nonrecurring and recurring costs
- Transfer orbit system and its costs
- Space Transportation System (STS) (Shuttle) costs
- TT&C system costs
- Terminal subsystem and unit costs
- Terminal quantity discount costs
- Total program costs for a given base year
- Total program costs spread over program life

2.0 GENERAL COSTING APPROACH

The general costing approach objective was to provide system costs and cost sensitivities as an input to overall program costing for providing defined communications services. Therefore, costs generated by the systems contractors were defined for a given base year and formed a basis for determining cash flows and revenues required to provide the different stated categories of user demand.

The general costing approach used by FACC for both the trunking and direct-to-user (DTU) systems was to define a baseline system and its costs and then generate cost deltas for the various alternatives considered in order to establish at least a first order cost optimization for a given service. Basically, the steps in this process were to:

a. Define baseline systems:
1. Trunking - FDMA/FDMA; TDMA
2. Direct-to-User - TDMA; FDMA/FDM
b. Use FACC parametric estimating models:
1. Generate spacecraft and terminal parameters.
2. Use modified SAMSO model for spacecraft costing.
3. Use FACC terminal costing model.
c. Make basic parametric changes and identify cost deltas:
1. Rf power
2. Number of spacecraft beams
3. Number of rf channels

Ford

Ford Aerospace &
Communications Corporation

4. Bit rates

A similar approach was followed for the earth terminals. The basic costing ground rules used included:

a. No year dollars; base year 1978
b. Trunking - total program costs only
c. Direct-to-user:
   1. Total program costs
   2. Estimated end-to-end costs
d. Spacecraft:
   1. Three flight models plus refurbished prototype
   2. Three launches
   3. Ten-year operating period
   4. Space Transportation System launch
   5. Three-year program to first launch
e. Terminals:
   1. Fifteen-year life, 10-year operating period
   2. Land, utilities, roads, fences, auxiliary power, radomes/windscreens not included
   3. Maximum production discount quantity of 100 units for DTU system
   4. Three-year program for first production quantity

Although estimated end-to-end costs for the DTU system were examined, the results were suspect and no detail is provided.

2.1 Spacecraft Cost Model

The spacecraft estimating model predicts spacecraft weights and costs based on derived factors and the use of a modified version of the same spacecraft cost model. The program has been designed to estimate spacecraft sizes and costs and the effect of increasing or decreasing communications capability on spacecraft size and cost. The model use is limited to communications payloads (or payloads that are equivalent) for estimating size and costs although the spacecraft parametric estimates can be used for sizing any type of spacecraft. Further the model is limited to three-axis spacecraft and the use of the Space Transportation System as a launch vehicle. Cost estimates generated are defined as *end-of-program should costs* and have a 95% confidence interval of approximately -8% to +14% of the predicted costs.

2.1.1 General Model Description

Figure B-1 depicts the general program flow of the model, which consists of four major routines.

2.1.2 Orbital Parameter Generator

Through the use of simple Keplarian formulas, ΔV's are estimated for the defined spacecraft orbits. An STS launch vehicle is assumed starting from a parking orbit of 160 nmi altitude at a 28.5° inclination (Eastern Test Range) or 75° inclination (Western Test Range).

2.1.3 Spacecraft Parameter Generator

Using the payload weight and power as inputs, the model generates estimates for:
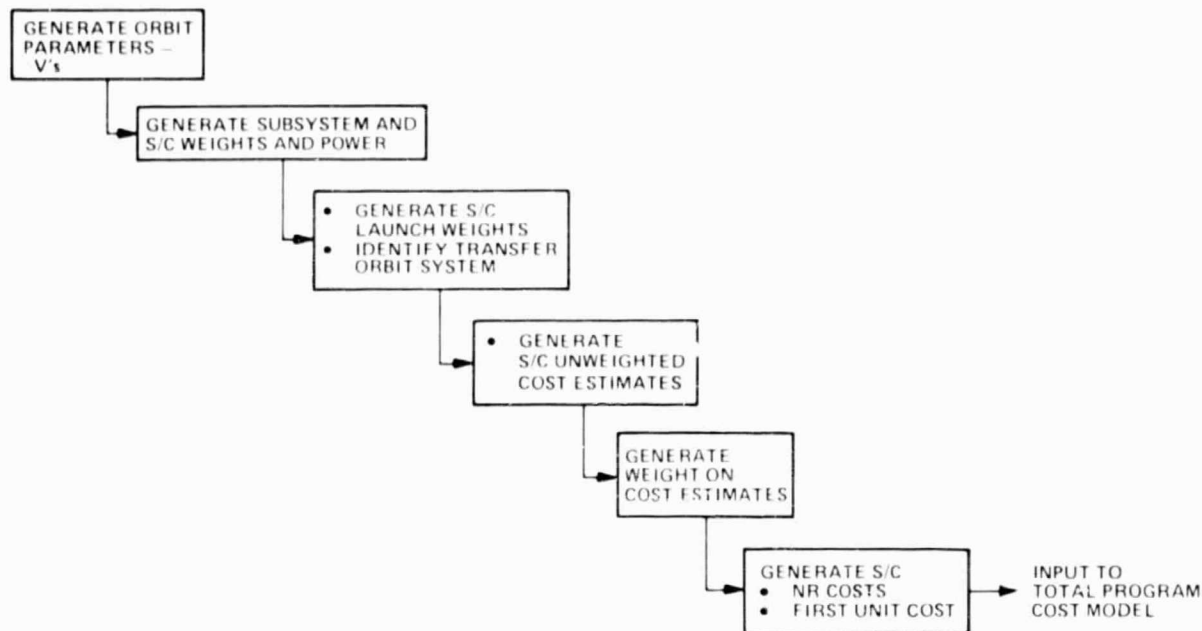
Figure B-1. Spacecraft Cost Model Flow

a. Structure Weight
b. TT&C Weight and Power
c. Attitude Control Weight and Power
d. Propulsion Weight
e. Electrical/Mechanical Integration Weight
f. Thermal Weight
g. Electrical Power Weight
h. Number of cells in the array
i. EOL & BOL Power (equinox)
j. On-Orbit Fuel Weight
k. Bus/Spacecraft On-Orbit Dry and Wet Weights
l. Spacecraft Launch Weight

In addition, the transfer orbit system is predicted.

2.1.4 Spacecraft Cost Generator

The estimated spacecraft subsystem weights and power are rearranged to fit the SAMSO Cost Estimating Relationship (CER) parameters, and Basic Cost Estimates at the subsystem level are generated using the SAMSO CERs. Complexity factors and weighted complexity factors are then generated and applied to the Basic Estimates to arrive at the cost estimates for the derived spacecraft. Both nonrecurring costs (prototpe and R&D) and recurring costs (first unit costs) are generated, including Management and Support, prototype refurbishment, and total space segment costs including profit and on-orbit incentives, transfer orbit system costs, and STS costs.

If the user has all of the spacecraft parameters, the model can be used to generate costs only.

2.1.5 Trade Generator

Tradeoffs can be accomplished using different payload weights and power. The model retains the initial computations as a baseline; checks to see if the new payload can be accommodated within the capabilities of the baseline bus; and either computes weight/cost deltas or recomputes all spacecraft parameters and costs. Based on the results of the trades, the user can retain or replace the stored baseline.

2.1.6 Technology Base

With the exception of the electrical power subsystem, the technology base for estimating spacecraft weights is essentially that which would be available for a spacecraft lauched in the 1985-87 time period. Although some increases in the technology base can be anticipated post-1985-87, they would have to be radical in nature for a significant difference to be seen. For the electrical power subsystem, two technology bases are included in the model: one for 1985-87 launch (up to 1984) and one for 1988+ launch (1985). Significant increase in power generating capability per pound of power subsystem weight is anticipated in the post-1985 period. Where an apogee motor capability is included in the spacecraft, use of a bipropellant system is factored into the model.

2.1.7 Cost Base

The cost base provided in the model has been set in terms of 1978 dollars. All computations are presented for that base year. To establish a cost estimate for base years beyond 1978, the generated cost estimates must be spread and appropriate inflation factors applied.

2.2 Terminal Cost Model

The Terminal Cost Model used for this study consists of a series of algorithms empirically derived by FACC. These algorithms are used to generate estimated cost of the major terminal hardware such as the antennas, HPAS, LNAs, up/down converters, and modems. Inputs are generally the predominent design factors such as antenna diameter, HPA power, LNA noise temperature, etc. Once these hardware costs have been generated using a block diagram to determine the number of each component, other terminal costs (test translator, frequency source, power suplies, racks, etc) are factored and summed with the hardware costs. This cost is then factored for installation, checkout, and site preparation costs. This latter cost is summed with the previous costs and a learning curve factor is applied based on the number of terminals to be manufactured.

The costs generated by this model are presented in 1978 dollars and do not include peculiar system costs such as diversity. Such costs plus initial and ongoing spares costs, operation and maintenance costs, utilities costs, roads, buildings, and land costs must be added, based on the system equipment/capabilities.

3.0 COSTING CONSIDERATIONS

The system configurations (as defined from a spacecraft standpoint) exceeded 20 in number and included:

a. *Trunking*
  1. FDMA
    (a) Baseline - FDMA/FDMA, 10 beams, 1 W power amplifiers
    (b) Alternatives
      (1) 4 PA levels, 20 beams
      (2) FDMA/FDM (3 carriers/power amplifier)
      (3) FDMA/TDM
  2. TDMA
    (a) Baseline - TDMA, 10 beams, 10 W power amplifiers
    (b) Alternatives - 3 PA levels; 20 beams
b. *Direct-to-User*
  1. TDMA
    (a) Baseline - TDMA, 25 beams, 25 W power amplifiers, no frequency reuse
    (b) Alternatives - 2 PA levels, 1 and 3 times frequency reuse
  2. FDMA
    (a) Baseline - FDMA/FDMA
    (b) Alternatives - FDMA/FDM (25 beams, 80 W power amplifiers, 1 frequency reuse)

From an earth terminal standpoint, configurations examined included:

a. *Trunking*
  1. With diversity
  2. Without diversity
b. *Direct-to-User*
  1. Uniform/nonuniform distribution per beam
  2. Total number of terminals

A significant cost element in all system configurations associated with the spacecraft was the transfer orbit system required and the STS launch costs. The transfer orbit system presented some difficulties in systems costing due to the limitation presented by existing/planned systems (SSUS-D, SSUS-A, IUS), which severely limits the spacecraft design in optimizing spacecraft systems from an STS cost standpoint as well as the basic spacecraft design. FACC has been working on a transfer-orbit system design to overcome these limitations.

The FACC approach is a bipropellant satellite propulsion module (SPM) that allows sizing transfer orbit propellants to a given spacecraft design. The basic design (Figure B-2) has eight tanks which accommodate 25,000 lb of fuel, and has inert and cradle weights of 2500 lb and 550 lb, respectively. The design allows for reducing or increasing the number of tanks employed when fuel requirements drop or increase. Therefore, the other basic SPM configurations have 4, 6, 16, 20, etc, tanks depending upon the total amount of fuel required. These configurations are also shown in Figure B-3. The basic capabilities of the various transfer orbit systems are:

TOTAL WEIGHT	28,050 lb
INERT WEIGHT	2,500 lb
CRADLE WEIGHT	550 lb
FUEL WEIGHT	25,000 lb
NOMINAL I_S	310 s
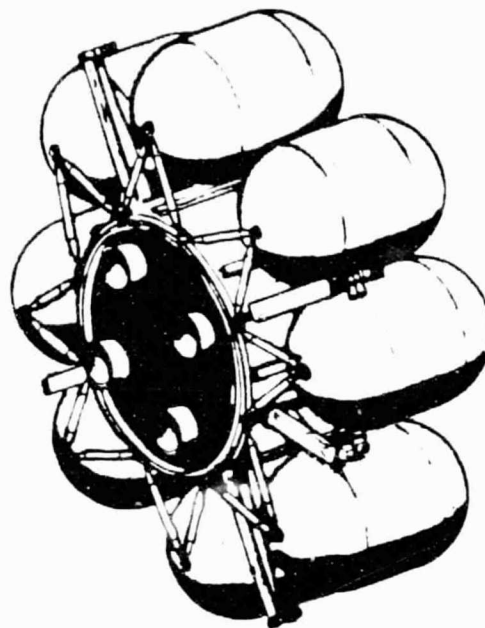
Figure B-2. Satellite Propulsion Module Basic Consideration

Transfer Orbit System	Spacecraft On-Orbit Weight (lb) (to sync equatorial)	Cost (78 $)
SSUS-D	Up to 1565	$ 2.5M each
SSUS-A	Up to 2475	$ 5M each
SPM (4 tank)	Up to 2930	$ 5M each
SPM (6 tank)	Up to 4390	$ 6M each
SPM (8 tank)	Up to 5850	$ 7M each
IUS	000 to 5000	$13M each

It is noted that program costing does not include the technology development costs for the SPM. STS costs *(STSC)* were generated on the basis of the latest NASA STS cost allocation formulas:

$STSC = PLF \times 1.33 \times \$18.3M \times IF$

Where

PLF is partial-load factor (spacecraft length in feet divided by 60 or spacecraft weight in pounds divided by 65,000, whichever is great.).

Ford Ford Aerospace & Communications Corporation
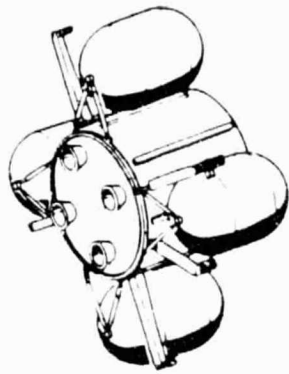
4-TANK 1-STAGE MODULE
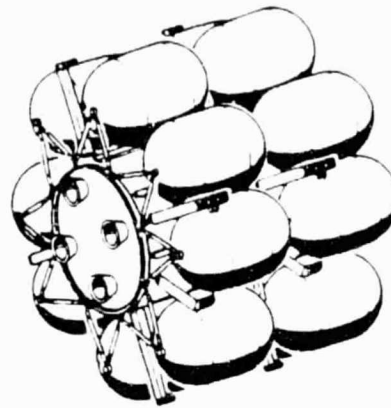
TWO-STAGE MODULE
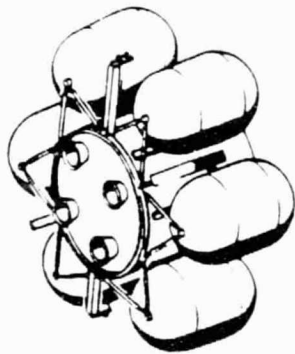
6-TANK 1-STAGE MODULE
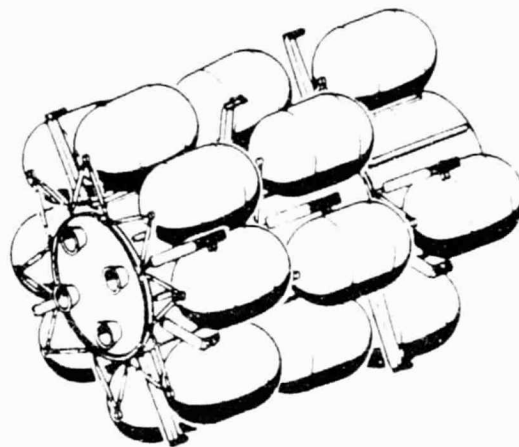
THREE-STAGE MODULE

Figure B-3. Off-Loaded and Staged SPM Configuration

IF is the inflation factor (8.5% used from a 1975 base year).

Another major system cost generated was the O&M cost associated with various earth terminal configurations. Historically, terminal O&M costs, particularly where a large number of terminals are involved, have tended to exceed (sometimes grossly) initial investment costs. In this area, initial and replacement spares and on/off equipment maintenance costs have proven to be the major cost drivers. Although there are several logistics support cost models in existence (MIL DEPS and RCA PRICE for example), the reduction and application of these models to this program was beyond the intended scope of the SOW. It is important to point out, however, particularly in the DTU system, that there is a major tradeoff involved between terminal MTBF and terminal O&M to minimize overall total program costs. This trade may well indicate a significant increase in unit investment costs in achieving

B-7

Ford Aerospace &
Communications Corporation

a high MTBF to offset ongoing O&M costs. For the purposes of this program, terminal O&M costs were empirically derived and are summarized below:

    a. *Trunking*
        1. Initial spares - 8% of total hardware
        2. OEM/year
         (a) Spares - 0.017% of total site costs
         (b) Operation and maintenance - 0.068% of total site costs
    b. *Direct-to-User*
        1. Initial spares - 8% of total hardware
        2. OEM/year
         (a) Spares - 0.024% of total site costs
         (b) Operation and maintenance - 0.048% of total site costs

Considerably more effort will be required in this area before valid total system costs can be defined.

4.0 COSTING RESULTS

Presented in this subsection are the results of the costing efforts on this program. Some general conclusions reached on the basis of the costing effort are:

    a. Ignoring technology development costs, TDMA configurations tended to be lower in cost than FDMA systems simply due to the number of rf channels required by FDMA systems.

    b. Higher rf power in the spacecraft generally tended to reduce overall program costs.

    c. A direct FDMA analogy to the TDMA baselne DTU configuration exceeded STS launch capabilities.

    d. Although TDM in the spacecraft downlink was less costly than FDMA/FDM or FDMA/FDMA for trunking, processing to individual signal baseband did not appear to be a significant, driving program requirement.

    e. Most spacecraft configurations fall outside of standard transfer orbit systems capabilities.

    f. In general, spacecraft length tended to dominate STS costs, which tended to allow increases in spacecraft rf power with a net decrease in total program costs.

    g. Major cost drivers in both systems tended to be:
        1. Number of spacecraft beams
        2. Number of rf channels per beam
        3. Spacecraft rf power
        4. Earth terminal HPA power
        5. Number of earth terminals (primary effort was O&M costs)

4.1 Baseline Configurations

The following paragraphs present the baseline spacecraft and earth terminal costing parameters and costs for the trunking and DTU systems. Costs presented are for nonrecurring and first unit costs. Included for the spacecraft are prototype refurnishment costs.

4.2 Spacecraft

Tables B-1 and B-2 present the estimated spacecraft parameters and costs for baseline

Ford   Ford Aerospace & Communications Corporation

trunking FDMA and TDMA spacecraft. Results of basic spacecraft trades for the trunking system are presented in Tables B-3 and B-4. Estimated spacecraft parameters and costs for the baseline DTU system TDMA and FDMA spacecraft are presented in Tables B-5 and B-6. Basic spacecraft DTU trades are shown in Table B-7.

4.3 Terminals

Trunking terminal estimates and trades are shown in Table B-8 with DTU terminal estimates and trades shown in Table B-9.

4.4 Notes

    a. Cost and cost deltas shown provided the basis for trade results shown in the main body of this report.

    b. FDMA/FDMA estimated spacecraft configuration for DTU exceeded STS weight capability so an FDMA/FDM configuration was baselined instead. Reference Table B-5.

    c. Reference Tables B-2 and B-6. Costs shown indicate constituent parts of total spacecraft program, eg, for three spacecraft and refurbished prototype, baseline trunking system.

			1978 $
Nonrecurring		**Recurring**	**X 1000**
Prototype	33,447.6	Prototype Refurbishment	09,851.6
Red	38,836.1	3 flight models	80,274.3
Total	72,283.7	3 SPM-4s	15,000.0
		3 STSs	46,403.0
		Total Recurring	151,529.0
		Total Nonrecurring	72,283.7
			223,812.7
		Profit & OOIs	32,481.9
		Total Spacecraft Program	256,294.6

    d. Reference Tables B-3, B-4, and B-7. Costs shown are deltas to baseline system costs, eg, for 2 W power amplifiers to baseline FDMA/FDMA trunking systems.

Baseline		**Trade Results**	**Total**
Prototype Refurbish	09,851.6	+0,209.4	10,061.0
3 flight models	80,274.3	3,141.0	83,415.3
3 SPM-4s	15,000.0	-	15,000.0
3 STSs	46,403.1	-	46,403.1
Total Nonrecurring	72,283.7	1,599.8	73,883.5
	223,812.7	4,950.2	228,762.9
Profit & OOIs	32,481.9	0,990.0	33,471.9
Total Spacecraft Program	256,294.6	5,940.2	262,234.8

    e. For terminal trades, the same general approach is followed as used for the spacecraft. *Note:* O&M is ratioed on a per terminal basis as indicated in section 3.0 above.

Ford Ford Aerospace & Communications Corporation

Table B-1. Trunking System Baseline Spacecraft Parameters

	FDMA/FDMA	TDMA
1 COMMUNICATIONS S/S (lbs)	995.9	453.7
2 TTEC S/S	50.0	50.0
3 ELECTRICAL POWER S/S	162.1	174.0
4 ELECT. INTEGRATION	107.6	49.0
5 ATTITUDE CONTROL S/S	158.0	131.0
6 PROPULSION S/S	72.1	136.3
7 STRUCTURE S/S	383.0	174.5
8 THERMAL CONTROL	62.7	28.6
9 MECHANICAL INTEGRATION	44.8	20.4
10 DRY SPACECRAFT	2036.2	1217.5
11 ON-ORBIT FUEL	381.0	275.7
12 SPACECRAFT ON-ORBIT WT.	2417.2	1493.2
13 SPACECRAFT THROW WT.	6535.0	2981.9
14 ALL-UP S/C LAUNCH WT.	15191.8	9201.8
15 XFER ORBIT SYSTEM	SPM-4	SSUS-D
16 SPACECRAFT LENGTH (ft)	21.0	21.0
17 STS INSTALLED LENGTH (ft)	27.5	28.0
18 TOTAL RF POWER (WATTS)	90.0	100.0
19 ARRAY: EOL (WATTS)	831.1	991.0
20 ARRAY: BOL (WATTS)	1138.5	1357.5
COSTING PARAMETERS		
1C COMMUNICATIONS S/S (lbs)	995.9	453.7
2C TTEC SUBSYSTEM (lbs)	50.0	50.0
3C ELECTRICAL POWER S/S (lbs)	269.7	223.0
4C BUS POWER (WATTS)	471.5	623.8
5C # CELLS IN ARRAY	7590	9050
6C ATTITUDE CONTROL S/S (lbs)	230.1	267.3
7C STRUCTURE S/S (lbs)	490.5	223.5
8C XFER ORBIT SYS.	SPM-4	SSUS-D
9C STS FACTOR (LENGTH) WT	27.5'	28.0'

Table B-2. Trunking System Spacecraft Cost Estimates

	NR CER	RCER	NR WCF	R WCF	NR EST.	R EST.
FDMA/FDMA						
COMMUNICATIONS S/S	18682.4	9234.8	1.715	1.534	31853.5	14166.2
TT&C S/S	1395.2	745.4	1.219	1.123	1700.7	837.1
Elec. Power S/S	1834.3	1083.9	1.000	1.000	1834.3	1083.9
ARRAY	379.5	303.6	1.316	1.957	499.4	599.1
ATTITUDE CONTROL S/S	10116.7	3196.5	1.301	1.097	13161.8	3506.6
STRUCTURE S/S	4697.2	881.3	1.346	1.377	6322.4	1213.6
TOTALS					55372.1	21406.5
MANAGEMENT & SUPPORT					16911.6	5351.6
TOTAL					72283.7 *	26758.1
PROTOTYPE					33447.6	
R&D					38836.1	
PROTO REFURBISH						5351.6
STORAGE						1500.0
PROTO LAUNCH						3000.0
TOTAL						9,851.6 *
FIRST UNIT COST						26758.1 *
XFER ORBIT SYST						3,000.0
STS COST						15,467.7
TOTAL FLY AWAY						47,225.8

* PLUS PROFIT & ON-ORBIT INCENTIVES (NOMINALLY 20%)

	NR CER	RCER	NR WCF	R WCF	NR EST.	R EST.
TDMA						
COMMUNICATIONS S/S	11598.8	5079.9	1.900	1.551	22032.0	7878.9
TT&C S/S	1395.2	745.4	1.323	1.183	1845.8	881.8
Elec. Power S/S	2141.4	1086.0	1.000	1.000	2141.4	1086.0
ARRAY	452.5	362.0	1.316	1.957	595.5	708.4
ATTITUDE CONTROL S/S	11,232.7	3600.4	1.383	1.176	15534.8	4234.1
STRUCTURE S/S	3103.3	482.2	1.346	1.377	4177.0	664.0
TOTALS					46326.5	15453.2
MANAGEMENT & SUPPORT					13898.0	3863.3
TOTAL					60244.5 *	19,316.5
PROTOTYPE					24145.6	
R&D					36078.9	
PROTO REFURBISH						3863.3
STORAGE						1500.0
PROTO LAUNCH						3000.0
TOTAL						8363.3 *
FIRST UNIT COST						19316.5
XFER ORBIT SYST.						2500.0
STS COST						18844.0
TOTAL FLY AWAY						40660.5 *

* PLUS PROFIT & ON-ORBIT INCENTIVES (NOMINALLY 20%)

Ford Ford Aerospace & Communications Corporation

Table B-3. FDMA/FDMA Trunking System Spacecraft Trades

Δ COST FACTORS		10 BEAM 2W PA's	10 BEAM 4W PA's	10 BEAM 6W PA's	10 BEAM 12W PA's	20 BEAM ½W PA's	10 BEAM 7.5W PA's-FDM	10 BEAM 15W PA's-FDM	10 BEAM 30W PA's-FDM	10 BEAM 100 PA's-TDM
(COMMUNICATIONS SUBSYSTEM	(lbs)	0.0	0.0	81.0	239.0	2575.3	⟨391.1⟩	⟨306.1⟩	⟨341.1⟩	⟨2643.⟩
ELEC POWER S/S	(lbs)	+23.7	+77.6	+163.3	+402.0	+357.2	+32.7	+88.0	+305.7	+71.3
BUS POWER	(watts)	+320.0	+1152.0	+1788.0	+3646.0	+5867	+6400	+3351.7	+3025.0	+1137.0
# CELLS		+2896.0	+8956.0	+15544.0	+34818.0	+35150.0	+4023	+10847	27852.0	+8788.0
TT&C S/S		0.0	0.0	0.0	0.0	0.0	0.0	0.0	0.0	0.0
AC S/S		0.0	0.0	0.0	0.0	20.0	0.0	0.0	0.0	0.0
PROP S/S		0.0	0.0	0.0	+22.3	+59.4	0.0	0.0	0.0	0.0
MECH INT		0.0	0.0	0.0	+13.7	+115.9	⟨37.0⟩	⟨13.2⟩	⟨5.7⟩	⟨11.9⟩
ELEC INT		0.0	0.0	0.0	+32.8	+278.1	⟨42.3⟩	⟨33.2⟩	⟨153.⟩	⟨28.6⟩
STRUCT S/S		0.0	0.0	0.0	+117.0	+940.5	⟨150.4⟩	⟨117.7⟩	⟨54.2⟩	⟨101.6⟩
Δ COSTS										
1/R COMM		0.0	0.0	+1841.9	+2875.9	+56,077.6	⟨5668.2⟩	⟨5217.2⟩	⟨5325.4⟩	⟨3026.7⟩
TT&C		0.0	0.0	0.0	0.0	0.0	0.0	0.0	0.0	0.0
EPS		+1040.0	+2304.0	+3576.0	+7342.0	1173.4	1280.0	27024	6050.0	+2274.0
ARRAY		+190.6	+588.9	+1022.0	+2284.3	231.3	264.7	713.7	1832.7	+577.8
ACS		0.0	0.0	0.0	+2120.1	2034.8	0.0	0.0	0.0	0.0
STRUCTURE		+6.0	0.0	0.0	+2058.7	8430.5	⟨2602.8⟩	⟨4642.1⟩	⟨983.2⟩	⟨1488.1⟩
TOTAL		+1,2306	+2892.9	+6434.9	+16,736.0	67,942.5	⟨4631.3⟩	⟨1450.2⟩	4574.1	⟨1674.0⟩
R. COMM		0.0	0.0	+2380.8	+5286.5	31,942.5	⟨7790.8⟩	⟨6466.1⟩	⟨36179⟩	⟨5112.3⟩
TT&C		0.0	0.0	0.0	0.0	0.0	0.0	0.0	0.0	0.0
EPS		+610.9	+915.0	+1174.7	+1208.6	1111.7	683.2	985.7	1520.3	815.7
ARRAY		+226.7	+701.1	+1555.4	+6354.2	275.2	314.9	935.4	5066.0	687.9
ACS		0.0	0.0	0.0	+490.2	1485.2	0.0	0.0	0.0	0.0
STRUCTURE		0.0	0.0	0.0	+293.5	2093.2	⟨349.0⟩	⟨290.2⟩	⟨161.5⟩	⟨286.7⟩
TOTAL		+837.6	+1616.1	+2750.1	+14138.0	36,907.9	⟨7121.7⟩	⟨7835.2⟩	2824.4	⟨3895.4⟩
1/R with RECURR & SUPPORT		+1,599.8	+3760.8	+8371.9	+21736.8	+89331.8	⟨6020.7⟩	⟨18853⟩	5946.3	⟨2176.2⟩
R " " "		+1047.0	+20201	+6412.6	+17672.5	46,134.5	⟨8902.1⟩	⟨6044.0⟩	3534.8	⟨4669.3⟩
PRORO RETURN " "		+209.9	+404.0	+1282.5	+3534.5	5227.0	⟨1180.4⟩	⟨1208.6⟩	707.4	⟨173.9⟩
XPER ORBIT SYST		0.0	0.0	0.0	0.0	+1,000.0	0.0	0.0	0.0	0.6
SYS COST		0.0	0.0	0.0	0.0	+89328	0.0	0.0	0.0	0.0

Table B-4. TDMA Trunking System Spacecraft Trades

Δ COST FACTORS	10 BEAM 20w PA's	10 BEAM 40w PA's	10 BEAM 80w PA's	20 BEAM 5w PA's
COMMUNICATIONS SUBSYSTEM (lbs)	46.8	82.8	118.8	340.1
ELEC. POWER S/S	0.0	40.0	120.0	17.7
BUS POWER	957.1	1623.8	2957.1	449.0
# CELLS	3195	9972	24484	2185
TTEC S/S	0.0	0.0	0.0	0.0
AC S/S	0.0	0.0	0.0	0.0
PROP S/S	0.0	0.0	95.2	95.2
MECH INT	0.0	0.0	20.4	20.4
ELEC INT	5.0	8.9	12.8	36.7
STRUCTURE S/S	0.0	0.0	177.9	177.7
Δ COSTS				
N.R. COMM	4238.8	6212.4	7912.4	16008.7
TTEC	0.0	0.0	0.0	0.0
EPS	1914.2	3247.5	5914.2	899.0
ARRAY	210.2	656.2	1647.8	143.8
ACS	0.0	0.0	6693.5	6693.5
STRUCTURE	0.0	0.0	2916.2	2916.2
TOTAL	6363.2	10,116.1	25084.1	26,661.2
R. COMM	1598.5	2452.2	3214.7	7075.2
TTEC	0.0	0.0	0.0	0.0
EPS	500.2	905.0	1269.4	705.9
ARRAY	250.2	750.6	1916.6	170.0
ACS	0.0	0.0	1840.9	1840.9
STRUCTURE	0.0	0.0	606.6	606.6
TOTAL	2348.9	4137.9	8,848.2	10,398.5
NR WITH MGMT & SUPPORT	8272.2	13,150.9	31355.1	34,654.6
R " " "	2936.1	5172.3	11060.3	12998.3
PROTO REFURB	587.2	1034.5	2212.0	2599.7
XFER ORBIT SYSTEM	0.0	0.0	1,000.0	1,000.0
STS COST	0.0	0.0	0.0	0.0

Table B-5. Direct-to-User System Baseline Spacecraft Parameters

	TDMA	FDMA [1]
1 COMMUNICATIONS S/S (lbs)	957.6	1392.7
2 TT&C S/S "	50.0	50.0
3 ELECTRICAL POWER S/S "	377.5	942.4
4 ELEC. INTEGRATION "	103.4	150.4
5 ATTITUDE CONTROL S/S "	158.0	178.0
6 PROPULSION S/S "	78.9	110.8
7 STRUCTURE S/S "	368.3	537.7
8 THERMAL CONTROL S/S "	60.3	87.7
9 MECHANICAL INTEGRATION "	43.1	62.7
10 DRY SPACECRAFT "	2197.1	3512.4
11 ON-ORBIT FUEL "	449.2	764.5
12 SPACECRAFT ON-ORBIT WT.	2646.3	4276.9
13 SPACECRAFT THROW WT.	6943.2	12076.4
14 ALL-UP S/C LAUNCH WT.	16106.4	27607.5
15 XFER ORBIT SYSTEM	SPM-4	SPM-6
16 SPACECRAFT LENGTH (ft)	15.0	15.0
17 STS INSTALLED LENGTH (ft)	21.5	21.5
18 TOTAL RF POWER (WATTS)	625.0	2000.0
19 ARRAY: EOL (WATTS)	3200.7	8135.9
20 ARRAY: BOL (WATTS)	4384.5	11145.1
COSTING PARAMETERS		
1C COMMUNICATIONS S/S (lbs)	957.6	1392.7
2C TT&C S/S (lbs)	50.0	50.0
3C ELECTRICAL POWER S/S (lbs)	480.9	1092.9
4C BUS POWER (WATTS)	2443.3	6468.5
5C #CELLS IN ARRAY	29230	74300
6C ATTITUDE CONTROL S/S (lbs)	236.9	288.9
7C STRUCTURE S/S (lbs)	471.7	688.1
8C XFER ORBIT SYS.	SPM-4	SPM-6
9C STS FACTOR LENGTH (WT)	21.5 ft.	27607.5 lbs

(1) FDMA/FDM CONFIGURATION: FDMA/FDM
EXCEED STS LAUNCH WT. CAPABILITIES

Table B-6. Direct-to-User System Spacecraft Cost Estimates

	NR CER	R CER	NR WCF	R WCF	NR EST.	R EST.
TDMA						
Communications S/S	18234.1	8969.5	2.004	1.870	36541.1	16773.0
TT&C S/S	1395.2	745.4	1.323	1.183	1845.8	881.8
Elec Power S/S	6283.2	1057.9	1.000	1.000	6283.2	1057.9
Array	1461.2	1168.9	1.329	4.643	1941.9	5427.2
Attitude Control S/S	10323.9	3271.2	1.248	1.141	12884.2	3732.3
Structure S/S	4597.0	855.3	1.346	1.377	6187.6	1177.7
Totals					65683.8	29049.9
Management & Support					19705.1	7262.5
Total					85388.9*	36312.4
Prototype					45390.5	
R & D					39998.4	
Proto Refurbish.						7262.5
Storage						1500.0
Proto Launch						3000.0
Total						11762.5*
First Unit Cost						36312.4*
Xfer Orbit Sys.						5,000.0
STS Cost						15,467.7
Total Fly Away						56,779.1

* PLUS PROFIT & ON-ORBIT INCENTIVES (NOMINALLY 20%)

	NR CER	R CER	NR WCF	R WCF	NR EST.	R EST.
FDMA/FDM						
Communications S/S	23043.2	11902.0	2.025	1.889	46662.5	22482.9
TT&C S/S	1395.2	745.4	1.219	1.123	1700.7	837.1
Elec Power S/S	15254.8	2400.3	1.000	1.000	15,254.8	2400.3
Array	3715.0	2992.0	1.333	5.643	4952.1	16771.0
Attitude Control S/S	11859.8	3828.7	1.150	1.062	13638.8	4066.1
Structure S/S	5693.7	1140.5	1.346	1.377	7663.7	1570.5
Totals					89872.6	48127.9
Management & Support					26961.8	12032.0
Total					116834.4*	60159.9
Prototype					75198.8	
R & D					41635.6	
Proto Refurb						12031.8
Storage						1500.0
Proto Launch						3000.0
Total						16531.8*
First Unit Cost						60159.9
Xfer Orbit Sys						7000.0
STS Cost						17,533.0
Total Fly Away						84,692.9*

* PLUS PROFIT & ON-ORBIT INCENTIVES (NOMINALLY 20%)

WDL-TR8457

B-15

Ford Aerospace &
Communications Corporation

Table B-7. Direct-to-User System Spacecraft Trades

TDMA Δ Cost Factors	25 Burny 50w PA's	25 Burny 75 w PA's	25 Burny w 1x Frg.Re.	25 Burn w 3x Frg.R.
Communications Subsystem	+95.0	+75.0	580.1	1160.2
Elec. Power S/s	303.5	562.3	332.5	674.7
Bus Power	2669.3	4871.7	3041.9	5753.6
# Cells	22672	44749	26243	53689
TTEC S/s	0.0	0.0	0.0	0.0
AC S/s	0.0	0.0	0.0	20.0
Pr&P. S/s	18.4	36.9	26.4	54.1
Mech Int	0.0	0.0	26.1	89.9
Elect Int	10.3	10.3	62.5	125.3
Struct X/S	0.0	0.0	223.1	451.2
Δ Costs				
N.R. Comm	2616.5	2616.5	12614.5	23751.4
TTEC	0.0	0.0	0.0	0.0
SPS	5338.5	9443.4	6083.9	11507.0
Array	1506.6	2973.6	1743.8	3567.6
ACS	651.9	2967.1	2308.2	5005.3
Structure	0.0	0.0	3390.9	5656.6
TOTAL	10,113.5	18,000.5	26,143.5	49,487.9
R. Comm	1418.5	1418.5	7213.3	13,768.2
TTEC	0.0	0.0	0.0	0.0
SPS	1489.7	1919.7	1607.7	2135.2
Array	4210.6	8310.8	4873.8	9971.1
ACS	479.6	836.8	640.2	1461.7
Structure	0.0	0.0	723.3	1314.1
TOTAL	7598.7	13,485.9	15,058.3	28650.2
NR with Mgmt & Support	+13,147.6	23400.8	33,986.3	64334.3
R	+9499.0	16,857.3	18,822.9	35,812.8
Proto Refurb	+1899.5	3371.5	3764.6	7162.6
Xfer orbit System	+1000.0	1000.0	1000.0	2000.0
STS Cost	0.0	1785.7	1,897.9	4,946.4

(1) Trades on SC Power (+36−) on FDMA/FDM
   DTU Baseline exceeded STS wt capacity.

Table B-8. Trunking System Terminal Estimates

Table B-8. Trunking System Terminal Estimates

Table B-8. Trunking System Terminal Estimates (Continued)

Table B-9. Direct-to-User System Terminal Estimates

Table B-9. Direct-to-User System Terminal Estimates (4.5 METER)

	TDMA SINGLE UNIT	100 UNITS	S/C EIRP +3dB (1)	S/C EIRP +3dB S/C G/T +3dB	S/C EIRP +6dB S/C G/T +6dB		FDMA SINGLE UNIT	100 UNITS	S/C EIRP +3dB	S/C EIRP +3dB S/C G/T +3dB	S/C EIRP +6dB S/C G/T +6dB
ANTENNA, PEDESTAL, DRIVE, TRACK + FEED	28.4	20.2					28.4	20.2			
TRANSMITTERS											
A 100W (1)	45.1	32.1		⟨8.2⟩	⟨8.2⟩	1 W (16)	99.0	70.4		⟨17.7⟩	⟨17.7⟩
B 1000W (1)	121.6	86.5		⟨22.3⟩	⟨22.3⟩	10W	16.7	11.9		⟨3.0⟩	⟨3.0⟩
C						50W	33.6	23.9		⟨6.2⟩	⟨6.2⟩
LOW NOISE AMPLIFIERS (2) (230°K)	45.6	32.4	⟨14.5⟩	⟨14.5⟩	⟨22.5⟩	(475°K)	26.9	19.1	⟨8.6⟩	⟨8.6⟩	⟨13.3⟩
UP CONVERTORS (3)	16.7	11.9				(13)	123.2	87.6			
DOWN CONVERTERS (3)	15.3	10.7				(13)	112.2	79.8			
MODEMS (3)	56.0	39.8				(13)	60.2	42.8			
MUX/DEMUX	18.0	12.8					—	—			
DEMAND ASSIGNMENT PROCESSOR	56.9	40.5					35.1	25.0			
TEST XLATOR	15.0	10.7					15.0	10.7			
CONTROL, MONITOR & ALARM	15.0	10.7					15.0	10.7			
FREQ STANDARD	3.9	2.7					3.9	2.7			
ORDER WIRE	3.5	2.5					3.5	2.5			
RACKS (w cables/power)	14.2	10.1					14.2	10.1			
TOTAL SITE HARDWARE	455.2	323.7	⟨14.5⟩	⟨45.0⟩	⟨53.0⟩		586.9	417.4	⟨8.6⟩	⟨35.5⟩	⟨40.2⟩
OTHER SITE EQUIPMENT	91.0	64.7	⟨2.9⟩	⟨9.0⟩	⟨10.5⟩		117.4	83.5	⟨1.7⟩	⟨7.1⟩	⟨8.0⟩
TOTAL HARDWARE	546.2	388.4	⟨17.4⟩	⟨54.0⟩	⟨63.5⟩		704.3	500.9	⟨10.3⟩	⟨42.6⟩	⟨48.2⟩
INSTALLATION & CHECKOUT	136.6	97.1	⟨4.4⟩	⟨13.5⟩	⟨15.9⟩		176.0	125.2	⟨2.6⟩	⟨10.7⟩	⟨12.1⟩
INITIAL SPARES	45.5	32.4	⟨1.5⟩	⟨4.5⟩	⟨5.3⟩		58.6	41.7	⟨0.8⟩	⟨3.6⟩	⟨4.0⟩
TOTAL INSTALLED TERM	728.3	517.9	⟨23.3⟩	⟨72.0⟩	⟨84.7⟩		938.9	667.8	⟨13.7⟩	⟨56.9⟩	⟨64.3⟩
			494.5	445.9	433.2				654.1	610.9	603.5

(1) Decrease Terminal Diameter by 3dB yields an increase in terminal 100 unit cost of $58.7K due to 3dB increase in PA output power required

REPRODUCIBILITY OF THE ORIGINAL PAGE IS POOR